Solar Energy on Demand: A Review on High Temperature Thermochemical Heat Storage Systems and Materials

Alfonso J. Carrillo [a*], *José González-Aguilar* [b*], *Manuel Romero* [b], *Juan M. Coronado*[c*]

(a) Instituto de Tecnología Química (Universitat Politècnica de València – CSIC), Avda. Los Naranjos s/n, 46022 Valencia, Spain

(b) IMDEA Energy Institute, Avda. Ramón de la Sagra, 3, 28935, Móstoles, Madrid, Spain

(c) Instituto de Catálisis y Petroleoquímica, CSIC, Marie Curie, 2, Cantoblanco, 28049 Madrid, Spain.

*Corresponding authors: alcardel@itq.upv.es; jose.gonzalez@imdea.org; jm.coronado@csic.es

Abstract

Among renewable energies, wind and solar are inherently intermittent and therefore both require efficient energy storage systems to facilitate a round-the-clock electricity production at global scale. In this context, concentrated solar power (CSP) stands out among other sustainable technologies because it offers the interesting possibility of storing energy collected from the sun as heat, by sensible, latent or thermochemical means. Accordingly, continuous electricity generation in the power block is possible even during off-sun periods, providing CSP plants with a remarkable dispatchability. Sensible heat storage has been already incorporated to commercial CSP plants. However, due to its potentially higher energy storage density, thermochemical heat storage (TCS) systems emerge as an attractive alternative for the design of next generation power plants, which are expected to operate at higher temperatures. Through these systems, thermal energy is used to drive endothermic chemical reactions, which can subsequently release the stored energy when needed through a reversible exothermic step. This review analyzes the status

of this prominent energy storage technology, its major challenges and future perspectives, covering in detail the numerous strategies proposed for the improvement of materials and thermochemical reactors. Thermodynamic calculations allow selecting high energy density systems, but experimental findings indicate that sufficiently rapid kinetics and long-term stability trough continuous cycles of chemical transformation are also necessary for practical implementation. In addition, selecting easy to handle materials with reduced cost and limited toxicity is crucial for large-scale deployment of this technology. In this work, the possible utilization of materials as diverse as metal hydrides, hydroxides or carbonates for thermochemical storage is discussed. Furthermore, especial attention is paid to the development of redox metal oxides, such as Co_3O_4/CoO, Mn_2O_3/Mn_3O_4 and perovskites of different compositions, as an auspicious new class of TCS materials due to the advantage of working with atmospheric air as reactant, avoiding the need of gas storage tanks. Current knowledge about the structural, morphological and chemical modifications of these solids, either caused during redox transformations, or induced wittingly as a way to improve their properties, is revised in detail. In addition, the design of new reactors concepts proposed for the most efficient use of TCS in concentrated solar facilities is also critically considered. Finally, strategies for the harmonic integration of these units in functioning solar power plants, as well as the economic aspects are also briefly assessed.

Contents

1. Introduction

1.1. Concentrating Solar Power

Solar energy is the most abundant renewable resource available in the Earth. Namely, 430 EJ (1 EJ = 10^{20} J) of sunlight energy impinge on the Earth per hour, which is approximately the total world energy consumption per year[1]. However, its collection, conversion, distribution and final use entail economic and technological challenges that must be overcome to enhance solar energy exploitation. Solar applications mainly comprise thermal processes and electricity generation. The first one focuses on transforming solar energy into heat for low-to-high temperature applications like active and passive water and space (in buildings) heating, solar cooling or industrial process heat. Electricity generation comprises direct solar-to-electricity conversion by photovoltaics (PV) and solar-to-mechanical and then to electricity transformation by concentrating solar power (CSP). By end-2017, solar energy represents less than 2% of total global electricity production, being PV 1.5% and CSP almost 0.4%[2]. Additionally, costs have been highly reduced in the last years, especially in PV, which results in higher competitiveness of solar energy technologies with respect to non-renewable electricity and their deployment worldwide. In fact, in 2014 investment in solar power grew a 25% in respect to 2013 [3].

Despite PV has experienced a higher deployment and currently presents lower cost than CSP [4] when no storage is considered, solar thermal power exhibits some advantages compared to PV, mainly in centralized electricity generation. The most distinguishing feature is the capability of using thermal energy storage in CSP plants that allows overcoming the inherent problem related to solar intermittency [4–6]. Electrochemical storage for PV is currently very expensive, which leads to hampering the use of PV with energy storage [4]. According to Feldman et al., comparison

between concentrating solar power using thermal storage and photovoltaic using electrochemical energy storage indicates that first technology is cheaper than the second one in terms of levelized cost of energy (LCOE) at longer storage periods (9 h).[7]

By end-2016, there were 4.8 GW of installed CSP in the whole world. CSP deployment had an important increase between 2008 and 2013, especially in Spain and USA and other countries such as India and Israel [8]. This trend has currently leveled-off, although significant contributions are expected in MENA region (Morocco, Saudi Arabia, Dubai, Kuwait) and South Africa, China and Chile (Fig.1) [9] .

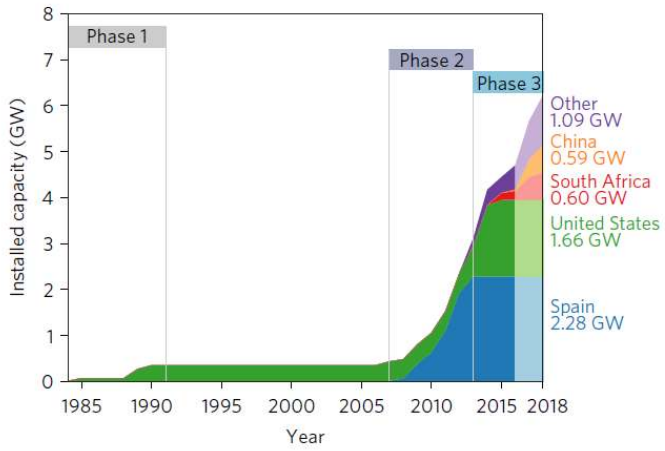

Figure 1. CSP installed capacity evolution from 1985 to 2018. Reprinted by permission from Springer Nature, Nature, Nature Energy. Empirically observed learning rates for concentrating solar power and their responses to regime change, Johan Lilliestam, Mercè Labordena, Anthony Patt, Stefan Pfenninger. Copyright (2017)

CSP plants basically comprise four main systems, collector, receiver, thermal storage and electric power generating subsystems[6]. Regarding concentrating solar thermal technologies, CSP plants are classified in point-focus and line-focus systems. The first one encompasses parabolic dishes and tower/central receivers, whilst the second one includes parabolic trough and lineal Fresnel reflectors. Fig. 2 depicts the schemes of these four optical configurations. Parabolic trough

and central receiver solar power plants are currently the most extended technologies, followed by a few linear Fresnel plants. Central receiver, for its part, is currently considered to have the highest potential for cost reduction due to its capability to reach higher working temperatures and use more-efficient thermodynamic cycles.[10,11]

Although each of the four types of concentrating systems presents interesting particular advantages, this section will just briefly explain the central receiver concept, since it is the most indicated for large-scale high-temperature thermochemical storage. As depicted in Fig.2, this system is composed by two main elements, a heliostat field and a solar receiver located on top of a tower, reason why plants working with this concept are also known as tower plants. Heliostats are mirrors of large dimensions that reflect sunlight and concentrate it on the central receiver [6]. Solar receivers are heat exchangers that transform concentrated solar energy into thermal energy by heating up a fluid, which flows through these radiation absorber components. Several heat transfer fluids (HTF) can be used for such purpose,[4,12,13] such as molten salts, liquid metals (like sodium), water/steam, air or even moving solid particle streams. However today commercial central receiver CSP plants used mainly (nitrate-based) molten salts and water/steam.[11] The HTF conveys thermal energy from the receiver to the power block. The choice of HTF depends on the temperature range within the HTF is thermally stable and its physical properties, for instance, the heat capacity, density and thermal conductivity. In general, gases can operate at higher temperatures than liquids, although they exhibit poorer thermal properties. In the power block, thermal energy is firstly transformed into mechanical energy through a thermodynamic cycle and, then converted into electricity by a generator. The most common thermodynamic cycle employed in commercial CSP plants is the Rankine type (working with steam). Another well-known thermodynamic cycle that can be implemented in CSP is the Brayton cycle, which operates with

gases (air). Both concepts are also revisited using new heat transfer fluids such as supercritical steam or supercritical CO_2[14] and combined cycles thereof (Rankine-Brayton) [4].

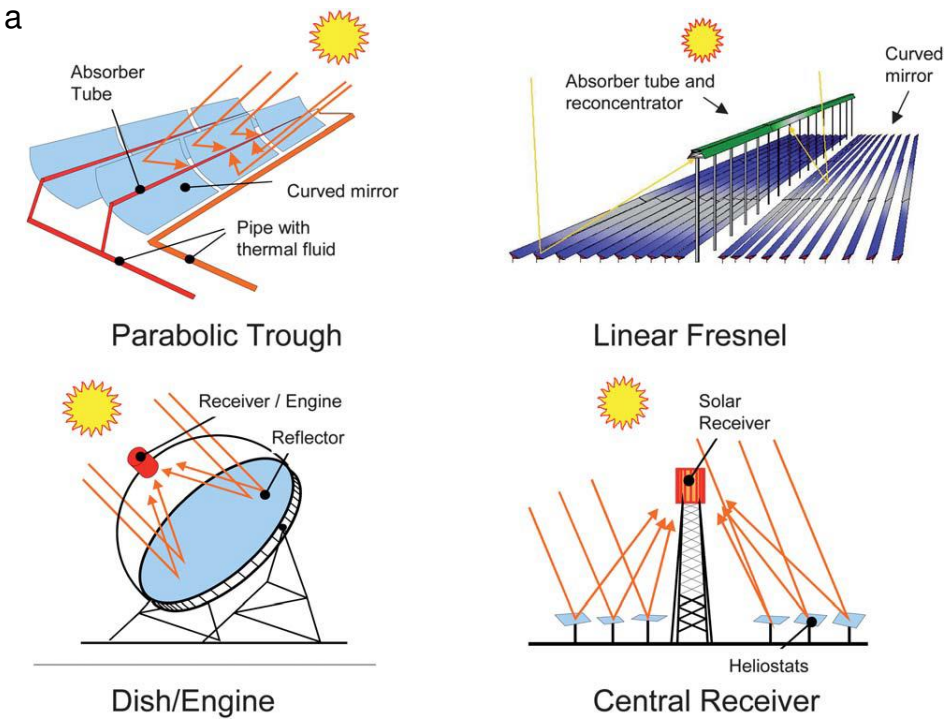

Figure 2. (a) CSP optical concentrator configurations. Reproduced from Ref. 5 with permission of The Royal Society of Chemistry. (b) Image on the solar field and the tower built in IMDEA Energy facilities at Móstoles (Madrid, Spain) within the framework of the project SUN-to-LIQUID.[15]

The great advantage of central receivers is that enables generation of temperatures up to 1000 ºC, which is higher than for parabolic troughs [6]. High temperatures are sought since they can boost the efficiency of the thermodynamic cycles, [5] however they lead to new challenges in terms of cost-effective materials and components development. In light of this, new receiver concepts are under research in order to obtain high temperatures at CSP tower plants. Namely, temperatures higher than 1000 ºC could be achieved utilizing volumetric air receivers. In such configurations, sun radiation is gradually absorbed inside an adequate porous material [16]. Ambient air enters in the absorber at the front, just where sun radiation is impinging. This makes that the outer part of the receiver is at lower temperatures diminishing radiation loses. On the other hand, in tube receivers the outer wall is heated by sun radiation and then heat is transferred from the wall to the HTF, implying higher radiation losses [16]. More information about volumetric receiver technology can be found in the review by Ávila-Marín[17]. Although high temperatures (~1000 ºC) can be reached with CSP tower plants coupled with volumetric air receivers, such technology has not been implemented commercially yet. To date the only plant operating with volumetric air receiver is the Solar Power Tower Jülich, located in Germany. This experimental facility heats atmospheric air at about 700 ºC, which is then used to produce steam in a heat exchanger that drives the turbine generating 1.5 MW of electricity [18]. The Jülich plant has a honeycomb-like sensible heat storage system made of alumina ceramic bricks [18].

Through this section, the principal components present in a CSP plant have been briefly described as to provide the reader with a general vision of such technology, with special emphasis in advances that will enable enhancing the temperature produced from concentrating solar radiation. Thermal energy storage (TES), which is one of the four main components in CSP plants

providing continuity to the process, will be discussed in more detail in the next sections, since it is the topic in which the present review is focused on.

1.2. Thermal energy storage

As commented above, a unique feature of CSP lies in its capability to incorporate thermal energy storage (TES) at large-scale, which leads to increase renewable electricity dispatchability and provide electricity on-demand [4–6]. As illustrated in Fig. 3, there is a mismatch between the electricity demand and solar electricity production since energy needs usually do not correspond to the solar resource availability. For instance, peak energy demand may occur in the evening, whereas peak solar power generation takes place at solar noon. The working principle is to collect solar energy in excess and store the fraction that is not used for immediate electricity generation, stage named charging, and to release it during the periods where the solar resource is not sufficient to produce electricity (night or during cloudy periods), stage known as discharging. CSP plants working with TES will require a larger solar field [19], which implies higher investment, but electricity production will be much higher (round-the-clock); hence, incorporation of storage system will increase its solar-to-electricity efficiency and decrease the annual LCOE [19].

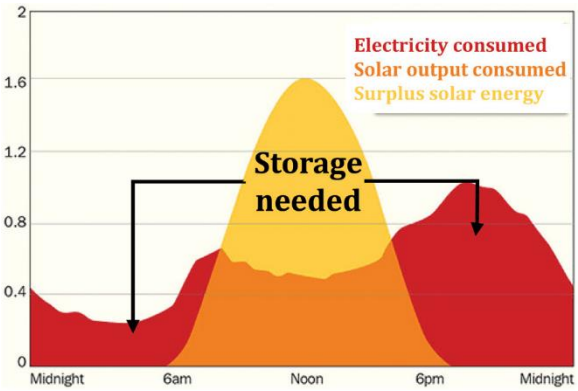

Figure 3. Daily electricity household demand (measured in kW) in Melbourne (Australia) versus solar production. Reproduced with permission from Ref. [20] with permission of The Royal Society of Chemistry.

TES is normally classified into sensible, latent and thermochemical heat storage according to the physico-chemical mechanisms involved. Sensible heat storage (SHS) systems store energy by temperature changes experienced by the storage medium, which can be either a liquid or a solid material. Latent heat storage (LHS) makes use of the latent heat involved in a phase change, being the most common case solid-liquid transitions. Thermochemical heat storage (TCS) is based on reversible chemical reactions. Charging and discharging steps are conducted by carrying out an endothermic and exothermic reaction, respectively.

Energy densities of even the most promising TES systems are remarkably lower than electrochemical storage devices such Li batteries (210 Wh kg^{-1})[21] and, this constitutes one important technical constraint of storage systems for next generation CSP with regards to future PV plants. Therefore, low cost systems with high-energy storage density and stability are sought, so as to reduce the expenses of CSP plants deployment. According to Zhang et al., the thermal energy storage sub-system represents around 18% of the total investment of a central receiver solar power plant[22]; consequently, TES cost reduction will positively impact on minimizing the levelized cost of energy (LCOE). This parameter is normally used to compare different technologies for power generation, and is calculated as the expected lifetime costs divided by the lifetime expected power output (kWh) of a particular system [22]. Besides storage capacity and costs, the temperature range at which the TES system will operate is also of high importance, since TES media must be stable at temperatures compatible with the working conditions of the other parts of the CSP plants (receiver, HTF and heat engine) [4].

Exergy efficiency (η_{ex}) of TES systems allows characterizing the thermal performance of the TES system, and it is defined as,

$$\eta_{ex} = \frac{Q_{out}\left(1 - \frac{T_c}{T_{out}}\right)}{Q_{in}\left(1 - \frac{T_c}{T_{in}}\right)} \quad (1)$$

where Q_{out} and Q_{in} are the heat recovered from and supplied to the TES system, respectively, and T_{out} and T_{in} are the temperatures at which discharge and charge take place. T_C is the minimum working temperature of the TES system [4]. Exergy efficiency mainly depends on the ratio between the released and stored heat and the difference between HTF temperatures in the TES charge stage [4]. Heat losses in TES components (i.e. thermal storage tanks) and inefficient heat exchangers lead to reduction in the exergy efficiency. In particular, TCS systems would be especially penalized if chemical reactions for heat storage and release proceed at different temperature range[4]. According to Eq. (1), maximum exergy efficiency is achieved by reducing heat losses and using temperatures at which heat is stored and released are as much similar as possible.

Optimum operation of TES system requires that both the storing medium and the conceptual design of the system meet a series of desirable characteristics [4,23,24]. Regardless the TES application, appropriate materials for thermal storage in future CSP plants ideally should have the characteristics summarized in Table 1.[4,19] In addition, reference parameters for solar salts, which is the technology currently in use in CSP plants, are also provided as a reference. However, taking into consideration that the development of these technologies is in progress, the lack of experience of these systems under realistic conditions is still significant and, accordingly, the values collected in this table should be considered only as a rough guide.

Table 1. Current and expected properties of TES materials for commercial applications in CSP

Property	***Relevance***	***Reasons***	***Current values: Solar salts***	***Targeted values***
Energy storage density	*Critical*	*As high as possible to reduce the required weight/volume of the system and, accordingly, material requirement*	*144 kWh.m^{-3} or 304 kJ.kg^{-1} (ΔT=200ºC)*[25]	*>300 kWh.m^{-3} or >1000 kJ.kg^{-1} as*
Cycling and thermal/chemical stability	*Critical*	*Elevated stability of the material delays its replacement and reduces maintenance costs.*	*30,000 hours tested for solar salts*[19]*, expected >30 years*	*Several years of continuous operation (> 1000 cycles) without significant degradation of performance.*
Operation temperature	*Critical*	*Increasing operation temperature improves the efficiency up to certain limit established by radiative heat losses*	*< 565 ºC*	*1500 ºC (directly irradiated) >T>700 ºC for the charge stage.* *Limited hysteresis: ΔT between charge and discharge*

				as low as possible
Thermal conductivity	*High*	*Necessary to facilitate an adequate heat transfer between the material and the HTF, especially for systems with rapid energy interchange (high power). Adequate chemical compatibility with the HTF, for configurations where it gets into direct contact with storage system is necessary.*	*λ= 0.5 W. $m^{-1}.K^{-1}$* [19]	*Significantly higher than thermal insulators: λ>1 W. $m^{-1}.K^{-1}$*
Kinetics of charging/discharging processes:	*High*	*Depends on the specific plant configuration, which establish the duration of the cycles*	*Minutes*	*In the range of minutes (<30min) for complete conversion. Higher rates may be needed for quick responses*
Mechanical properties	*High*	*Adequate to ensure physical integrity of the material in the*		

		long term. Low thermal stresses, limited volume change and, in the case of fluidized beds, resistance to attrition are desirable		
Toxicity, flammability and corrosion	*High/Medium*	*As low as possible to facilitate handling and operation of the plant, and, eventually, safe disposal. Experience in chemical industry may facilitate the use of dangerous chemicals if necessary, but this can increment operation cost.*	*Low toxicity*	
Cost	*Critical*	*Inexpensive and abundant materials to facilitate economic viability and to guarantee a steady supply*	*20-33 $/kWh* [25]	*< 25 $ MJ^{-1} (90 $\$.kWh^{-1}$) (2017)* [26] *4.2$ MJ^{-1} (15 $\$.kWh^{-1}$) DOE (2020)*[27]

In addition to the materials considerations, the selection of a TES system should be also address, such as its integration in the plant [19]. To date only SHS has reached commercial implementation, being the most mature technology. For instance, Torresol's Gemasolar plant located in Seville, Spain, has a 15 h storage capacity based on a two-tank molten salt SHS system [19]. On the other hand, TCS presents lower degree of development, and, despite its potential advantages, in most cases research in TCS is still at lab-scale[4], although larger facilities are currently under study.

These facts summarize briefly the advantages of TES implementation in CSP plants. In the next subsections, each type of TES will be briefly described.

1.2.1. Sensible heat storage

Stored sensible heat (Q) depends on temperature changes (ΔT) in the storage medium, which can be either a liquid or a solid, according to the expression:

$$Q = V \rho C_P \Delta T \tag{2}$$

With V, ρ and C_p, the volume, density and specific heat capacity of the material (Eq.2), respectively [19,23,28].

A plethora of solid and liquid compounds is available for SHS [4,19,28]. Selected materials with their thermal properties and working temperatures can be found in the reviews by Weinstein et al. [4] and Kuravi et al. [19]. Most commonly used liquids are water, oils (mineral, synthetic, silicone) and molten salts (mixture of nitrates like Solar Salt, $NaNO_3$–KNO_3, and nitrides and nitrates such commercial Hitec, $NaNO_3$–$NaNO_2$–KNO_3)[4]. Molten salts mixtures allow for achieving very-high storage temperatures and therefore are the preferred option for concentrating solar power plants. However, they present drawbacks related with minimum working temperature,

which is constraint by salt freezing, and corrosion[29]. Nitrate solar salt mixtures are currently used in commercial CSP and are able to operate up to approx. 600 ºC, since their decomposition and the subsequent buildup of important vapor pressure occur at higher temperatures. A summary of the main properties of this system can be found in Table 1. Research on CSP plants with improved efficiency is driven investigation on other salts based on carbonates and chlorides as well as pure sodium or potassium nitrates[30]. The aim is developing storage media able to delivered and stored heat at temperatures required by advanced power cycles like supercritical steam Rankine, supercritical CO_2 or air Brayton cycles. In this regard, chloride and carbonate salt mixtures and pure sodium nitrate and potassium salts are also promising candidates mainly due to good thermo-physical properties (high energy density) for carbonates and relatively low cost for chlorides; molten chloride- and carbonate-based salts stables up to 800 ºC have been reported [4,19,29]. Furthermore, the onset of decomposition of a eutectic ternary mixture of Na, K, Li carbonates in CO_2 was observed to be above 1,000 ºC [31]. In supercritical CO_2 Brayton cycles, expected cold temperature of salts is 420 ºC, which is higher than melting point of pure Na or K nitrate salts and then it allows their use in this thermodynamic cycle. Corrosion by chloride salt mixtures is a crucial issue and important efforts are focusing on understanding the mechanisms and analyzing several mitigation strategies (adding corrosion inhibitor, use of alumina-forming Ni-based alloys, alloying with refractory elements (W/Co), coatings, and cathodic protection)[32,33].

Two-tanks, thermocline and steam accumulators are the main thermal storage configurations currently used in commercial CSP. This arrangement is an active-type thermal storage, in which the storage medium circulates between a cold tank and a hot one through one or two heat exchangers. The first heat exchanger allows for transferring the heat from the storage medium to the power block. The second heat exchanger is required in indirect-type thermal

storage, for which the heat transfer fluid circulating in the solar collectors is also the thermal storage carrier. Single-tank or thermocline can be designed as active and passive-types. Passive systems normally consisted of packed bed made of concrete, rocks or sand, which are the heat storage medium [19,23]. Optimum performance of thermocline systems lies in thermal stratification, which is obtained with an appropriate distribution of the heat transfer fluid passing through the storage tank.

Besides concrete other inexpensive solids used as SHS medium are sand or gravel with working temperatures between 200 and 400 ºC [4]. For higher temperatures ceramic bricks, such as those made of magnesia or alumina have been proposed [4] and recently Becattini et al. cycled Alpine rocks up to 600 ºC [34]. In addition, Calvet et al. have suggested the use of ceramic material made from industrial treatment of asbestos wastes (Cofalit®) as high temperature TES system (up to 1100 ºC) [35]. A detailed review that covers other solid wastes such by-products of steel manufacturing tested for sensible heat storage can be found in the work of Gutiérrez et al.[36]

In summary, sensible heat storage is currently considered a mature technology installed in commercial concentrating solar power plants. SH-TES usually makes use of inexpensive materials and presents low energy storage densities (typically in the order of ~150 kJ kg^{-1} per 100 ºC), which implies large storage volumes and good insulation in order to avoid large heat losses in long-term [37,38].

1.2.2. Latent heat storage

Latent heat storage (LHS) makes use of the heat involved in phase changes, mainly solid-liquid phase transitions. The heat stored is given by the mass of storage material (m) and latent heat related to the phase change, Δh_m (Eq. 3).

$$Q = m\Delta h_m \quad (3)$$

Materials used for LHS are known as *phase change materials* (PCM). Lists of relevant PCM utilized for CSP heat storage and their thermal properties can be found in Weinstein et al [4], Gil et al. [23], Nomura et al. [39] and Khare et al. [40], being the last two focused on high temperature applications. Available PCMs for CSP cover a broad range of temperatures, viz. 250 – 800 ºC [4] and comprise metals (Zn, Al), metal alloys (Mg-Zn), salts (alkali nitrates, hydroxides or chlorides) or salt mixtures (KNO_3-KCl) [4]. Organic compounds have been also proposed but in general there are used in low- and mid-temperature applications due to their low melting temperature (< 250 ºC) [23]. Among the aforementioned inorganic materials, metals present better thermal properties and higher latent heat values, but they are more expensive than salts [4]. The energy storage density range is quite broad, varying from 74 kJ kg^{-1} of KNO_3−KCl (95.5−4.5) salt mixture to 498 kJ kg^{-1} of Al−Si (88−12) alloy or 530 kJ kg^{-1} of $LiNaCO_3$−C (90−10) composite.[4] However, some of these compounds such hydroxides or chlorides are corrosive and they require the use of more costly special containers

Commercial PCMs are usually characterized by low thermal conductivities (around 1 W m^{-1} K^{-1}); consequently, techniques to enhance heat transfer are sought[19]. For instance, by incorporating structures that maximize the surface available for heat transfer (i.e. fins, cylindrical tubes, plates, rods, etc.) [19], encapsulating PCMs or inserting them in a matrix; or even dispersing high-thermal conductivity materials in PCMs.[41–43]

Compared to SHS, LHS presents higher energy density (which implies lower volume required) for most temperature intervals of practical interest and almost constant temperatures for charging and discharging. However, further advances in unraveling the complexity of the heat transfer processes involved in latent heat storage are necessary. Besides, the development of PCM

and encapsulated materials, with enhanced properties and reduced cost, can facilitate the implementation of other LHS systems at commercial scale

1.2.3. Thermochemical heat storage

Thermochemical heat storage (TCS) is based on storing chemical energy making use of reversible chemical reactions (Eq. 4). In the simplest case, a reactant A is transformed in the products B and C in an endothermic reaction during the charging step[44]. B and C compounds are normally stored separately. Discharge then accounts for the reversible process, in which B and C are recombined releasing thermal energy.

$$A + \Delta H_r \leftrightarrow B + C \tag{4}$$

Examples of this general process include gas-gas reactions, such ammonia dissociation, in which NH_3 gas (A) is split into N_2 (B) and H_2 (C) and gas-solid reaction, such as the decomposition of carbonates like $CaCO_3$ (A) into a solid oxide, CaO (B) and CO_2 (C). A detailed account of all these systems can be found in the following sections.

The stored heat (Q) is proportional to the molar reaction enthalpy (ΔH_r), the number of moles of one of the products (n_B) and the conversion achieved (X) according to:[4]

$$Q = X n_B \Delta H_r \tag{5}$$

Growing interest on TCS lies in their advantages compared to sensible and latent heat storage, namely higher energy storage densities, with no losses of thermochemical energy for long-term storage when kept away from the relevant reagents. In addition, higher flexibility is possible with this technology due to the plethora of reversible reactions that allows choosing the most adequate one for a targeted working temperature range at the solar receiver and power block. As a

counterpart, TCS systems are usually more complex because they require the management of heterogeneous chemical reactions and the handling of solids, which is more unwieldy than dealing with fluids.

The use of chemical reactions for thermal heat storage of solar energy was proposed in the mid-1970s. At that time, oil crisis fostered R&D activities in solar energy [5]. Several reactions were suggested and theoretically analyzed [45–52]. During the following years, the first experimental studies covering thermodynamics, reaction kinetics and reversibility assessments were reported [50,53–57] and the first prototypes were designed and installed [58–60]. On the following decades (1990s and 2000s) the interest on thermochemical heat storage decreased remarkably. Only the work carried out at the Australian National University (ANU) on ammonia-based TCS system has seen continuation from the mid-1970s until the present days [61]. In last decade TCS has experienced a revived and growing interest, which was boosted by the deployment of CSP plants and R&D initiatives aiming significant cost reduction of this technology [4,19,38,62]. Thus, only in US, six projects addressing as the use of reactions based on carbonates, hydrides, ammonia or mixed metal oxides started in 2014 within the CSP ELEMENTS program[63], funded by the SunShot Initiative of the U.S. Department of Energy (DOE) with an overall budget of 10 M$. The DOE SunShot Initiative aims at making solar energy cost-competitive with other technologies for electricity production.[63] CSP ELEMENTS program targeted to reach 15 $/kWh using TES able to operate at temperatures higher than 650 ºC. European Union (EU) has also supported R&D on TCS systems for CSP within its instruments for funding research in Europe like the Seventh Framework Program for Research and Technological Development. These EU-funded projects will be described in next sections.

According to the nature of the reactants and products, TCS is classified into gas-gas, gas-liquid or gas-solid reactions, being gas-gas and gas-solid processes the most commonly used. Steam methane reforming and ammonia dissociation are the most investigated gas-gas reactions [44]. On the other hand, gas-solid reactions are categorized depending on the composition of the solid reactant, being the most prominent those based on hydrides, hydroxides, carbonates and oxides [62]. All these types will be described in more detail on Section 2. At this point, it is worth mentioning the recent use of computational chemistry based on density functional theory (DFT) modeling in order to perform a systematic search of promising reversible reactions that allows identifying materials that have been scarcely (or have not been) explored for thermochemical storage applications such as sulfates.[64]

The type of reaction (or the nature of the reactants) has profound implications on the design of the reactor and the system integration. For instance, TCS based on gas-solid reactions can be also divided into *open* and *closed systems* [44]. In an open system, the reactant gas is not stored separately but released to the atmosphere. TCS based on redox reactions, where air is used as a reagent, usually fits on this category. On the other hand, TCS based on carbonates, hydrides and hydroxides are closed systems, since the gaseous product (CO_2, H_2 and H_2O) must be stored in a separate tank. In this respect, condensable gases such steam can be easily kept in simple reservoirs, while non-condensable gases require pressurized tanks. In contrast, evaporation of condensed vapors on demand need dedicated equipment, which can have an impact on the overall cost of the facilities. On the contrary, open systems present less complexity since gas storage can be avoided. However, this also implies that oxygen partial pressure is fixed at 0.21 atm (atmospheric air,) restraining redox reactivity. Furthermore, the reaction can also be affected by the quality of the gas (ambient air) and it might require elimination of critical impurities [44].

Regarding the reactor concept (cf. section 3.2.1), moving beds like fluidized beds, rotary kilns or screw extruders are the most common systems for gas-solid reactions[62] due to their flexibility in terms of heat and mass transfer, although solids can suffer attrition or erosion[22]. Additionally, reactors can be located on top of the solar tower and heated up by concentrated solar radiation. In this case, reactors are classified into directly or indirectly heated, depending on whether solar radiation is absorbed by the heat transfer fluid, or impinges on the external wall of reactor and then is transferred to the heat transfer fluid by conduction/convection. This classification is commonly used for solar receivers [65–69].

Wentworth and Chen established certain criteria for selecting the most suitable chemical reactions for thermochemical storage [46]:

- High reaction reversibility in both directions, without side reactions
- High reaction enthalpy (less storage volume required)
- Low degradation/deactivation of the reactants and catalysts
- Fast reaction rates and stable kinetics over prolonged cycling

Furthermore, reaction thermodynamics plays a crucial role in the selection of the most appropriate reaction, defining the working temperatures and the enthalpy of reaction. The enthalpy of reaction is commonly used as the figure of merit in TCS since it establishes the amount of energy that is exchange. However, it should be taken into account that TCS systems can additionally store thermal energy as sensible heat. Preliminary thermodynamic analyses are required for determining the suitability of a reversible reaction given a specific power block cycle. For instance, a TCS system with the exothermic reaction occurring at a discharging temperature ca. 1000 ºC is not adequate for implementation in a Rankine but in an Air Brayton cycle. Additionally, it is desirable that the difference between charging and discharging temperatures is

as narrow as possible since, as mentioned before, it will imply higher exergy efficiency. Pressure has also high operational and technical implications. Some gas-gas or gas-solid reactions might involve gas storage at high pressure. For example, the ammonia-based TCS requires pressurized reservoirs at 100-300 bar. Thus, this system necessitates high-pressure components with the subsequent parasitic energy losses and the corresponding economic implications and safety concerns.

Besides thermodynamic considerations, TCS requires proper evaluation of critical parameters such as reaction kinetics, long-term cyclability (total conversion reached in each step over several cycles) and materials degradation in the case of solid reagents. Here we would like to emphasize the importance of cyclability as key parameter to identify the feasibility of a TCS system, since thermochemical materials and processes are meant to last long periods in a CSP plant. The use of reversible chemical reactions in a cyclic way implies a careful monitoring of the cycle-to-cycle stability and a complete understanding of the physicochemical changes that can take place at the high temperatures at which thermochemical reactions take place. Especially for the case of reactions involving solids, these materials can suffer morphological degradations or microstructural transformations over cycling that could affect to the total storage capacity of given TCS material. Processes like particle sintering or agglomeration can pose physical hurdles to the gas-solid contact interphases that might result in slower reactions and eventually loss of the chemical activity after prolonged cycling. Formation of additional solid phases, such as oxide segregation in multi-cationic compounds that do not actively participate in the storage/release of heat can have a detrimental effect, lowering the total energy storage density of a TCS system. Thus, cyclability is one of the main aspects to take into account when evaluating the potential of TCS systems and, therefore, research has been focused on developing materials with long-term

stability under such severe high-temperature operational conditions. The ability to withstand numerous charge/discharge cycles and the engineer approaches utilized to improve long-term materials durability will be thoroughly discussed along the present review.

Additionally, design of efficient reactors is as relevant as materials development. The nature, physicochemical properties and working temperatures of the reagents are decisive factors for the selection of the optimum reactor configuration. The different setups selected for each TCS type will be described in the corresponding section. Furthermore, research and development activities also focus on the study of the most effective way of TCS system integration in the CSP plant. These three main areas, which reveal the fascinating multiscale nature of TCS research, are closely interrelated and a detailed evaluation of all of them is required for further advance of this technology.

Fig. 4 summarizes the main advantages and disadvantages of each TES type. After this brief overview of the three main thermal energy storage concepts for CSP plants, the next section will cover in more detail the most prominent thermochemical heat storage systems that have been explored so far for such application.

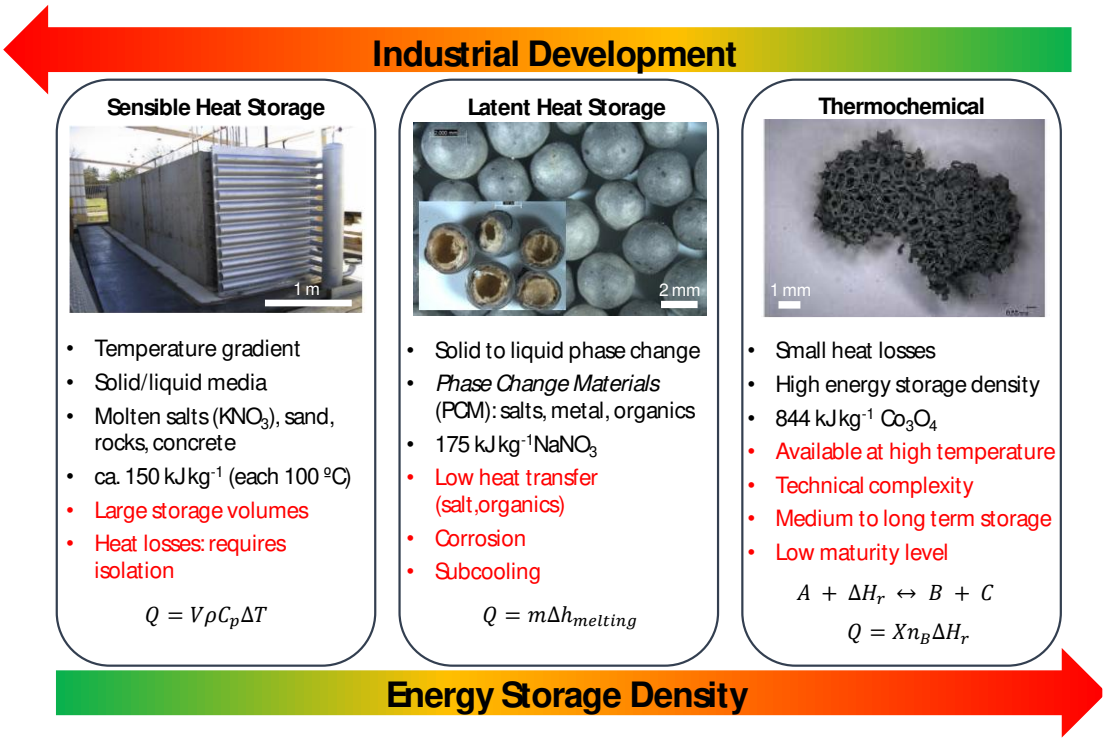

Figure 4. Schematic representing the advantages and disadvantages of the three main thermal energy storage systems. From left to right images represent a sensible heat storage concrete module (source Ref [70]), encapsulated phase change material (source Ref [71]) and Co_3O_4-based foam for redox-based thermochemical heat storage. Reprinted from Solar Energy, 114, Christos Agrafiotis,Stefania Tescari,Martin Roeb,Martin Schmücker,Christian Sattler, Exploitation of thermochemical cycles based on solid oxide redox systems for thermochemical storage of solar heat. Part 3: Cobalt oxide monolithic porous structures as integrated thermochemical reactors/heat exchangers, 459-475, Copyright (2015), with permission from Elsevier.

2. Thermochemical heat storage systems

2.1. Ammonia-based heat storage

The ammonia-based concept was proposed in the mid-1970s by Carden and has been developed for 40 years, especially at the Australian National University (ANU) [61]. It is surely the most investigated thermochemical heat storage concept [44]. This section only addresses the most important aspects of this technology. A more detailed description is provided by Dunn et al. [61].

Ammonia thermochemical storage makes use of the dissociation of this molecule into hydrogen and nitrogen for storing solar heat (Eq.6), which presents an enthalpy of reaction of 66.8 kJ mol^{-1} at 20MPa and 300 K.

$$2NH_3(g) \leftrightarrow N_2(g) + 3H_2(g) \qquad \Delta H_r = 66.8\ kJ\ mol^{-1}\ (3.9\ MJ\ kg^{-1}) \tag{6}$$

The endothermic step, through which solar energy is stored in the chemical bonds of the gaseous products, occurs at around 700 ºC. When H_2 and N_2 gases recombine (ammonia synthesis), the stored heat is released. The discharge step usually takes place between 350 and 550 ºC. Each reaction is conducted in a different reactor (endo and exo) and both steps require the use of catalysts disposed in packed beds[66]. Several commercial metal-based catalysts (Ni, Co, Fe, normally supported in Al_2O_3) have been tested for both reactions [61].

Gaseous products and ammonia pass alternatively from the endothermic to the exothermic reactor, pumped by large compressor units. Heat exchangers are placed between the reactors and the separation and storage units [66], as observed in Fig. 5.

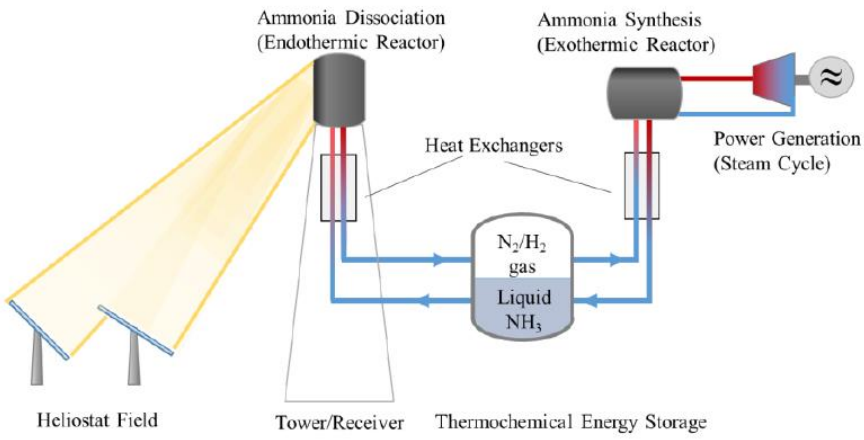

Figure 5. Schematic of the ammonia-based heat storage system. Reprinted from Solar Energy, 155, Chen Chen, Hamarz Aryafar, Keith M. Lovegrove, Adrienne S. Lavine, Modeling of ammonia synthesis to produce supercritical steam for solar thermochemical energy storage, Copyrigh (2017).

Ammonia-based thermochemical heat storage in concentrating solar processes has been traditionally developed using parabolic dishes. Researchers at ANU developed a 10-kW_{chem} synthesis reactor, achieving a closed loop 24-h storage and release of solar heat based on the ammonia dissociation reaction [61]. The dish collector prototype was further up-scaled from a 20 m^2 to a 489 m^2 area of aperture [61].

Lately, a project led by researchers from University of California, Los Angeles (UCLA) within DOE SunShot Initiative CSP-ELEMENTS program targeted improving this system [72,73]. Chen and co-workers have recently evaluated the use of the ammonia dissociation reaction for heat storage coupled with supercritical steam as HTF, by both experimental and modelling studies.[74] Experiments were performed using a concentric-tube packed-bed reactor in which the thermochemical reversible reaction is carried out in the outer side, whereas the steam flows in the inner side. For the ammonia synthesis, authors used a porous bed of iron-based catalyst. Chen et

al. demonstrated that with such reaction it was possible to heat up steam in the 350-650 °C temperature range, ascribing the main system limitations to heat transfer. Further parametric studies, evaluating dimensions, flow rates and temperatures revealed the positive influence on reducing the reactor diameter on enhancing the heat transfer [75].

This technology presents several advantages. First, the ammonia synthesis is a well-known industrial process (Haber-Bosch) developed at commercial scale in 1910. In addition, no side reactions are expected, which eases the system development. On the other hand, high operational pressures (100-300 bar [61]) may add economic limitations and operational complexity if compared with other systems [44], although so far none TCS system has reached the level of maturity of the ammonia-based one.

Finally, it should be mentioned that an alternative ammonia-based TCS was proposed in the mid-1970s and uses the decomposition of ammonium hydrogen sulfate (Eq. 7) [45–47]. This process presents a high energy storage density [62], but it involves several steps, liquid and gas reagents and did not overpass the conceptual scale [50,55].

$$NH_4HSO_4(l) \leftrightarrow NH_3(g) + H_2O(g) + SO_3(g) \quad \Delta H_r = 336\ kJ\ mol^{-1} \tag{7}$$

2.2. Hydrocarbon-based heat storage

Methane reforming was proposed for thermochemical heat storage in the mid-1970s [47]. Such reaction can be performed with either steam (Eq. 8) or CO_2 (Eq. 9) resulting in both cases in H_2 and CO (syn-gas), reason why these reactions are currently used for industrial hydrogen production [62].

$$CH_4(g) + H_2O(g) \leftrightarrow 3H_2(g) + CO(g) \quad \Delta H_r = 250\ kJ\ mol^{-1} \tag{8}$$

$$CH_4(g) + CO_2(g) \leftrightarrow 2H_2(g) + 2CO(g) \quad \Delta H_r = 247\ kJ\ mol^{-1} \tag{9}$$

In the late-1980s researchers from the Weizmann Institute of Science (Israel) tested TCS based on the reforming with CO_2 (Eq. 9) on a tubular receiver/reactor filled with Rh/Al_2O_3 catalyst. Such experimental work was carried out with a 20 kW solar furnace [60]. Years later they tested the system on a closed-loop configuration over 60 cycles [76].

The main drawback of these processes for further implementation, if compared with other systems such as the ammonia-based, is the presence of side reactions. For steam methane reforming, there is the Water Gas Shift (WGS) reaction, which consumes CO and increase the proportion of H_2. Temperatures for the endothermic reaction are about 1000 ºC for the two reversible reactions [62]. Additionally, the use of catalyst is needed. Noble metal catalysts showed good performances, but their prices can be prohibitive for large scale applications [38]. Additional drawbacks are related with H_2 and CO storage, due to the flammability of these gases and also to the toxicity of CO, methane price and low reversibility attained in the reactions [62].

The use of dry reforming of methane (Eq.9) and ammonia was recently assessed by Peng et al., in which, to the best of our knowledge, is the first techno-economic evaluation of TCS systems incorporated into a CSP plant [20]. In such study, authors evaluated two gas storage options, pressurized vessel or underground, which they found to be the costliest component of such gas-gas TCS options. [20] This relevant study will surely pave the route of such type of assessment to other promising TCS systems.

Cyclohexane dehydrogenation (Eq. 10) was also proposed as TCS system in the early-1980s [77]. The endothermic step is the formation of benzene and hydrogen and it takes place at temperatures close to 300 ºC [62,77]. Similar to the previous reactions, C_6H_{12} dehydrogenation is a commercial process, with years of industrial experience. Nevertheless, it exhibits problems of

reversibility, possible secondary reactions, toxicity (benzene), hydrogen storage and requires the use of catalysts [62]. In summary, it is a process of difficult implementation in CSP plants.

$$C_6H_{12}(l) \leftrightarrow C_6H_6(l) + 3H_2(g) \qquad \Delta H_r = 207\ kJ\ mol^{-1} \tag{10}$$

2.3. Sulfur-based heat storage

In the late 1970's, Chubb and co-workers proposed the use of the catalytic dissociation of SO_3 (Eq.11) as a possible route for thermochemical heat storage.

$$2SO_3(g) \leftrightarrow 2SO_2(g) + O_2(g) \quad \Delta H_r = 98\ kJ\ mol^{-1} \tag{11}$$

The system worked in a temperature range between 500 ºC and 1000 ºC. A helix type receiver/reactor was developed to test it, working as countercurrent heat exchanger which contained the catalyst [51,52,58]. However, after those initial developments, this technology did not gather further attention.

The sulfur-based heat storage concept is a three-step process, rather than a two-step reversible reaction, recently developed by the American company General Atomics in collaboration with the German Aerospace Center (DLR). The project, which was funded by the DOE, finished on November 2014 [78], and has seen continuation under the Pegasus Project[79]. The three steps involved in the overall process are as follows:

$$H_2SO_4(aq) \rightarrow H_2O(g) + 0.5O_2(g) + SO_2(g) \tag{12}$$

$$2H_2O(l) + 3SO_2(g) \rightarrow 2H_2SO_4(aq) + S(l) \tag{13}$$

$$S(g,l) + O_2(g) \rightarrow SO_2(g) \tag{14}$$

The first step is the solar-driven sulfuric acid decomposition (Eq. 12). Here sulfuric acid decomposes in water and SO_3 and then this product is transformed into SO_2 and O_2. The first

reaction occurs at ~500 ºC, while the second takes place between 650 and 900 ºC [78]. Sulfuric acid dissociation requires the use of efficient catalysts for reaching stable conversions (e.g. Fe-Cr based catalysts) [78]. The second step is the recovery of sulfuric acid and the formation of sulfur (Eq. 13). This is the low-temperature step, taking place at around 150 ºC. Finally, sulfur combustion proceeds at temperatures ca. 1200 ºC (Eq.14), releasing the heat that was stored in its chemical bonds through the first two steps. One of the interesting features of this technology is that the exothermic step (discharge) that liberates the heat occurs at 1200 ºC, whereas it was stored at about 900 ºC, when in traditional gas-solid TCS systems the heat release occurs normally at lower temperatures than the charging step as it will be shown on the following sections. The energy storage density of the sulfur-based system is ca. 9 MJ kg^{-1}_{Sulfur} [78], which is one of the great advantages of this technology if compared with any other TES process.

However, as it can be observed in the flowsheet plotted in Fig. 6, this three-step thermochemical cycle is more complex than two-step cycles proposed for TES, requiring the implementation of additional components. Furthermore, sulfur-containing chemical used in this process are highly corrosive, implying higher cost for its storage and operation. In summary, sulfur-based heat storage exhibits an outstanding energy storage density; however, up-scaling presents further technological challenges due to the great number of steps required and the complexity of the equipment involved in the overall process.

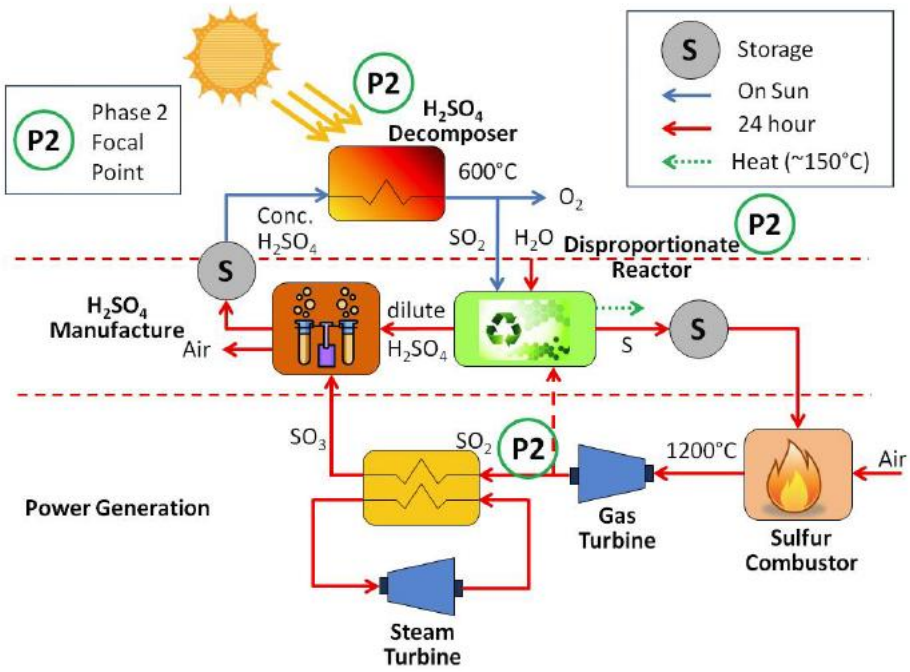

Figure 6. Flowsheet of sulfur-based heat storage system. Source Ref [78].

2.4. Hydrides-based heat storage

Metal hydrides are another class of promising materials for TCS applications. In this case, solar energy is utilized in the dehydrogenation of a metal hydride (MH), resulting in the formation of gaseous H_2 and the solid metal (Eq. 15). Then, when energy is required, the backward reaction is conducted, releasing the heat that was stored in the chemical bonds of the reaction products. These reactions have been studied over decades for hydrogen storage applications [80]:

$$MH(s) + \Delta H_r \leftrightarrow M(s) + 1/2H_2(g) \quad (15)$$

The main advantage of metal hydride-based TCS is the outstanding energy storage density that these materials present. Table 2 collects the most prominent metal hydrides proposed for TCS implemented in CSP plants. For instance, a TES system based on molten salts has an energy

storage density of about 150 kJ kg^{-1} per each 100 ºC of temperature change, whereas for a TCS system based on MgH_2 is 2811 kJ kg^{-1} (and for other hydrides is even higher) [81].

Table 2. Metal hydrides candidates for TCS [81].

Reaction	Temperature (ºC)	Energy storage density (kJ kg^{-1} hydride)
$Mg_2NiH_4 \leftrightarrow Mg_2Ni_3 + 2H_2$	250-400	1158
$MgH_2 \leftrightarrow Mg + H_2$	300-400	2811
$Mg_2FeH_6 \leftrightarrow 2Mg + Fe + 3H_2$	350-550	2096
$NaMgH_3 \leftrightarrow NaH + Mg + H_2$	430-585	1721
$NaMgH_2F \leftrightarrow NaH + Mg + H_2$	510–605	1416
$TiH_{1.7} \leftrightarrow Ti + 0.85H_2$	700-1000	2842
$CaH_2 \leftrightarrow Ca + H_2$	>1000	4934
$LiH \leftrightarrow Li + 0.5H_2$	>850	8397

Progress on research in metal hydrides for TCS applications was recently reviewed by Harries et al. [80]. Besides high energy storage density, another advantage of these materials is the maturity reached in small scale applications for vehicle, where hydrogen storage devices have been developed to manage waste heat on board [80]. This niche is obviously very different from CSP requirements but such systems can provide valuable information about the behavior of hydrides in more realistic conditions. On the other hand, one of the main disadvantages of metal hydride systems is the need of a hydrogen storage sub-system (Fig. 7), since H_2 is one of the products of the solar driven step. For that end, it has been suggested the use of a second metal/metal hydride pair that works on the same scheme as Eq. 15 but at lower temperatures [80], bringing the concept of a self-regulated system. The high-temperature metal-hydride decomposes in a metal and H_2 when a certain temperature is reached, hence, H_2 pressure increases and the gas moves to the low

temperature H_2 storage system, where it is absorbed. During the discharging process, the energy storage reactor is cooled down, thus, H_2 is no longer released with the subsequent decrease of H_2 pressure. In that moment, the hydrogen that is stored in the low-temperature sub-system moves back to the high-temperature reactor, driven by the pressure drop. This triggers the exothermic reaction releasing the heat that was stored in the solar driven step [80].

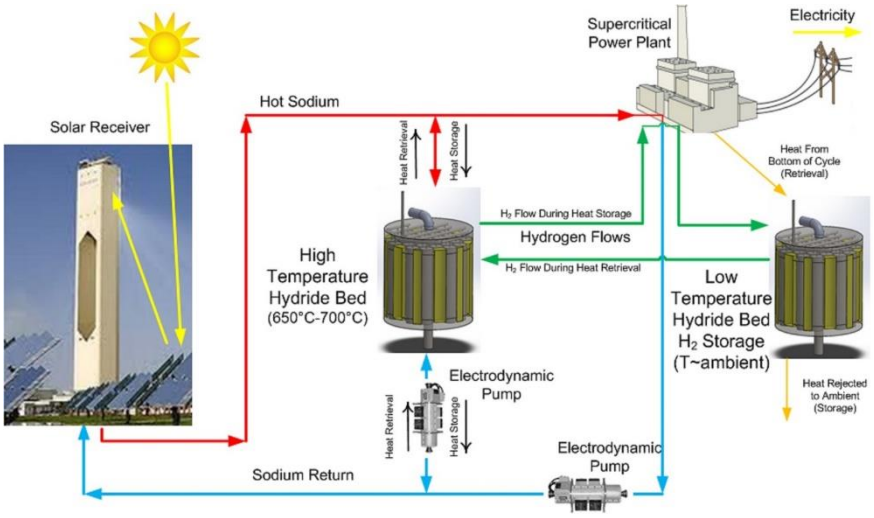

Figure 7. Layout of a CSP plant working with metal hydride TCS as proposed by PNNL (source http://energy.gov/eere/sunshot).

Mg-based hydrides are the most studied for this application. Paskevicius et al. built a prototype to test these materials at gram-scale, using supercritical water as heat transfer fluid [82]. They observed problems during hydrogen uptake, which is slower that H_2 release, probably due to Mg powder compaction, which resulted in slower absorption kinetics [82]. Another drawback of metal hydrides is their low heat conductivity. For instance, MgH_2 presents a value of 1 W m^{-1} K^{-1}. An interesting approach to improve this property is to add graphite, as demonstrated by Chaise et al [83], who enhanced the thermal conductivity up to 8 W m^{-1} K^{-1} by adding 10% of expanded natural graphite. Rönnebro et al. applied the same approach to titanium hydride increasing its thermal conductivity from 10 to 20 W m^{-1} K^{-1} at 500 ºC [84].

Metal-Mg alloys have been also suggested for TCS. Some of them result in increased working temperatures but lower energy storage density as in the case of Mg_2FeH_6 (Table 2). Recently Urbanczyk et al. developed a heat storage unit consisting of a reactor with a 13-tube bundle, using molten salts as heat transfer fluid and Mg_2FeH_6 as TCS material (Fig.8), with a heat storing capacity of 1.5 kWh[85]. However, authors reported several technical issues with insulation and pumping that need to be solved to guarantee a higher process efficiency. [85]

Sheppard et al. [86] developed an alternative chemical modification of Metal-Mg alloys based on anion doping with F^-. A techno-economic study of several metal hydrides concluded that $NaMgH_2F$ (1416 kJ kg^{-1}) resulted in lower cost than for MgH_2 (2814 kJ kg^{-1}), due to higher operating temperature, despite the fact that the heat storage capacity was lower [86]. $NaMgH_2F$ releases H_2 at 545 ºC and 10 bar [87]. According to Sheppard et al., even though the anion-doping strategy results in lower energy storage densities, TES system costs decreases due to lower price and higher stability of metal fluorides and less H_2 needed to run the reaction, since H^- anions have been replaced by F^- (one F substitute one H per formula in $NaMgH_3$). This implies that less H_2 need to be stored, with the consequent cost reduction on the secondary H_2 storing unit. [87]

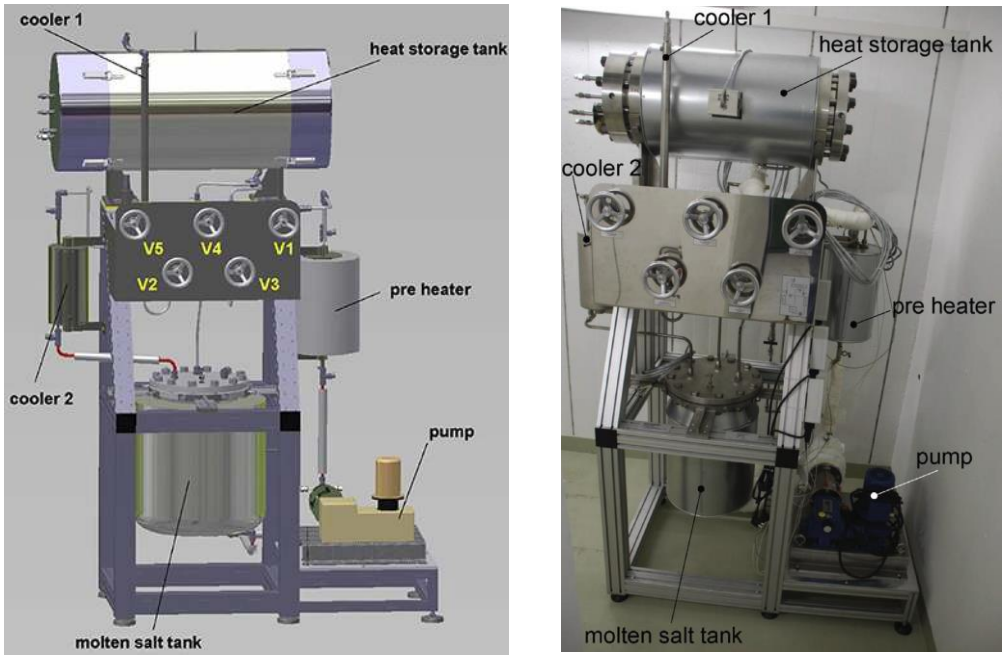

Figure 8. Schematic and picture of the unit developed by Urbanzcyk et al. for hydride-based thermochemical heat storage. Reprinted from International Journal of Hydrogen Energy, 42, R. Urbanczyk, K. Peinecke, S. Peil, M. Felderhoff, Development of a heat storage demonstration unit on the basis of Mg_2FeH_6 as heat storage material and molten salt as heat transfer media, 13818-13826, Copyright (2017), with permission from Elsevier.

Other promising hydrides for TES in CSP are $TiH_{1.7}$, CaH_2 and LiH because their higher working temperatures. TCS performance of Ti hydride is being evaluated in a project leaded by Pacific Northwest National Laboratory (PNNL), also funded by the CSP: ELEMENTS program. A detailed report on the research performed by the PNNL on this subject can be found in the work of Rönnebro et al. [84], which was performed in the frame of the ARPA-E HEATS DOE program. These authors built a prototype able to work during 60 cycles, between 635 and 645 ºC, with a titanium hydride-based TCS [84].

Li hydride exhibits an impressive energy storage density; however, such material has not been proposed for large-scale TCS in CSP plants. Harries et al. suggest that is due to the high

reactivity and safety concerns of LiH and Li, which makes more difficult to find suitable container materials [80]. Additionally, Li is less abundant (33rd element on the Earth Crust) than Ti (9th) or Ca (5th) and its growing demand for the battery sector can render LiH in a much costly option compared with CaH_2, since Ca is an abundant and inexpensive element. In fact, Ca hydride-based TCS has been tested at kg-scale for TCS by the Australian company EMC, which developed a TCS reactor with 50 kg of CaH_2, coupled to a Stirling engine [80]. $TiH_{1.7}$ can be also a costly option if compared with CaH_2 since Ti is a metal much difficult to obtain. Finally, it is worth mentioning that hydrides-based TCS systems of complex composition has also been applied to reutilized waste heat in vehicles at lower working temperatures (T<130 °C), using $LaNi_{4.85}Al_{0.15}$ and Hydralloy C5® ($Ti_{0.95}Zr_{0.05}Mn_{1.56}V_{0.46}Fe_{0.09}$) [88].

In summary, metal hydrides present remarkably high energy storage densities and the advantage of covering a broad window of temperatures (250-1000 °C) which makes these materials interesting candidates for any available concentrator configurations in the market. In addition, this technology has reached certain level of maturity with several demonstration storage units already commissioned. Besides, in other completely different context, the use of TCS based on metallic hydrides has been also proposed to increase the overall efficiency of electric vehicle provided with fuel cell[89]. However, the high pressures required to operate this technology and the need of a secondary unit for storage of the H_2 produced during the endothermic charge step may pose limitations to the development of this technology if compared with the other types describe in the following sections.

2.5. Hydroxides-based heat storage

Solar heat can also be stored by means of dehydration/hydration reactions of metal hydroxides (Eq. 16). In the solar-driven step, a metal hydroxide splits into a metal oxide and water (steam), which are stored separately. When heat is required, the metal oxide is hydrated with steam releasing the stored energy. Alkaline earth-based hydroxides have been the most studied for this application, namely $Mg(OH)_2$ and $Ca(OH)_2$ (Table 3). These two materials were firstly evaluated by Ervin[47], who studied the reversibility of these reactions over 500 and 200 cycles for Mg and Ca-based hydroxides respectively.

$$M(OH)_2(s) + \Delta H_r \leftrightarrow MO(s) + H_2O(g) \quad (16)$$

Mg hydroxide is an interesting candidate due to its low cost and high energy storage density (1340 kJ kg^{-1} [90]) but the charging temperatures of this system are low (T_{eq} = 350 ºC) for implementation in future CSP tower plants. Furthermore, hydration (discharging) stage is appreciably slower than dehydration and requires temperatures below 125 ºC. Nevertheless, this TCS system might be suitable for CSP plants working with parabolic troughs. In addition, it has been widely studied as a chemical heat pump for up-grading of waste heat of exhaust gases from combustion engines [91], which is another niche of application of thermochemical heat storage. Mg hydroxide decomposition is a complex process comprising several steps. However, it was proved that addition of exfoliated graphite or carbon nanotubes remarkably improved its reactivity by means of enhanced hydration reaction rate and higher dehydration/hydration conversion.[92] Mastronardo et al. also evaluated different synthesis methods for preparing the carbonaceous/hydroxide composites, finding that smaller particle size favored the dispersion of $Mg(OH)_2$ crystals over the exfoliated graphite, which in turn facilitated achieving higher dehydration/hydration conversions (84 and 79%, respectively) than for the $Mg(OH)_2$/MgO system

(52 and 50%).[93] Through the suggested fabrication route (Reverse Deposition-Precipitation), authors reported Mg-hydroxide hybrid materials with heat storage capacity of 1163 kJ per kg of $Mg(OH)_2$.[93] Additional modifications include the use of surfactants, *viz.* cetyl trimethyl ammonium bromide, resulting in hydroxide materials with enhanced volumetric energy density and multi-cycle stability.[94]

Shkatulov et al. utilized vermiculite (silicate-based clay) as an additive for improving $Mg(OH)_2$/MgO system behavior, observing that Mg-hydroxide/vermiculite composite exhibited a 50 ºC lower decomposition temperature with 540 kJ kg^{-1} heat storage capacity [90]. These authors also found a decrease on the dehydration temperature of 20 ºC by doping the $Mg(OH)_2$ with $NaNO_3$. Additionally, doping with sodium nitrate enhanced dehydration kinetics[95]. Other chlorides, sulfates, acetates and nitrates were examined for that end, finding that doping with $LiNO_3$ was beneficial for Mg hydroxide on reducing dehydration temperature, and exhibiting 1168 kJ kg^{-1} of heat storage density.

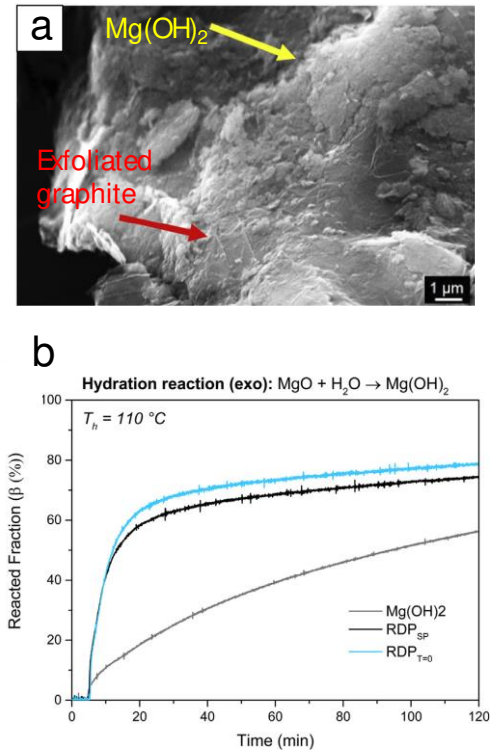

Figure 9. (a) SEM image of the hybrid material based on exfoliated graphite and $Mg(OH)_2$ prepared via Reverse Deposition-Precipitation. (b) Comparison of hydration conversion for hybrid and $Mg(OH)_2$ materials. Reprinted from Applied Thermal Engineering, 120, Emanuela Mastronardo,Lucio Bonaccorsi,Yukitaka Kato,Elpida Piperopoulos,Maurizio Lanza,Candida Milone, Strategies for the enhancement of heat storage materials performances for $MgO/H_2O/Mg(OH)_2$ thermochemical storage system, 626-634, Copyright (2017), with permission from Elsevier.

Ca hydroxide-based cycle works at higher temperatures than Mg-based one (400-600 ºC at pH_2O = 0.1-5 bar [44]) and also possesses a higher energy storage density (1406 kJ kg^{-1}) and lower price. Proposed in the mid-1970s as many others TCS systems [47,48,96], it has been widely studied and during the last years it has arisen high interest among the TCS scientific community. The German Aerospace Center (DLR) has been deeply involved in its research for TCS in CSP plants with projects such as the EU funded TCS Power (http://www.tcs-power.eu/). Years before Darkwa evaluated a heat storage system based on Ca-hydroxide for its application in vehicles [97]. Although

working temperatures are still low if compared with other high-temperature TCS options, such as $CaCO_3$ or CaH_2, $Ca(OH)_2$ can fit very well the operation conditions of parabolic trough CSP plants.

Ca hydroxide has been explored from different approaches, covering material development, reactor design and process modelling. One of the main drawbacks of this system concerns the poor mechanical stability of CaO due to the volume change during hydration/ dehydration cycles, which leads to fragmentation of the particles.[98,99] These characteristics might pose severe problems for different reactor configurations due to the formation of fines that eventually can cause pressure drops in fixed beds or material losses in fluidized systems. Several strategies for enhancing the mechanical properties of Ca-based materials while maintaining high degrees of conversion for both the hydration and dehydration reaction have been proposed. In this respect, molecular dynamics simulations have revealed that sintering of $Ca(OH)_2$ particles is determining the agglomeration of the material, and the rate of this process is slower for particles of larger diameter.[100] This study has also suggested that additives such SiO_2 can act as barrier preventing agglomeration of $CaO/Ca(OH)_2$ particles.

Criado et al. proved that $CaO/Na_2Si_3O_7$ composites exhibited superior crushing resistance due to the generation of a cementitious matrix of calcium-silicates[101], reporting a mechanism for the formation of such compound, as depicted in Fig.10a[102]. With such approach, fast hydration/dehydration rates were also achieved, favored by the porosity obtained (Fig. 10b) utilizing such fabrication route. However, although such composites presented 4 times higher crushing strength, low conversions were obtained for both reactions over 100 cycles, limiting this approach due to lower energy storage density[102]. Incorporation of Al as oxide [103] or silicate [99,104] was found to have a similar effect. Formation of Ca/Al oxides or Ca/Al silicates favored the resistance to fragmentation by increasing the crushing strength[103] and showing stable hydration

capacity over 200 cycles [104]. However, in both cases, the hydration/dehydration capacity decreased if compared with pure CaO [99,103,104].

A novel morphological modification consisting in semipermeable $Ca(OH)_2$ encapsulation was recently reported by Afflerbach et al. [105] The storage material was covered by a ceramic oxide-based capsule (Fig. 10c). These encapsulated materials exhibited about 8-fold increase in crushing strength if compared with pure $Ca(OH)_2$ granules, both before and after a 10 dehydration/hydration cycles, although hydration conversion values were still lowered if compared with pure $Ca(OH)_2$ granules (56 vs. 90%, respectively).

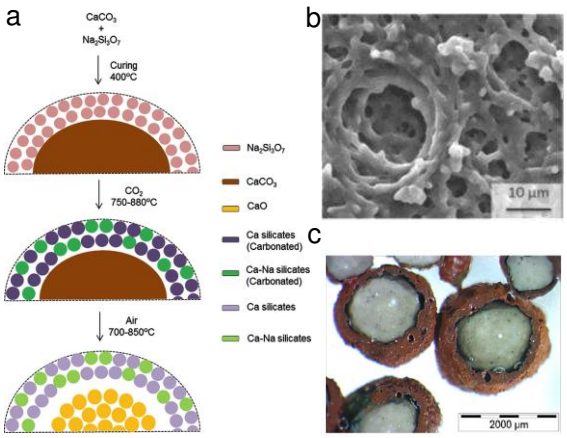

Figure 10. (a) Steps involved in the formation of Ca and Ca-Na silicates around CaO for enhancing the crushing strength of Ca-based composite materials. (b) SEM micrograph of a Ca-based composite materials after 40 hydration/ dehydration cycles (pure steam, 450 ºC-550 ºC, respectively). Both reprinted from Solar Energy, 135, Yolanda A. Criado,Mónica Alonso,J. Carlos Abanades, Enhancement of a CaO/$Ca(OH)_2$ based material for thermochemical energy storage, 800-809, Copyright (2016) with permission from Elsevier. (c) Encapsulated Ca oxide materials used for thermochemical heat storage. Reprinted from Solar Energy, 148, S. Afflerbach,M. Kappes,A. Gipperich,R. Trettin,W. Krumm, Semipermeable encapsulation of calcium hydroxide for thermochemical heat storage solutions, 1-11, Copyright (2017) with permission from Elsevier.

Roβkopf et al. identified problems of powder agglomeration and formation of flow channels in an indirectly-heated fixed bed reactor (Fig. 11a-b) that hampered the thermochemical cycling of $Ca(OH)_2$/CaO [106]. In order to solve this agglomeration problem they added a commercial

hydrophilic additive based on SiO_2 called Aerosil® that improved the bulk properties and, in turn, the cyclability [106]. Roßkopf et al. further tested Aerosil®-coated $Ca(OH)_2$ cycling behavior in a reactor (Fig. 11c-d), observing the formation of mixed Ca-Si by-products due to reaction between coating, water and CaO [107] that led to a capacity loss of the TCS reactor. On the other hand, dehydration/hydration reactions of $Ca(OH)_2$/CaO, without incorporation of any additives, were also analyzed via thermogravimetric analyses, demonstrating total reversibility over 100 cycles [108], which indicates the influence that the testing setup poses on the cyclability studies. Chemical modifications were suggested by Yan and Zhao who performed a first-principle numerical analysis of $Ca(OH)_2$/CaO doped with Li or Mg, finding that incorporation of Li resulted in a reduction on the working temperature [109], whereas heat storage efficiency for Mg-doped Ca-materials was maintained. They further analyzed the thermodynamics and kinetics of Li-doped $Ca(OH)_2$/CaO thermochemical cycle experimentally, finding that dehydration of Li-doped material followed a 2-step decomposition, fitted to a 1st-order model and a contracting surface model respectively [110]. In addition, Shkatulov et al. found that addition of KNO_3 also diminished the dehydration temperature by 40 ºC, presenting stability over 5 cycles. Although such results are promising, cyclability of these materials should be tested over prolonged periods [111].

Kinetics of pure $Ca(OH)_2$ dehydration was studied by Schaube et al., finding as well that dehydration was composed by two consecutive steps. They also found that the conversion plots of the reverse reaction presented a sigmoid-shape, which could be related to an Avrami-Erofeev mechanism [108]. Álvarez Criado et al. also analyzed the kinetics of both processes, describing the two reactions with a shrinking core model, using thermogravimetric data with enhanced temporal resolution [98]. Accordingly, differences on the model governing the hydration/dehydration kinetic could arise from the use of different raw materials and/or experimental equipment.

Development of efficient reactors has been also subject of research, trying to find the best configuration taking into account the working conditions and the material characteristics. Schaube et al. analyzed the effects of direct and indirect heat transfer and pointed out that the direct contact of the HTF with the solid reagents was the best choice, since the gas flow through the solid bed did not exhibit heat transfer limitations [112]. Schaube et al. further built a gram-scale fixed bed reactor prototype, in which the cycle stability over 25 cycles was tested [113]. Additionally, they developed a 2D model for comparing experimental and simulated results and reported a good agreement between both of them in most of the studied cases [114]. A numerical heat and mass-transfer model for hydration of CaO in a packed-bed can be also found in the work of Ströhle et al. [115], whereas Shao et al. presented a study with more detailed aspects of the chemical model of both charge/discharge steps [116]. However, difficulties for upscaling without inducing significant mass and heat transfer limitations, among other practical issues, render fixed-bed reactors an unattractive choice for using CaO in CSP plants. This is partially caused by agglomeration, which reduces contact with steam and can result in channeling of the Ca-based solid bed, being these effects clearly detrimental for the performance of the system [106]. To circumvent this issue and to improve mass and heat transfer, Álvarez Criado et al. proposed a fluidized-bed reactor, using steam as the fluidizing gas [117]. Pardo et al. further evaluated experimentally the fluidized-bed TCS batch reactor. For improving fluidization of Ca-based particles (low powder flowability), they tested the setup with ca. 2 kg of a mixture containing 70% of inert Al_2O_3 to facilitate fluidization, since particle of small size (<50 µm) cannot fluidize properly. Using this set-up they performed 50 cycles with a mean conversion of 80% for both the dehydration and hydration processes [69]. Additionally, by using a fluidized-bed batch configuration, 5.5 kWth power reactor, Criado et al. observed that the discharge step was controlled by slow kinetics of CaO hydration, whereas dehydration was

limited by mass transfer [118]. Fluidized-bed concept was further evaluated under continuous operation [119]. Rouge et al. demonstrated the suitability of a bubbling fluidized-bed reactor for this TCS system under continuous feed of gas and solid reactants in a 20 kW power pilot plant [119].

Alternatively, Schmidt et al. built a plate heat exchanger-like reactor (Fig. 11c-d) and tested 10 dehydration/hydration cycles of 20 kg of $Ca(OH)_2$, exhibiting conversions around 77% [120]. Recently, the feasibility of using this system in an indirectly heated configuration was evaluated at low steam partial pressures; the reason for selecting such operation conditions is that the temperature decrease obtained by performing dehydration at low pH_2O favors the exploitation of lower grade heat flows for the charging step.[121] In addition, energy supply required for steam generation is also lowered, turning more feasible the use of heat sources at lower temperatures, which can be integrated in the plant for improving the overall energy efficiency. Schimdt and co-workers assessed such working conditions in a relatively large scale system (2.4 kg of $Ca(OH)_2$), finding that for the dehydration, a pH_2O of 10 kPa and temperature higher than 445 °C are needed for ensuring the best balance between sufficiently faster reaction rate and high power densities[121]. In addition, the same research team developed a moving bed pilot plant with a 10-kW thermal power reactor with capacity for 270 kg (Fig.11e-f), although such design is still on a preliminary stage of development. [122]

Table 3. Promising alkaline-earth hydroxides and carbonates for TCS.

Reaction	Temperature (°C)	Energy storage density (kJ kg^{-1})
$Mg(OH)_2 \rightarrow MgO + H_2O$	350	1340
$Ca(OH)_2 \rightarrow CaO + H_2O$	400-600	1406
$CaCO_3 \rightarrow CaO + CO_2$	850	1790
$SrCO_3 \rightarrow SrO + CO_2$	1200	1585

Dehydration/hydration reactions of Ca-based materials are a promising TCS candidate and through the several ongoing research efforts focused in addressing several critical aspects (reactor configuration and improvement of material mechanical properties while guaranteeing high chemical reactivity), this system has reached a certain level of maturity. However, the medium temperatures at which this TCS system works might detract its applicability in future CSP plants that will generate higher-temperature HTF.

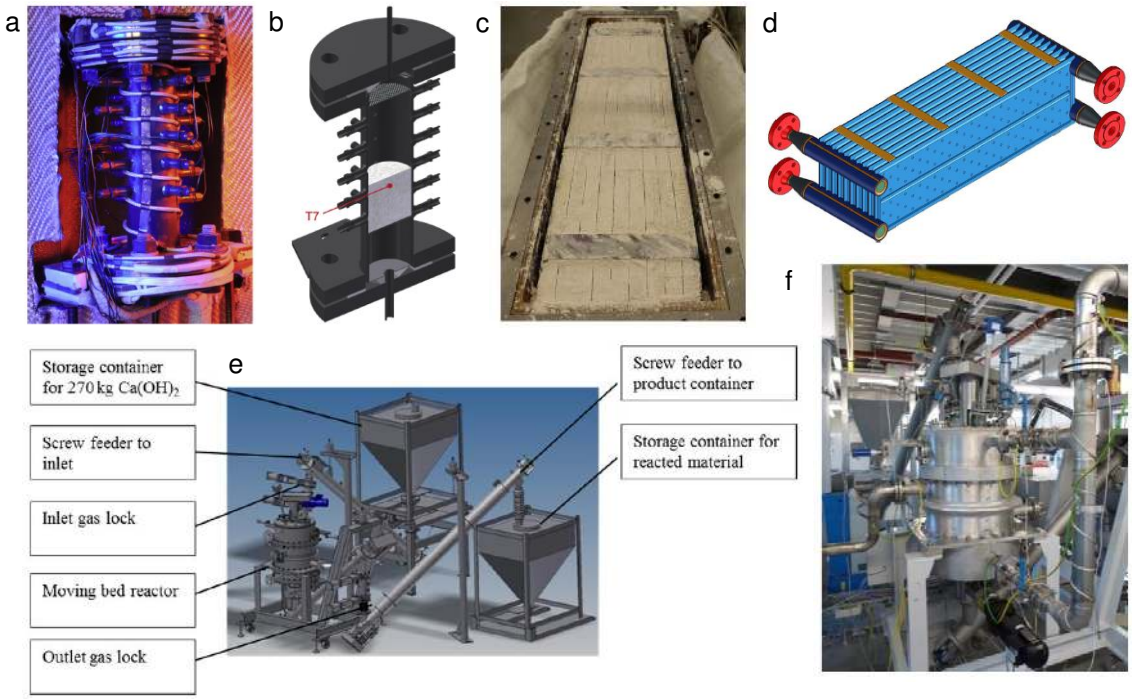

Figure 11 Reactors developed by DLR for TCS using $Ca(OH)_2$/CaO cycle: (a-b) fixed bed reactor. Reprinted from Energy Conversion and Management, 86, C. Roßkopf, M. Haas, A. Faik,M. Linder, A. Wörner, Improving powder bed properties for thermochemical storage by adding nanoparticles, 553-559, Copyright (2014), with permission of Elsevier. (c-d) plate heat exchanger-like reactor. Reprinted from Applied Thermal Engineering, 62, Matthias Schmidt, Christoph Szczukowski, Christian Roßkopf, Marc Linder, Antje Wörner, Experimental results of a 10 kW high temperature thermochemical storage reactor based on calcium hydroxide, 93-98, Copyright (2014), with permission of Elsevier.. (e-f) moving bed reactor pilot plant Reprinted from Ref. [122], with the permission of AIP Publishing.

2.6. Carbonates-based heat storage

TCS can be also performed through decarbonation/carbonation reactions. In this case, heat absorbed at the solar receiver is used to carry out the endothermic decomposition of a carbonate. The products of such reaction are CO_2 and a metal oxide (Eq.17). Both reaction products are stored separately, until heat is needed. Heat release proceeds by carbonation of the metal oxide. This TCS type is a gas-solid reaction and operates as a closed system.

$$MeCO_3(s) + \Delta H \leftrightarrow MeO(s) + CO_2(g) \quad (17)$$

The use of these reactions was also proposed in the mid-1970s [47] for heat storage applications. According to Ervin, one of the drawbacks of this system is CO_2 storage, since CO_2 must be compressed, adding an energetic penalty [47]. Alternatives to compression are storing the CO_2 with an adsorbent (amines, metal organic frameworks or zeolites) or by carbonation of other oxides with lower working temperatures as suggested by Kyaw et al. [123]. These authors evaluated the decarbonation and carbonation reactions of $CaCO_3$ and CaO, respectively, which is the carbonate-based TCS system that has caught more attention. Additionally, this system has been widely explored for post-combustion CO_2 capture, in the context of sequestration to avoid greenhouse gases emissions, using a technology known as the Ca-looping (CaL) cycle, with some pilot plants located in Spain and Germany [124,125]. The incorporation of the CaL cycle as energy storage system in CSP plants was evaluated by Chacartegui et al. suggesting the use of CO_2 for both the CaL process and the power cycle.[126] Such analysis reported plant efficiencies above 45%. Same authors evaluated different power cycle concepts, viz. directly-integrated Brayton cycle and indirectly-integrated Rankine cycle; finding that the former offer the best performance.[127] Additionally, Aloviso et al. evaluated several layout configurations in a recent process

optimization study, observing that by introducing additional gas-solid heat recovery systems, cycle efficiencies increased up to 46% at 50% CaO conversion[128].

First experimental studies about the use of $CaCO_3$ as TCS material date from 1980, when Flamant et al. analyzed the solar-driven decomposition of calcium carbonate [129]. Years later, Kyaw et al. analyzed in more detail such system for thermal energy storage coupled to nuclear reactors [123]. Decarbonation takes place at around 850 ºC, although temperature can be lowered within certain limits by decreasing the partial pressure of CO_2, according to the practical constraints established by the pumping capacity of the system required to evacuate the gas released by solid decomposition. This temperature range will fit perfectly with the requirements of several thermodynamic cycles in central receiver plants. As additional benefits, those materials are abundant, inexpensive and present low toxicity [130]. Furthermore, the energy storage density is quite high (ca. 1790 kJ per kg $CaCO_3$) and there are not side reactions involved. These characteristics render this system a promising candidate for TCS.

One of the great advantages of this thermal energy storage technology is the natural abundance and availability of non-toxic Ca-carbonates minerals, which ensures an inexpensive source of TCS material. Natural carbonates such, limestone, chalk and marble, and dolomite ($CaMg(CO_3)_2$) have been recently assessed for TCS purposes under multicycle charge/discharge experiments monitored via thermogravimetric analyses [131–133]. Despite the good expectations of utilizing such low-cost materials, authors have encountered several drawbacks from the cyclability point of view related with low reversibility and particle agglomeration/sintering, that eventually might cause partial deactivation, exhibiting a cycle-to-cycle decrease on the carbonation conversion (Fig. 12a). Benitez-Guerrero et al. found that an outer layer of sintered CaO is formed on the surface of a porous structure of CaO (Fig. 12b) [133]. When carbonation proceeds, CO_2 reacts

with the outer layer of CaO forming an outer shell of $CaCO_3$ that blocks the access of CO_2 to the inner core of porous CaO, which remains unreacted. This process in turn lowers the efficiency of the decarbonation/carbonation cycle. Interestingly, same authors found that such pore-plugging effect did not affect to the same manner to carbonation/decarbonation cycles performed to dolomite, due to the presence of MgO clusters that facilitate CO_2 diffusion into the CaO porous structure.[132] Recently, good reversibility of natural dolomites has been obtained using a molten salt eutectic (NaCl and $MgCl_2$ mixture) and this good behavior has been attributed to the anti-agglomeration effect of impurities such as quartz.[134] Additionally, Perejón et al. experimentally evaluated the use of chemically-treated steel slag (containing CaO with impurities of Si, Al, Fe, Ti, Mg, Mn and Cr), which is an industrial by-product, as TCS material and observed high material cyclability when carbonation was performed at around 850 °C under high pCO_2 and calcination was carried out under inert atmosphere (He).

Several approaches have been adopted in order to improve the cyclability of the $CaCO_3$/CaO couple. For instance, Aihara et al. evaluated different synthesis procedures as to enhance the reversibility. They found that addition of $CaTiO_3$ was beneficial for avoiding sintering, which in turn stabilized both reactions over prolonged cycling [135]. Additionally, the use of high temperature thermal pretreatment was also reported as a positive way to reactivate CaO when subjected to multiple carbonation/calcination cycles [136]. Carbonation reaction seems to be well-described by a two-stage reaction, a kinetic-controlled fast step followed by a diffusion-limited stage [136]. Zhao et al. found that addition of polymorphic spacers, *viz*. Ca_2SiO_4 could alleviate the sintering effects, which in turn enhanced the multi-cycle reactivity [137]. In order to counteract the cycle-to-cycle deactivation phenomenon, Obermeier et al. explored CaO/Al_2O_3 composites and the hydration of natural CaO as an intermediate step to reactivate such material [138]. Aluminum

incorporation led to the formation of the mixed phase $Ca_3Al_2O_6$, which shows higher concentration with increased Al contents, and eventually contributes to a higher resistance to sintering and a better multicycle stability. A Ca/Al ratio of 95/5 appears to be the optimum for guaranteeing proper cyclability, although it comes at the expense of a slight decrease in the energy storage density.[138] On the other hand, regeneration by the intermediate hydration process was found to just moderately improve the decarbonation/carbonation cyclability.[138] In a another strategy, a recent report explored the utilization of calcium magnesium acetate as precursor, which gives rise to platelet-like morphologies of CaO and aids to retain certain porosity after cycling due to the stabilizing effect of MgO nanoparticles.[139]

Morphological modifications have been employed in a lower extent for improving carbonation reaction. The most successful is probably the one proposed by Benítez-Guerrero et al. who applied the replica method for the fabrication of macroporous CaO-SiO_2 composites by using rice husk as a template [140]. Such bio-templating approach allowed formation of pores in the nano-range (< 10 nm) that overcomes the pore-plugging effect described above, resulting in a higher multi-cycle effective conversion when compared with limestone (Fig. 12a) [140]. Additionally, CaO-coated honeycombs used as monolithic reactors/heat exchangers have been suggested for preventing materials deactivation, although such structures suffered degradation [141]. This research was conducted in the frame of the NESTOR project (A Novel Energy STORage and transportation concept based on concentrated solar irradiation-aided CaO-looping http://apt.cperi.certh.gr/). This project aims at using the Ca-based reversible reactions for solar heat storage but transporting the CaO to the location where heat is needed. For instance, the endothermic reaction is carried out in a solar plant in a desert area; then, CaO is transported to regions with lower solar resources but higher energy demand, such as central-Europe [130]. Obermeier et al. carried out a sensitivity

analysis of this trans-regional storage concept, stating the importance of carbonation temperature, reaction conversion and the heat recovery on the effective storage density [130]. However, still a life-cycle assessment of the overall carbon footprint of the suggested concept should be provided, especially considering that large CaO volumes must be transported long distances.

Other carbonates proposed for TCS applications are the $PbCO_3$, $BaCO_3$ and $SrCO_3$ [62, 142, 143]. The former was analyzed as a chemical heat pump [62], however this system presents low interest for further development due to its high toxicity and lower energy storage capacity than Ca-based reversible reaction. $BaCO_3$ requires high calcination temperatures (1200-1400 ˚C) and presents melting problems of the eutectic phase $BaCO_3$/BaO that hamper the carbonation reaction, both factors limiting its applicability for commercial thermochemical heat storage [142]. On the other hand, calcination/carbonation reactions of $SrCO_3$/SrO have been recently reported as a promising route for high temperature solar heat storage [143]. This system operates at around 1200 ºC, which is the calcination temperature, and presents a high energy storage density ca. 1585 kJ per kg $SrCO_3$ [143]. However, as in the case of CaO, SrO particles suffered sintering processes owing to the high working temperatures attained, which hampered the carbonation reaction due to a decrease of active surface, affecting negatively to its multicycle performance [143]. Rhodes et al. found that materials with 40 wt% SrO supported over yttria-stabilized zirconia could withstand 15 cycles with high stability. However, in the last cycles of a 45-charge/discharge test carbonation reaction showed slow kinetics (Fig. 12c) [143]. Additionally, André and Abanades obtained stable carbonation reactions with high conversions during four calcination/carbonation cycles by adding 32%wt. of MgO [142]. $CaSO_4$ and $Sr_3(PO_4)_2$ have been also tested as supports for this system. [144] Calcium sulfate was tested as a polymorphic spacer and strontium phosphate as sintering inhibitor. Although both materials stabilized the carbonation/decarbonation cycles, the phosphate support

resulted in higher gravimetric energy storage densities (ca. 500 kJ/kg).[144] These works demonstrated that there is room for further development by applying chemical modifications, which makes $SrCO_3$ an interesting candidate for temperatures above 1000 ºC, particularly considering its low price: less than $22/kg for the carbonate and less than $45/kg for the YSZ support. [145] However, although addition of supports can stabilize the carbonation step, it should be noted that it comes at the cost of lowering specific energy storage density, since the supports are normally inert to the chemical heat storage/release.

Another different concept based on the exothermic transformation of orthosilicate of lithium, Li_4SiO_4, into Li_2CO_3 and methasilicate, Li_2SiO_3, under CO_2 atmosphere at around. This process presents an interesting enthalpy, 780 kJ kg^{-1}, and it has showed reversibility in 5 cycles. However, lithium is less abundant and more expensive that the carbonates previously mentioned, and it requires the use of relatively high pressures (pCO_2= 1 atm) and, even so, the kinetics are sluggish [146]. Overall, all these alternative carbonate cycles require further long-term studies to confirm their stability for real applications.

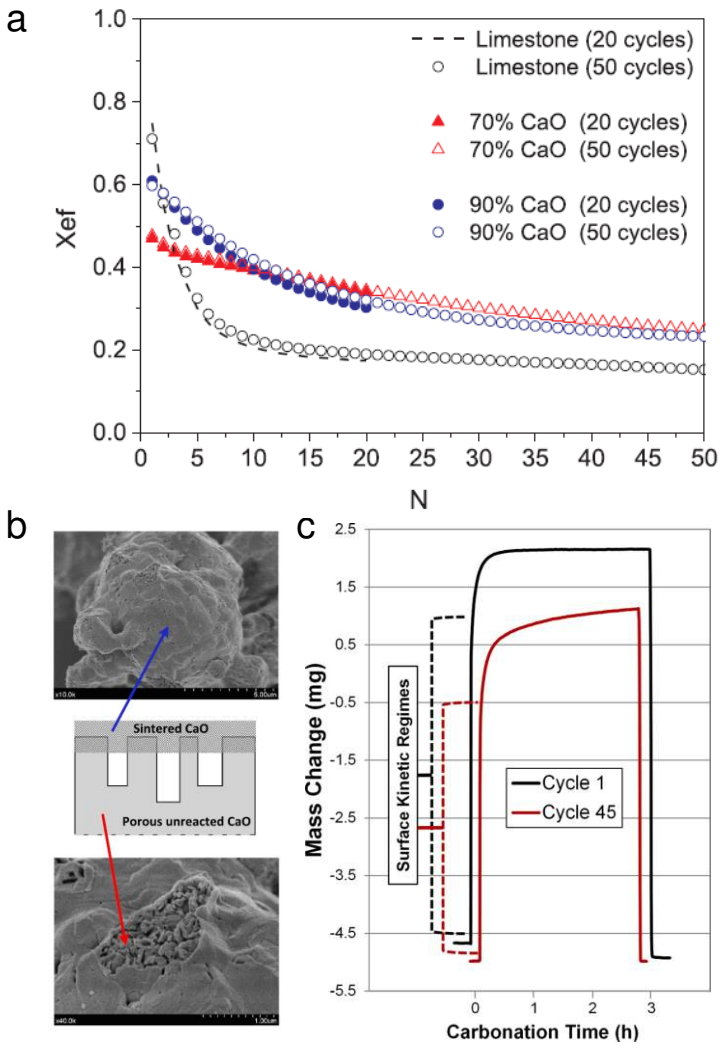

Figure 12. (a) Multi-cycle conversion comparison for the carbonation of limestone (white circles), composite with 70 (red circles) and 90% of CaO (blue circles) in CaO/SiO_2 composites. Reprinted from Applied Energy, 210, Monica Benitez-Guerrero,Jose Manuel Valverde,Antonio Perejon,Pedro E. Sanchez-Jimenez,Luis A. Perez-Maqueda, Low-cost Ca-based composites synthesized by biotemplate method for thermochemical energy storage of concentrated solar power, 108-116, Copyright (2018), with permission from Elsevier.(b) SEM micrographs and schematic illustrating the sintering phenomenon that causes cyclability problem in the $CaCO_3/CaO$ system. Reprinted from Solar Energy, 153, Monica Benitez-Guerrero,Jose Manuel Valverde,Pedro E. Sanchez-Jimenez,Antonio Perejon,Luis A. Perez-Maqueda, Multicycle activity of natural CaCO3 minerals for thermochemical energy storage in Concentrated Solar Power plants, 188-199, Copyright (2017), with permission of Elsevier. (c) Cycle 1 and 45 carbonation conversion analyzed by TGA for a SrO/YSZ material. Reproduced from Ref [143], with permission of John Wiley & Sons, Inc

Carbonates are a very promising class of material for TCS due to its high-energy storage density, suitable working temperatures to be coupled with tower CSP plants, low-cost, abundancy and low toxicity. Efforts in improving materials chemical activity over prolonged cycling seem encouraging. Determination of optimum reactor configuration and process up-scaling and testing of charge/discharge cycle stability utilizing kg-scale rectors should still be evaluated as to guarantee the feasibility of this TCS concept. An initial techno-economic analysis reveals that for $CaCO_3$ capital cost is slightly larger than 15 \$. MJ^{-1}, while for other alkaline earth carbonates such Ba or Mg are around 25 \$.MJ^{-1}.[26] These values are considered already competitive for commercial applications. On the other hand, system integration analysis of $CaCO_3$ in solar plants shows an overall efficiency of the storage system between 32 to 44%, depending on the specific configuration.[147] In addition, this attractive technology can clearly benefit from existing R&D efforts on CO_2 capture by the CaL process, which in turn might facilitate a faster implementation in commercial CSP plants.

However, it is important to take into account the energetic and economic penalties of the gas (CO_2) storage process, issue that carbonate-based TCS shares with hydride and hydroxide-based systems. Generally, in order to reduce the size of the tank supercritical condition are selected and this requires high pressure at ambient temperature. Recently, costs for the compression of CO_2 up to 150 bars has been estimated in 18.4 \$ per tonne[148]. Meroueh et al. evaluated two different options for CO_2 storage for the $SrCO_3$ system, gas compression and CO_2 sorption, finding that the use of sorbents is more economic (153±64 USD kWh^{-1} and 48 ±18 USD kWh^{-1}, respectively), although a higher energy efficiency was observed for gas compression (96 vs 71%).[149]

Additionally, the origin and quality of CO_2 should be also evaluated; so far, lab-scale experiments with pure CO_2 streams have been carried out. Capture of CO_2 at large scale in cement

or power plants is usually based on amine (usually monoethalnolamine-MEA) scrubbing, although the use of zeolites, MOF's and polymeric membranes has been also proposed for this process.[150] However, depending on the source of the CO_2 might contain impurities, such SO_2, which could affect negatively to the carbonation process, and they should be removed before introduction into the storage loop.

2.7. Redox-based heat storage

This TCS type is based on reduction-oxidation (redox) reactions of metal oxides (Eq. 18). Reduction (charge) is the endothermic solar-driven process. Heat is needed to conduct the reduction of a metal oxide, which decreases its oxidation state releasing lattice oxygen. In this case, the gaseous product theoretically does not require storage since oxygen could be released to or taken from the atmosphere. When heat is required, discharge occurs by re-oxidizing the reduced phase with ambient air, liberating the stored energy owing to the exothermic nature of the reaction (Fig. 13).

$$MO_x(s) + \Delta H_r \leftrightarrow MO_{x-y}(s) + y/2O_2(g) \quad (18)$$

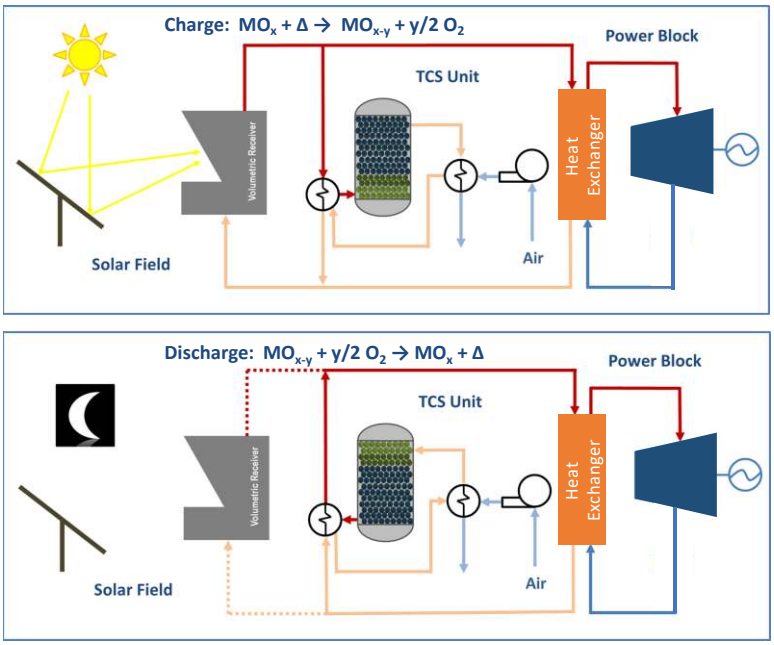

Figure 13. Scheme of a CSP plant working with an indirect-type redox-based TCS and volumetric air receiver.

In this system, air is used both as a HTF (reduction) and reactant (oxidation), hence it can be a suitable candidate for implementation in future CSP plants working with volumetric air receivers, since their designs will allow generating high temperature air (HTF). The fact that gas storage is avoided presents beneficial economic implications. However, other factors related to the effect of air purity (especially the CO_2 and H_2O content) in the gas-solid reaction should be addressed before commercial implementation, which in turn might imply the incorporation of air purification units in the CSP plant.

First experimental work concerned the thermodynamic, kinetic and reversibility assessment of the BaO_2/BaO and CuO/Cu_2O redox couples [53, 54]. Decades later a project leaded by the American company General Atomics, in collaboration with DLR, re-evaluated the concept of using redox reactions for TCS purposes [151]. The project finished in 2011 and evaluated various redox couples for that end covering a wide range of temperatures. General Atomics analyzed potential redox couples through thermodynamic calculations. However, many of them were

discarded on a first basis due to its low (Cr_5O_{12}, Li_2O_2, MgO_2) or high (V_2O_5) working temperature, toxicity (U_2O_3, PbO_2; in addition the latter did not show redox reversibility in a recent study [152]) or prohibiting high price (PtO_2, Rh_2O_3) [151]. Others were rejected on a first reversibility assessment, such as Sb_2O_5 or MnO_2, since they did not exhibit re-oxidation reaction [151]. This let BaO_2/BaO, Mn_2O_3/Mn_3O_4, Co_3O_4/CoO, CuO/Cu_2O and Fe_2O_3/Fe_2O_3 as the most promising candidates. Fig. 4 shows the Ellingham plots of these selected redox materials, from which the transition temperature can be discerned. It is clear that due to its higher transition temperature (1350 ºC), the iron oxide-based system is the less attractive of these redox candidates, especially considering mid-term implementation in existing CSP plan technologies.

In the next section (section 3), the current status of the research progress performed on such interesting redox pairs, based on binary metal oxides, and the recently-proposed use of perovskites for TCS applications at high temperatures will be described in more detail. That section will cover material related aspects, with special focus on the strategies suggested for improving TCS performance (kinetics, thermodynamics, energy storage density and materials stability) and the proposed thermochemical reactor concepts.

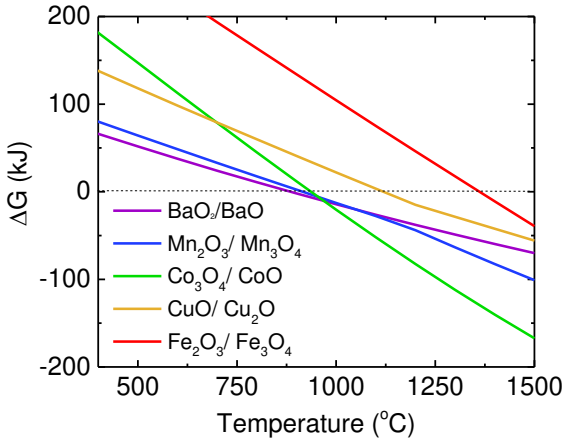

Figure 14. Ellingham plot for the most promising redox reactions selected as candidates for thermochemical heat storage. Thermodynamic simulations were performed considering 1 atm of pressure using the software package HSC Chemistry 6.1 from Outotec Research Oy.

In this section, we have described chemical reactions explored for thermal energy storage suitable for use in concentrated solar power plants. However, some of these systems might find applications in other technologies or industries in which exploitation of exhaust low-grade heat from high temperature process, e.g. metallurgy, would be beneficial for increasing process efficiency. For such applications might be especially interesting TCS systems working in low-mid temperatures, such as Mg or Ca hydroxides. The great advantage of TCS gas-solid systems (hydrides, hydroxides, carbonates and redox) is the vast room for tailoring the solid materials involved in such reactions through morphological or chemical modifications, enabling proper adjustment of each system for the desired operational working parameters. Fig. 15 briefly summarizes the advantages and disadvantages of each of these systems. Ongoing R&D efforts on materials and reactor development and system integration might contribute in the future to palliate some of the disadvantages here described, paving the route for market incorporation of these TCS technologies.

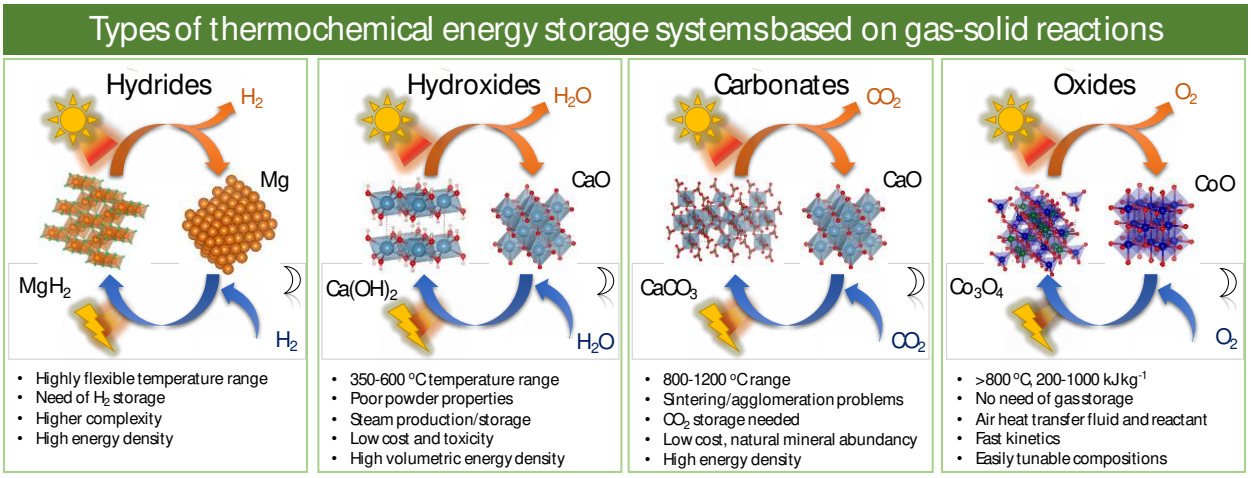

Figure 15. Summary of the reaction schemes, advantages and disadvantages of the thermochemical heat storage systems based on gas-solid reactions. All the crystalline structures were simulated with software Vesta[153].

3. Thermochemical heat storage based on redox cycles of metal oxides

3.1. Redox materials

3.1.1. Barium oxides

The redox transition between BaO_2 (barium peroxide, tetragonal crystal lattice, space group I4/mmm) and BaO (barium oxide, cubic, Fm-3m) was the first redox couple proposed for TCS purposes by Ervin in 1977 [47]. This couple presents the peculiarity that the monovalent cation, Ba^{2+}, does not participate in the redox trade, since the electron transfer occurs in the anion site when its transformed from peroxide (O_2^{2-}) to oxide (O^{2-}). Ervin stated the advantages of working without gas storage, a high energy storage density and a moderate price, although it could be high enough for discarding this redox pair [47]. A year later, Bowrey and Jutsen performed the first experimental studies on barium peroxide. They evaluated the thermodynamics of such system, stating that heat could be discharged at temperatures below 754 ºC [49]. One of the main problems associated with this redox pair is that is highly hygroscopic, and the high capacity of BaO, as a basic oxide, to easily react with atmospheric CO_2 [49,154,155]. Thus, the reactor should be completely free of those gases in order to avoid a serious material degradation. Additionally, barium hydroxide species present much lower melting points ($Ba(OH)_2$, 408 ºC; $Ba(OH)_2$ H_2O, 78 ºC), which might pose severe material degradation issues considering the high temperatures attained for TCS operation [156]. Bowrey and Jutsen further performed reactivity analyses in an electric furnace,

varying the operational conditions, such as the heating rates, maximum temperature, etc. These very preliminary tests proved that the redox reactions of BaO_2/BaO could be performed under air atmosphere [49]. Some years later, Fahim and Ford conducted the first complete assessment of such redox pair, dealing with thermodynamics, kinetics and reversibility studies [53]. Reduction and oxidation kinetics were evaluated through isothermal and non-isothermal methods. They observed that above 850 ºC reduction was hindered by diffusion, and they recommended not to apply the oxidation rate above 580 ºC due to the reverse reaction becoming significant [53]. Those authors also reported a reversibility study in which they subjected BaO_2 to 20 charge/discharge cycles. Results showed a loss of cyclability in terms of progressive conversion decay with each cycle. Namely, total conversion for reduction and oxidation were only obtained in the first cycle. They attributed this behavior to the formation of a layer of BaO_2 during oxidation of BaO [53]. General Atomics also evaluated the use of BaO_2/BaO but in their analysis the materials showed almost no reversibility [151].

However, recently the interest in this redox couple emerged again. Firstly, for oxygen chemisorption, also known as the Brin process, which is one of the oldest ways to produce pure oxygen. Recently, researchers demonstrated that Sr and Mg co-doping was beneficial in order to improve the oxygenation/deoxygenation cyclability of BaO [157–159]. More importantly, the applicability for TCS of BaO_2/BaO redox couple was re-visited by Agrafiotis et al. [160] and by Carrillo et al. [156]. Carrillo et al. showed that commercial BaO_2 thermally pre-treated was able to withstand 30 redox-cycles without losing performance (Fig. 16), demonstrating a very promising redox reversibility for heat storage in CSP plants. Authors found that by such high-temperature thermal treatment impurities mainly associated with barium carbonates could be removed favoring the redox cyclability of the system [156]. As well, there is an interesting feature regarding redox

reactions of metal oxides: the hysteresis process due to the difference between reduction and oxidation temperatures. Indeed, it has been shown that there is an interval of about 10 ºC between the onset temperatures of reduction and oxidation reactions for Ba-based cycle. This interesting feature that takes place in all the redox pairs, is described in more detail in section 3.1.4.

In summary, barium-based redox TCS is an interesting candidate due to its capacity to withstand prolonged redox cycling, availability (barium is the 14th most abundant element in the Earth's crust), energy storage density (474 kJ kg^{-1}), and moderate working temperature (charge at ~800 ºC and discharge at 600-700 ºC). These operation conditions could make this system more appealing for CSP plants working with volumetric receivers in a short-medium term development. On the other hand, up-scaling system has not been tested yet, and this redox couple has only been evaluated in the lab at mg-scale. However, preliminary techno-economic analysis indicates that the cost of using BaO_2/BaO for thermochemical storage, 23.93 $ MJ^{-1}, is very attractive for use in future solar plants. Nevertheless, issues regarding BaO reactivity with H_2O and CO_2 should be addressed as they can drastically affect the material stability, to the point of rendering this system a non-suitable option for TCS if working with unpurified air [160]. Although long term studies will be necessary to better define the tolerance of the BaO_2 to these pollutants, most likely air with dew temperatures well-below 0 ºC will be required. Although dry air with that quality can achieved with conventional equipment, this additional purification stage adds cost and complexity to the system.

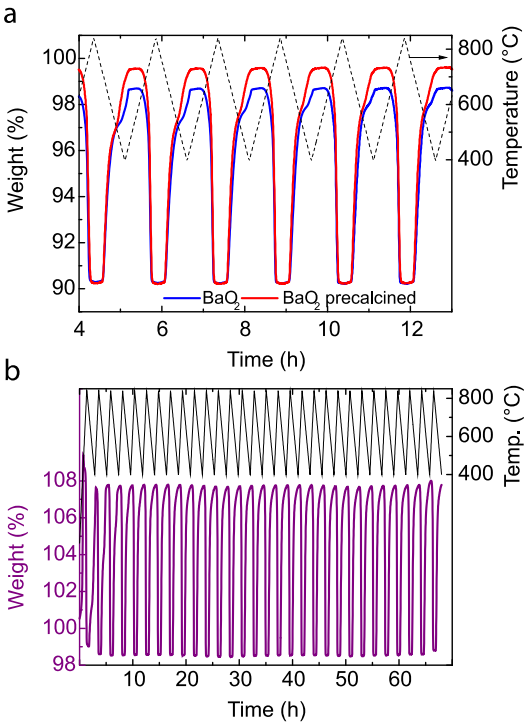

Figure 16. (a) Cyclability comparison of a BaO_2 commercial sample without pre-treatment and a BaO_2 sample pre-calcined at 1000 ºC in Ar. (b) 30-redox cycles carried out on the pre-calcined BaO_2 sample under an air atmosphere measured by thermogravimetric analyses. Reproduced from Ref [156], with permission of the PCCP Owner Societies.

3.1.2. Copper oxides

The copper-based redox cycle is also one of the systems proposed in the 1980s, however it has been scarcely evaluated. It presents a high energy storage density (811 kJ kg^{-1}), which is one of the great advantages for this redox couple. However, its transition temperature is high, about 1120 ºC. This becomes an important issue owing to the fact that Cu_2O melting temperature is 1232 ºC, providing a very narrow temperature window for operation [151,161]. This implies serious constraints in the reactor design, since homogeneous heat profiles will be required as to avoid hot points that could favor Cu_2O melting, which in turn might lead to an important material degradation.

Chadda et al. conducted a reversibility assessment demonstrating that this redox couple showed high cyclability over 20 redox cycles [54]. Even though high reversibility was obtained, copper oxides suffered a morphological change, probably caused by particle sintering due to the high temperatures attained. Chadda et al. also performed a kinetic analysis of both reactions, reporting activation energy values of 332 kJ mol^{-1} for CuO reduction and 84 kJ mol^{-1} for oxidation [54]. Agrafiotis et al. re-evaluated through thermogravimetric analyses the cyclability performance between reduction for CuO (tenorite, monoclinic crystal structure, space group C2/c, Cu (II)) and Cu_2O (cuprite, cubic, Pn-3m, Cu (I)) [160]. They found that thermal reduction (heating up to 1090 ºC) of CuO is much faster than re-oxidation of Cu_2O. The slow kinetics of oxidation eventually prevents reaction from reaching complete conversion. In this way, even at the most favorable conditions tested (isothermal at 1020 ºC) re-oxidation of Cu_2O is not complete after two hours and remarkable deterioration of the performance is observed in only five cycles. Authors also found powder shrinkage probably caused by particle densification after cycling experiments [160].

Conversely, by performing the study isothermally (950 ºC), driving reduction/oxidation reactions by changes in oxygen partial pressure, Deutsch et al. reported stability over 20 cycles monitored by TGA [162]. This result reflects the positive impact of lowering the maximum process temperature at which reduction is attained by decreasing the oxygen partial pressure. Materials structural stability can benefit from these milder conditions, since sintering increases exponentially with temperature. However, the same authors observed extensive sintering of CuO using a larger scale fixed-bed reactor (50 g of solid) and, as a consequence, only partial conversion was attained with the concurrent loss of cyclability of the system. [64]

Lowering the reduction temperature can be achieved by using sweep inert gases or by applying vacuum, although it must be taken into account that both options add energy (and economic) penalties to the overall TCS process. In the same work, authors performed a kinetic study of both reactions applying a novel non-parametric kinetic (NPK) method, observing that Cu_2O oxidation slowed down with increasing temperature, which in turn resulted in a negative activation energy [64]. This behavior has been reported for other oxidation reactions of metal oxides and will be discussed in more detail in section 3.1.4. A further assessment of Cu_2O oxidation reaction evaluating the influence of pO_2, conversion and temperature revealed that the model was well described by an Avrami-Erofeev two-dimensional nucleation model.[163]

Several Cu-based solid solutions were studied by Block et al. for TCS purposes, *viz.* Cu-Co, Cu-Cr and Cu-Fe [161]. Addition of Co led to the formation of two phases, Co-Cu spinel and CuO, in which probably some Co^{2+} or Co^{3+} cations are substituting Cu^{2+}. At Co concentrations lower that 50%, reduction follows with the creation of several Cu-Co mixed oxide compounds, at ca. 870 ºC, having those transitions lower reaction enthalpy (from 29 kJ kg^{-1} for Co 10% to 286 kJ kg^{-1} Co 50%) than pure Cu oxides. Although such redox reactions showed reversibility, these lower energy storage values render Co-doped Cu oxides a less attractive option for TCS. Higher enthalpy decrease was exhibited by Mn- and Fe-doped Cu oxides, with reduction temperatures at about 965 ºC and 1040 ºC, respectively; whereas Cr-Cu oxides did not show redox reversibility.

Very recently, Jafarian et al. proposed a new concept that exploits the proximity of the melting point of Cu_2O with the TCS working temperatures for increasing the energy density of the system [164]. These authors suggested for the first time a thermal energy storage system that combine both sensible, latent and thermochemical heat storage. The thermochemical contribution comes

from the CuO/Cu_2O redox pair, whereas the phase change occurs as the melting of Cu_2O. Jafarian et al. assessed thermodynamically the suggested concept, assuming a directly-irradiated TCS reactor and the need of a liquid-solid quenching unit. They obtained that approximately 29% of the energy is stored chemically, 37% as sensible heat and the rest as latent heat [164]. Besides the high thermodynamic efficiency of the suggested novel concept, concerns arise considering the operation of molten oxides. These might comprise corrosion issues, heat transfer limitations and liquid handling problems (e.g. possible plugging due to solidification); which eventually might require the use of encapsulated materials as in the case of latent heat storage PCM's. Such encapsulation might involve high technical complexity since the metal oxide requires good gas-solid contact for ensuring fast kinetics and avoid mass transfer hurdles. Accordingly, further research is warranted to determine the feasibility of this approach for practical applications.

3.1.3. Cobalt oxides

Owing to its high energy storage density (884 kJ kg^{-1}) and working temperature (~900 ºC), Co-based redox couple is a very attractive candidate for TCS and it is probably the most studied redox-based system for that end. This redox couple involves the transition between Co_3O_4 (cubic spinel, space group Fd3m, with cobalt in oxidation states 2^+ and 3^+) and CoO (cubic, Fd3m, with cobalt in oxidation state 2^+). On the other hand, Co-based redox couple presents two important drawbacks. First, its price is higher than that of other metal oxides proposed for this application (58.5 $ per kg of Co compared to 2.06 $ per kg of Mn) [161, 165]. Indeed, Co is the 32th most abundant element in the Earth's crust, whereas Mn is the 12th and Ba the 14th. In addition, ore reserves of this strategic metal are concentrated in a few countries, being Democratic Republic of Congo, China, Canada and Finland the main exporters. The second issue is related with its high toxicity, since cobalt oxides are suspicious to be carcinogenic [166].

Similar to other TCS systems, to date most of the literature about this redox couple focusses on kinetic and reversibility assessments. As it is usually the case in single oxides, oxidation of CoO is the slower process of the cycle and, although the rate is significantly higher than for other redox couples, it can take up to 2h for completion keeping the sample isothermally at 860 ºC[167]. On the other hand, Agrafiotis et al. have confirmed the good structural stability of porous foams of Co_3O_4 after 30 cycles, which does not show either any significant loss of redox activity.[168] Nevertheless, several approaches have been applied in order to improve the cycling stability of such redox pair, mainly based on morphological and chemical modifications. Doping with other metals has been explored by various authors. Agrafiotis et al. prepared metal-doped Co_3O_4 with divalent cations, such as Zn, Cu, Mg and Ni, via solid-state reaction. Thermogravimetric analysis on the reversibility of those doped-Co oxides revealed that such compositions did not show any improvement in comparison with pure Co_3O_4/CoO [167]. In addition, tests carried out to the pure oxide by those authors revealed that reduction rate was 2-fold faster than oxidation reaction (5.8 and 12.2 min respectively[161]). Mn-doped Co oxides were also evaluated, revealing that pure Co oxide presented better performance since it exhibited faster redox reactions and Mn-doped oxides presented a decrease on the energy storage density [169]. Block et al. evaluated the effect of Fe-incorporation on the Co-oxide redox behavior. As well, a decrease on the energy storage density was observed for increasing amounts of Fe. However, with low Fe concentrations, the energy storage density was still high and the long-term stability (more than 30 redox cycles) was improved [166]. André et al. revisited Co/Fe mixed oxides, corroborating that small additions (5% Fe) resulted beneficial. Increasing the Fe content on Co oxides also led to a raise in the reduction temperature, which matches well with reported Co-Fe-O phase diagrams [166,170]. This indicates the remarkable usefulness of reported mixed-oxide phase diagrams as thermodynamic predicting tool

for redox transitions. Block et al. further explored Cu-doped Co oxides. At concentrations of Cu less than 7% Co_3O_4 crystal phase prevails, with the appearance of CuO phase when increasing Cu amount. Interestingly, addition of 10% improved remarkably the reaction rates over a 40-cycles reversibility test [161]. Authors attributed this improvement to the microstructural stabilization caused by the presence of low amounts of CuO, which counteracted the negative effects of sintering [161]. 10% Cu-doped Co oxide also exhibited a lower reduction temperature (865 ºC), but also lower energy storage density (457 kJ kg^{-1}) [161]. Using a wide composition range, André et al. concluded that the redox properties of the Cu-Co-O systems are determined by the cobalt, so introducing Cu results in linear decrease of the oxygen storage capacity of the solid and, therefore, in lower reaction enthalpies.[171] Coming to this point, it is worth mentioning the experimental difficulties encountered in the TCS community when measuring the reaction enthalpy of the redox transition of pure Co oxides by differential scanning calorimetry (DSC). Block et al. could confirm theoretical value by using Calvet calorimetry, 828 kJ kg^{-1}; whereas by DSC they reported 576 kJ kg^{-1} [161]. They ascribed this discrepancy to the Co^{3+} spin-state change, process that involves and energy change of about 221 kJ kg^{-1}, and, according to the authors, is not possible to be measured by simultaneous DSC-TGA equipment [161]. Recently, Tamayo et al. studied redox reactions of Cu-Co spinels, with a detailed analysis of the surface cationic distribution via XPS and its implications on the TCS capacity of such materials [172]. Authors observed that the amount of Cu and the processing route affected to the presence of Cu^{2+} on either octahedral, tetrahedral or both positions, and that a higher presence of cations on tetrahedral positions favored the oxygen release during the reduction step. [172]

The second approach investigated, regarding the material development, was through morphological modifications and shaping. Agrafiotis et al. evaluated the behavior of porous

ceramic structures coated with Co_3O_4, namely foams and honeycombs; since this kind of configuration presents advantages for heat exchange processes [173]. Redox behavior of Co_3O_4-coated ceramic foams and honeycombs made of several redox-inert materials (Al_2O_3, ZrO_2, SiC, cordierite) was evaluated via thermogravimetric analyses over several cycles. In particular, Co_3O_4-coated on a cordierite foam exhibited stable redox reversibility over 100 charge/discharge cycles [173]. In light of these results, a step further was taken by Agrafiotis and co-workers and they fabricated and tested porous structures entirely made by cobalt oxide. With this concept, the total amount of porous material is redox-active, which lead to a higher energy storage density than in the case of coated-ceramic porous structures [168]. They found that dense pellets presented cracks after thermal cycling probably due to chemical expansion. However, the Co-based foams that they fabricated (Fig. 17a) showed redox reversibility and structural integrity over 30 redox cycles, which rendered this approach in a very promising method for up-scaling this redox-couple [168]. Pagkoura et al. studied cobalt oxide-based monolithic bodies, with several compositions. They found that addition of ceria could improve redox kinetics, although the monoliths suffered from cracking after various cycles. On the other hand, thermo-mechanical stability was improved with incorporation of Al_2O_3 [174]. The same authors corroborated the benefits of Al-addition when shaping Co_3O_4 as ceramic honeycombs, proving redox reversibility over 104 cycles (Fig. 17b). Kinetic analyses of both reduction and oxidation reactions have been recently reported. Reduction rate was fitted to an Avrami-Erofeev mechanism. Such reaction presented an activation energy of 247 kJ mol^{-1}. On the other hand, oxidation was described by a 3D diffusion mechanism, since authors proposed that CoO oxidation was limited by ionic diffusion through the Co_3O_4 layer that is being formed. Activation energy for oxidation was equal to 58 kJ mol^{-1} [175].

In summary, Co_3O_4/CoO is the redox couple that has caught more attention for TCS purposes. Besides the drawbacks related with high toxicity and price, this redox pair is able to withstand prolonged charge/discharge cycle in different setups and with several composition and/or structures. Recent efforts point towards implementation in CSP demonstration plants that will be described in more detail in section 3.2. The level of maturity reached, coupled with the high energy storage density and cycling stability, makes this TCS system one of the most promising for future CSP plants working with volumetric receivers.

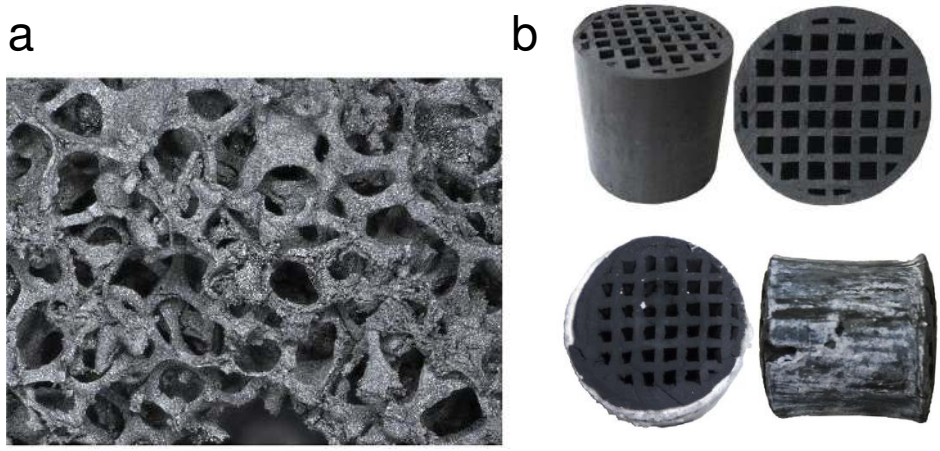

Figure 17 (a) Micrographs of Co_3O_4-based foams. Reprinted from Solar Energy, 114, Christos Agrafiotis,Stefania Tescari,Martin Roeb,Martin Schmücker,Christian Sattler, Exploitation of thermochemical cycles based on solid oxide redox systems for thermochemical storage of solar heat. Part 3: Cobalt oxide monolithic porous structures as integrated thermochemical reactors/heat exchangers, 459-475, Copyright (2015), with permission from Elsevier. (b) picture of Co_3O_4/Al_2O_3-based honeycombs (top: freshly made, bottom: after 104 cycles) made for TCS applications. Reprinted from Solar Energy, 133, George Karagiannakis,Chrysoula Pagkoura,Eleftherios Halevas,Penelope Baltzopoulou,Athanasios G. Konstandopoulos, Cobalt/cobaltous oxide based honeycombs for thermochemical heat storage in future concentrated solar power installations: Multi-cyclic assessment and semi-quantitative heat effects estimations, 394-407, Copyright (2016), with permission from Elsevier.

3.1.4. Iron oxides

The Fe_2O_3/Fe_3O_4 couple is the less explored redox system among the metal oxides, probably owing to the extreme high temperatures required for achieving the reduced phase. Temperatures close to 1400 ºC must be reached to attain the transformation of Fe_2O_3 (hematite, rhombohedral crystal structure, R-3c space group, Fe^{3+}) into Fe_3O_4 (magnetite, cubic spinel, Fd-3m, Fe^{2+} and Fe^{3+}) [176,161]. The experimental energy storage density of this pair has been reported to be 600 kJ kg^{-1} [161]. Additions of Co, Cu or Mn were found to be effective in decreasing the reduction temperature, but at the expense of a lower energy storage density [161]. Among them, the most interesting material was that obtained by the incorporation of 33% of Cu, exhibiting fast reduction and oxidation reactions occurring at temperatures around 1040 ºC, and a measured enthalpy of reaction of 330 kJ kg^{-1} [161]. Conformation of Fe_2O_3 powder into foams or pellets was also investigated for TCS purposes in each of these shapes, materials showed rigid structures and redox reversibility over few cycles [176]. However, detail observation of the porous architecture through SEM revealed micro-cracking, probably caused by the high temperatures attained, that could be seriously detrimental for the materials stability considering prolonged charge/discharge operation [176].

More recently, Bush and Loutzenhiser evaluated the iron redox pair thermodynamics, kinetics and cycle stability.[177] They found that reduction follows an Avrami-Erofeev reaction mechanism, while for oxidation a precise model could not be experimentally inferred due the most likely existence of two kinetic regimes depending on the oxidation extent. Cyclability was study for 10 pressure-swing isothermal cycles at 1400 ºC observing high degree of repeatability, although oxidation at such temperature only reached 80% conversion due to thermodynamic limitations. However, 100% oxidation conversion could be attained by lowering the temperature, increasing the thermodynamic driving force.

Although the application of Fe_2O_3/Fe_3O_4 has been examined to a lower extent for energy storage cycles, it has to be mentioned that the use of ferrites for thermochemical hydrogen production has been widely studied in the last decade, especially by Weimer and Kodama´s groups [178–183]. This progress in materials development, especially, in chemical modifications for lowering the reduction temperature by cationic doping or application of new redox crystallographic transitions[184], could find extensive applications in TCS.

3.1.5. Manganese oxides

Due to the multivalent nature of Mn and the abundancy of Mn ores (12th most abundant element in Earth's crust), these oxides emerge as interesting redox candidates. From low to high temperature, the oxide transitions are MnO_2 (pyrolusite, tetragonal structure, space group $P4_2/mnm$, Mn^{4+}), Mn_2O_3 (bixbyite, cubic structure, Ia3, Mn^{3+}), Mn_3O_4 (hausmannite, tetragonal, $I4_1/amd$, Mn^{2+} and Mn^{3+}), MnO (manganosite, cubic, Fm3m, Mn^{2+}) (Fig.18). There is an additional manganese oxide metastable phase with composition Mn_5O_8 (monoclinic, C2/m) [185].

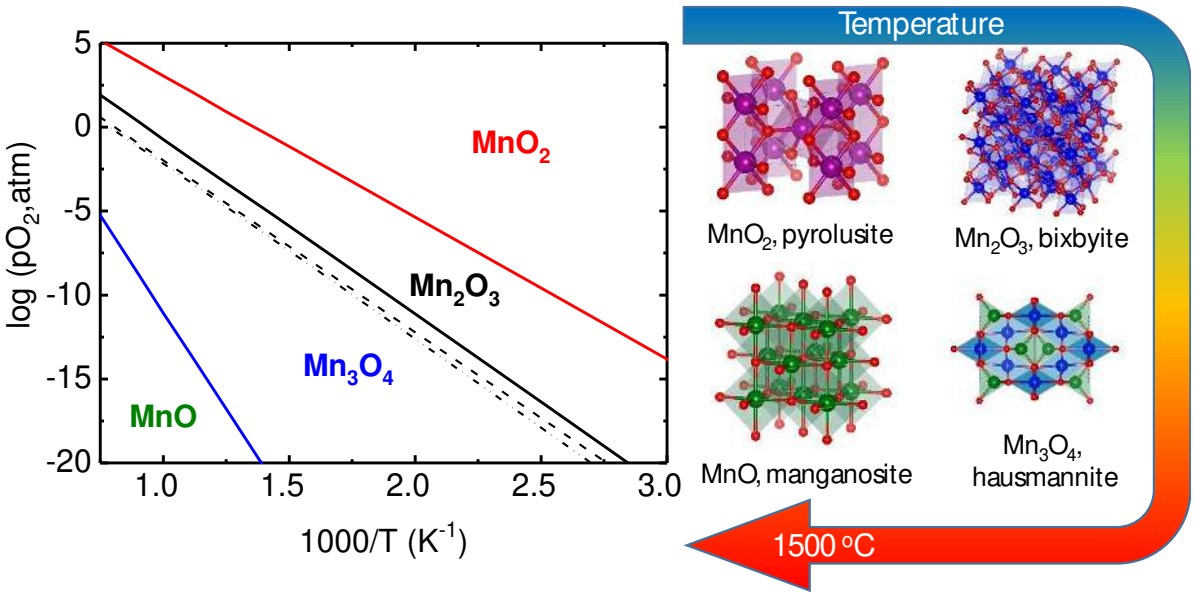

Figure 18 Left side shows manganese oxides phase stability diagram. Solid lines from ref. [186], dashed line from ref. [187] and dashed-dot line from data of ref. [188]. Right side, crystal structures of Mn oxides (All the crystalline structures were simulated with software Vesta[153]).

The transition occurring at lower temperature (MnO_2/Mn_2O_3) did not exhibit redox reversibility as it has been experimentally confirmed [189]. The decomposition from Mn_2O_3 to MnO has been widely studied for H_2 production as it is one of the processes involved in the Mn-Na-based 3-step thermochemical cycle [190–194]. Researchers from ANU have proposed the use of such Mn_2O_3/MnO redox cycle also for TCS purpose [195]. It works at high temperatures, since first Mn_2O_3 is transformed to Mn_3O_4 at around 950 ºC (with an energy consumption of 202 kJ kg^{-1}) and secondly Mn_3O_4 is reduced into MnO close to 1500 ºC, which has an enthalpy of reduction equal to 897 kJ kg^{-1}. In addition, at temperatures around 1170 ºC, the polymorphic transformation of α-Mn_3O_4 into β-Mn_3O_4 with cubic structure takes place, which adds 80 kJ kg^{-1} to the total energy storage density [196]. The high global energy storage density of this combination of reactions is promising, however, to the best of our knowledge, MnO to Mn_3O_4 redox reversibility has not been reported in literature yet. Furthermore, the influence of the high temperatures attained on the oxides morphological and chemical stability, which eventually could affect to the process kinetics, deserves careful analysis. In this respect, recently it has been studied the addition of Mg as a sintering inhibitor to guarantee the redox reversibility of that system. [197] Randhir et al. evaluated the incorporation of Mg at different doping levels in the Mn_3O_4/MnO redox couple, finding that the materials with higher magnesium content presented lower degree of sintering after 10 redox cycles carried out with a maximum temperature of 1500 ºC. Based on experimental analyses of O_2 release and uptake, thermodynamic data extracted from CALPHAD, and calorimetric measurements[198], Randhir et al determined that the gravimetric energy storage of that system to be 1070 kJ kg^{-1} for the material with a Mn:Mg ratio of 2:3, which is among the highest values for

redox-based TCS. However, despite the promise, the high operation temperatures might delay the implementation of this redox system at industrial scale.

Therefore, based on its more moderate working temperature, the most attractive redox transition and, thus, the most studied deals with the Mn_2O_3/Mn_3O_4 redox couple. Thermochemical heat storage using the Mn_2O_3/Mn_3O_4 redox pair entails a crystal phase transition in which Mn undergoes an oxidation state transition from +3 in the oxidized form, to an average of +2.67 in the reduced phase, with a thermochemical energy storage density of 202 kJ kg^{-1}. The reduced phase, tetragonal α-Mn_3O_4, presents a spinel structure of AB_2O_4 type with A = Mn^{2+} cations occupying the tetrahedral sites, and B = Mn^{3+} cations placed on the octahedral ones. α-Mn_3O_4 spinel structure presents tetragonal distortion due to a Jahn-Teller effect on Mn^{3+} [185]. General Atomics was the first in suggesting and evaluating its use for thermochemical heat storage [151]. Later, the EU-funded TCS Power project was dedicated to the development of this system both focused on the materials and reactor development and system integration, results that will be described in the present section and section 3.2.

Besides presenting the lowest energy storage density of all the redox couples explored for TCS purposes, the main drawbacks of this system are the slow oxidation kinetics of Mn_3O_4 reaction with O_2 [160,161,176,199,200], and material degradation problems induced by particle sintering that cause a cycle-to-cycle efficiency decrease or even, the total loss of cyclability. The higher thermal hysteresis (temperature gap between reduction and oxidation reactions) that Mn_2O_3/Mn_3O_4 (ca. 200 ºC) exhibits (Fig. 19b) respect to other redox couples (30-50 ºC for Co_3O_4/CoO) [168,169] poses an additional problem, both from operational and energetic perspectives. Based on the TES exergy efficiency (η_{ex}) definition given on Eq. 1 (cf. Section 1.2), the higher the difference between the charging and the discharging temperature, the lower the efficiency of the

system. On the following, strategies, mainly covering morphological and chemical modifications of such materials, to overcome the limitations are described.

Carrillo et al. evaluated the influence of the particle size on the Mn_2O_3/Mn_3O_4 cyclability. Mn_2O_3 materials with different particle size were synthesized by altering the Mn precursor concentration during the precipitation with ammonia [200]. Larger particles with lower specific surface area values were obtained when utilizing more concentrated precursor concentrations. In particular, synthesized materials with an initial mean particle size of 266 nm exhibited 30-cycle stability (Fig. 19c). However, sintering effects caused by the high temperatures attained in redox cycling (1000 ºC maximum temperature) induced changes in the morphology that eventually caused an exponential decay on the oxidation rate [200]. Conversely, Mn oxides with lower initial particle size (< 88 nm) and higher surface area showed a total loss of cyclability after the second redox cycle. This result was ascribed to a higher degree of sintering, by more pronounced effect of coarsening and densification, driven by a higher tendency to sintering of particles with smaller size [200]. Alteration of the Mn_2O_3 morphology by induced-macroporosity was explored by the same authors [201]. Faster reactions rates were achieved, although the macroporous bodies also suffered from a high degree of sintering that remarkably modified the initial structure, affecting negatively to the multicycle rate stability [201]. Agrafiotis et al. tested Mn_2O_3-coated, porous cordierite honeycombs and foams for a cascade-reactor concept coupled with Co_3O_4/CoO (more details in section 3.2.1) [202]. Same authors also fabricated Mn_2O_3-foams prepared by the replica method, finding that these porous structures totally collapsed after ceramic sintering at high temperatures [176]. Small fragments from that porous structure and pellets prepared from Mn_2O_3 were evaluated under redox cycling monitored in TGA, exhibiting poor reversibility performance [176].

Several cationic dopants have been explored as to modify chemically Mn_2O_3 and Mn_3O_4. The advantage of this approach respect to morphological modifications is that not only kinetics and chemical stability over cycling can be improve, but also thermodynamics can be altered, which in turn can positively affect to the energy storage density capacity or narrowing of the hysteresis gap. Co- and Al-doping were found to contribute negatively to the re-oxidation inducing even slower reactions or no reversibility [161,169,201]. By Cu-doping, it is possible to lower the reduction temperature to 915 ºC, when using 3-5% [161,201] or 10% Cu incorporation. Block et al. reported energy storage value of 157 kJ kg^{-1} for 3% Cu and slightly faster oxidation reaction [122]. Conversely, Carrillo et al. reported lower oxidation rates for 5% Cu content during 30-redox cycle analyses [149]. Addition of 5% of Cu caused the appearance of two crystal phases after cycling: Mn_2O_3 with Cu cations partially substituting Mn on the cubic bisbyite lattice and $CuMn_2O_4$ spinel [201]. In general, phase segregations are not desired in the Mn_2O_3/Mn_3O_4 system, since their presence can contribute to a decrease on the gravimetric energy storage density if such oxides are not redox active on the working temperature window. Cr-doping was evaluated in 5% molar content, resulting in slight increase on the onset reduction temperature (966 ºC) and, generally lower, but more stable oxidation rate values tested in multicycle TGA analyses [201].

Fe-doping has been found to be the most effective way to remarkably improve the TCS characteristics of the Mn_2O_3/Mn_3O_4 redox couple [161,170,176,201,203–207]. Carrillo et al. evaluated Fe-doping from 1 to 40 mol.%, finding that, in general, Mn oxides benefit from Fe incorporation by showing faster oxidation rates, which in turn implied more stable cycle stability; narrower thermal hysteresis, and more elevated energy storage density [204]. One of the great advantages of Fe doping is that Fe^{3+} and Mn^{3+} exhibit identical cationic radium [204], which facilitates Fe incorporation into the bixbyite crystal structure up to 50% Fe without the appearance of hexagonal hematite phase,

or other segregations, according to Mn-Fe-O phase diagrams [170]. Carrillo et al. found the best performance for a 20% Fe-doped Mn oxide synthesized via the Pechini method. This material presented a slight higher reduction temperature (995 ºC), narrower hysteresis (ΔT = 113 ºC), higher energy storage density than pure Mn oxide and remarkable multicycle redox reversibility (75 cycles) [204, 205]. Agrafiotis et al. corroborated the high redox stability of this composition, but prepared though a solid-state route, confirming the notable performance of this material regardless the fabrication route [176]. In the same work, authors also evaluated this material composition shaped as foams, presenting also redox reversibility, although without reaching stoichiometric reaction extents [176]. Redox kinetics of the $(Mn_{0.8}Fe_{0.2})_2O_3/(Mn_{0.8}Fe_{0.2})_3O_4$ couple were evaluated using dynamic and isothermal TGA experiments finding that both reactions follow nucleation and growth kinetic mechanism [205]. Crystallographic transitions were investigated via in situ X-ray diffraction, which revealed the presence of two spinel polymorphs (cubic jacobsite and tetragonal hausmannite) in the reduced form (Fig. 19d) [205]. Furthermore, Carrillo et al. proposed, based on Raman spectroscopy analyses, that a plausible reason for oxidation kinetic improvement was an enlargement of Mn-O distance caused by the presence of Fe in the crystal lattice, that eventually facilitated bond rearrangement during the cationic diffusion involved in the oxidation of Mn^{2+} cations [205]. Metal co-doping with both Cu-Fe was further investigated to diminish the hysteresis gap, finding a synergetic effect in which Fe increases the oxidation temperature and Cu lowers the temperature at which reduction takes place [208].

Recently, Wokon et al. elaborated a profound thermodynamic and kinetic analysis of the $(Mn_{0.75}Fe_{0.25})_2O_3/(Mn_{0.75}Fe_{0.25})_3O_4$ redox couple, using both a thermobalance and a fixed-bed reactor [206,207]. Authors reported the highest energy storage density for the Fe-doped Mn oxides, 271 kJ kg^{-1}, and remarkably stable redox reversibility over 100 cycles (Fig. 19b). Their kinetic

analyses also reported a nucleation and growth mechanism in accordance with work by Carrillo et al. [205,206]. Besides, both works reported an interesting kinetic feature occurring in several oxidation reactions of metal oxides. It has been observed that rate slowdown is experienced at high temperatures, while the system follows Arrhenius-temperature dependency at temperatures far from equilibrium [205,206]. In summary, these latest results support Fe-doped Mn oxides as one of the most promising redox couple for TCS due to the abundancy of the raw elements, not-toxicity, low-cost, increased energy storage density, fast reduction and oxidation kinetics and notable structural and chemical stability over prolong cycling operation. However, due to its still low energy storage density, can be less attractive than other systems such those based on cobalt oxide. In addition, mechanical stability can also be an issue as recently demonstrated by Preisner et al.[209] who evaluated CeO_2, ZrO_2 and TiO_2 as supports in order to improve the resistance to particle attrition. They found that the best particle stability was obtained for ZrO_2 or CeO_2 supports, whereas TiO_2 addition formed pseudobrookite phase leading to material deactivation.

Mixed oxides of Mn with well-defined stoichiometry have been also proposed as alternative for TCS applications. A novel redox scheme based on Li-Mn spinels has been proposed by Varsano et al. [210]. These works under the reaction shown in Eq. 19, and presents an experimental energy storage density of ca. 200 kJ per kg of $LiMnO_2$ [210]. Reduction proceeded at 970 ºC, whereas oxidation at 886 ºC, illustrating a narrow hysteresis gap. In addition, redox reversibility was confirmed over 45 cycles, revealing the promise of this system in this first assessment. More recently, Hlongwa et al. evaluated the redox properties of Li-Mn-spinels, finding that under low pO_2 (~$5 \cdot 10^{-3}$ bars) reduction the reaction proceeds by Eq. 20 [211].

$$Li_2MnO_3 + LiMn_2O_4 + \Delta H_r \leftrightarrow 3LiMnO_2 + + {}^1/_2\, O_2(g) \quad (19)$$

$$LiMn_2O_4 + \Delta H_r \leftrightarrow LiMnO_2 + {}^1/_3\, 3Mn_3O_4 + {}^1/_3\, O_2(g) \quad (20)$$

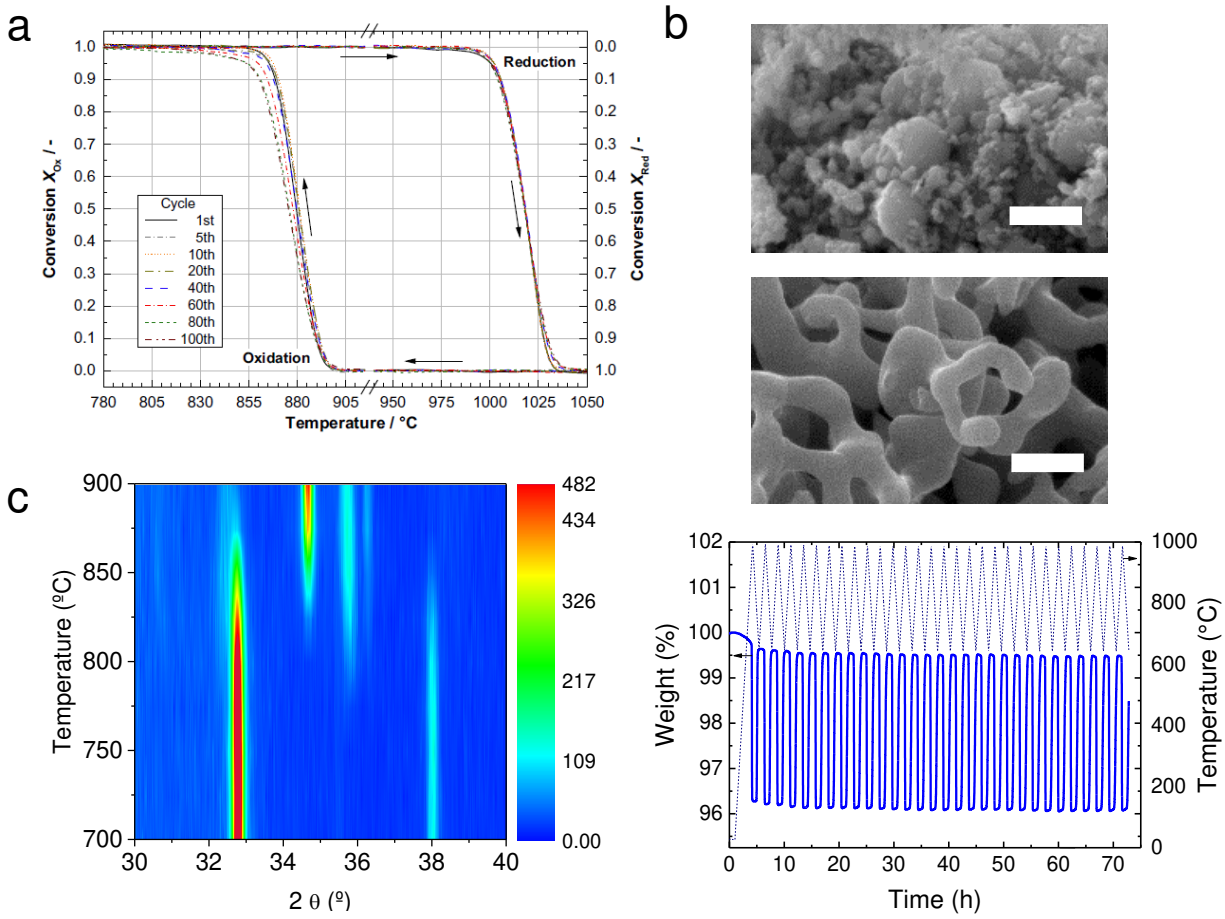

Figure 19. (a) Conversion vs. temperature plot for 100 cycles performed to the redox couple $(Mn_{0.75}Fe_{0.25})_3O_4/(Mn_{0.75}Fe_{0.25})_3O_4$, illustrating the thermal hysteresis of reduction/oxidation reactions. Reprinted from Solar Energy, 153, Michael Wokon,Tina Block,Sven Nicolai,Marc Linder,Martin Schmücker, Thermodynamic and kinetic investigation of a technical grade manganese-iron binary oxide for thermochemical energy storage, 471-485, Copyright (2017), with permission from Elsevier. (b) SEM micrographs of Mn_2O_3 material synthesized via precipitation with ammonia before (top) and after (middle) a 30-redox cycling test in TGA (bottom). Adapted from Ref [200], with permission of the Royal Society of Chemistry. The initial micron-size particles that formed aggregates of Mn_2O_3 powders suffered from remarkable coarsening and densification, resulting in open macro-porous sintered structures. Scale bar equal to 2 µm (c) Contour plot of an in situ XRD test, showing the crystallographic transition occurring in the reduction of $(Mn_{0.8}Fe_{0.2})_3O_4$ to $(Mn_{0.8}Fe_{0.2})_3O_4$. Adapted with permission from Carrillo, A. J.; Serrano, D. P.; Pizarro, P.; Coronado, J.

3.1.6. Perovskites

Perovskites are mixed-metal oxides of the form ABO_3, in which A is a large cation and B normally a transition metal cation of smaller size. Redox cycles of perovskites are currently subject of investigation for several energy-related applications, such as thermochemical solar fuel production [212], membranes for H_2 production [213] or CO_2 reforming [214], oxygen separation [215] or as oxygen carriers for chemical looping combustion [216,217]. The main difference between redox cycles of perovskites and stoichiometric metal oxides (as those described before) is that for perovskites reduction is accompanied by the creation of a limited amount of oxygen vacancies and generally not involve the formation of a different phase with well-defined stoichiometry. Accordingly, in contrast with stoichiometric oxides, perovskites do not show well-defined redox transition but, beyond a certain threshold temperature, which strongly depends on pO_2, exhibit a continuous, quasi-linear oxygen release/uptake within a very wide temperature range. This leads to a more gradual weight loss/gain during thermogravimetric experiments when compared to the sharp transitions of stoichiometric materials. During oxidation, such vacancies are re-occupied by oxygen anions through an exothermic reaction with the consequent release of heat. The amount of lattice oxygen released is also the extent of reaction and the non-stoichiometry of the reduced oxide, denoted as δ (Eq.21).

$$ABO_3 + \Delta H_r \leftrightarrow ABO_{3-\delta} + {}^{\delta}/_{2}\, O_2(g) \quad (21)$$

The fact that perovskites can perform redox cycles without suffering any crystallographic transition, as is the case of the redox couples described on previous sections, can be considered

advantageous. This directly affects to the materials longevity since crystal phase transformations imply also severe lattice reorganization that might be detrimental for the long-term stability.

Perovskites were proposed as TCS materials for high temperature applications by two projects launched in 2014 in the frame of the CSP ELEMENTS program. The projects are respectively led by Sandia National Laboratories and by Colorado School of Mines. Sandia researchers evaluated $La_xSr_{1-x}Co_yM_{1-y}O_{3-\delta}$ (M = Mn, Fe) perovskite materials as thermochemical energy storage media. More than 30 different compositions were analyzed via thermogravimetry, finding that $La_{0.3}Sr_{0.7}Co_{0.9}Mn_{0.1}O_{3-\delta}$ exhibited the higher enthalpy of reaction (250 kJ kg^{-1}) [218]. One of the most particular features of non-stoichiometric redox cycles based on perovskites is that the energy stored (and released) and the amount of oxygen vacancies created during the reduction step, δ, are proportional (see Fig. 20a).

Zhang et al. analyzed oxygen release and uptake from several compositions with Ba, Sr on the A-site and Mn, Co, Fe on the B-site. From all the materials tested on their study $BaCoO_{3-\delta}$ exhibited the highest reduction enthalpy (292.1 kJ kg^{-1}) [219]. Babiniec and co-workers further found Ti-doped Ca manganites to have a superior energy storage density if compared with Co-based perovskites at even lower values of δ. Namely, $CaTi_{0.2}Mn_{0.8}O_{3-\delta}$, shows 390 kJ kg^{-1} [220]. In addition, researchers from the Colorado School of Mines also analyzed experimentally the influence of A- and B-site doping of Ca manganites and probed that $Ca_{0.95}Sr_{0.05}MnO_{3-\delta}$ can store chemically 554.7 kJ kg^{-1} if reduced at 1000 ºC and $pO_2 = 10^{-4}$ bar [221]. Total energy storage density of 985 kJ kg^{-1} is reported when sensible heat storage contribution is also taken into account [221]. The TCS concept proposed by this group is depicted in Fig. 20b, aimed to be integrated with thermodynamic cycles operating with supercritical CO_2. This system comprises a fluidized bed reactor (left –hand side), where perovskite particles are oxidized and the heat generated (discharge

stage) is exchanged with the supercritical CO_2 used as HTF, and a solar receiver (top right-hand side, where the solid is heated and reduced (charging stage). In addition, the storage unit is also provided with two reservoirs for loading, respectively, the hot and cold perovskite, and a screw conveyor for moving the solid from the cold tank to the receiver. Therefore, circulation of the perovskite is achieved by combining gravity-assisted systems with pneumatic and mechanical impulsion. Imponenti et al. further tested the stability of Sr-doped Ca manganites over 1000 cycles, using a fixed-bed lab-scale reactor, demonstrating the high stability of perovskites materials over prolonged cycling [221,222]. More recently, Jackson et al. evaluated the impact of Sr-doped $CaMnO_3$ for TES versus inert oxide particles, such as Al_2O_3.[223] At temperatures lower than 800 ºC, matching supercritical CO_2 thermodynamic cycles, use of perovskite reactive particles helped in reduction of tank storage respect to the inert particles, which impacts on reducing costs[223].

These preliminary results illustrate the great potential of redox cycles Mn-based perovskites for thermochemical heat storage. The easy modulation of perovskite thermodynamic properties by addition of small quantities of dopants provides room for improving the thermochemical energy storage efficiency. Ideal perovskite candidates for the present application should present high oxygen release at temperatures below ~1000 ºC. In addition, the materials durability must be guaranteed, since segregation of phases is undesirable for stable energy charge/discharge operation. Computational methods are key for preliminary evaluation of potential perovskites due to the broad variety of chemical compositions. Based on data from thermodynamic libraries rules for designing more efficient materials can be established, as it was recently shown for solar-to-fuels production using data from CALPHAD [224] or Density Functional Theory (DFT) [225] or for Chemical Looping Combustion using Materials Project database [226].

In general, reduction and oxidation kinetics of perovskite materials are much faster than for stoichiometric redox couples (e.g. Mn_2O_3/Mn_3O_4, Co_3O_4/CoO), the reason being that O^{2-} diffusion in non-stoichiometric oxides is much faster than cationic diffusion in stoichiometric ones. Perovskite oxides can be re-oxidized in air within seconds [221], while re-oxidation of $(Mn_{0.8}Fe_{0.2})_3O_4$ takes around 10 min [205] and pure Mn_3O_4 can in some cases take more than one hour [161]. The easy recombination of reduced perovskites with gaseous O_2 poses several operational constraints of TCS using these systems. The solar-reduced perovskite phase must be stored under low pO_2 atmosphere to avoid precisely re-oxidation until heat released is required. This fact implies the use of sweep gas or vacuum in the storage tank, which increases operational costs. In fact, both alternatives are technologically feasible and the specific choice depend on economic considerations. Oxygen partial pressure lower than 10 Pa (0.1 mbar) requires medium and high-vacuum technologies, which are commonly used in industrial applications (for instance, steel degassing, vacuum induction melting, freeze drying or vacuum distillation). Use of sweep gas is constrained by the cost of the gas itself when it is released to the atmosphere or, if recycled, by the cost of auxiliaries for gas purification and cleaning. Traditionally, reduction of non-stoichiometric oxides has been performed under sweep gas in order to reach high δ values, which correlates with a higher energy density. However, Imponenti and co-authors have demonstrated that the reduction of Sr and Cr-doped calcium manganites can be performed also under O_2 rich atmospheres[227], although increasing pO_2 for the reduction also increases its transition temperature. Namely, for $CaCr_{0.1}Mn_{0.9}O_{3-\delta}$, reduction at $pO_2=10^{-4}$ bar occurs between 805-825 ^oC, whereas at $pO_2=0.17$ bar it increases up to 890-910 ^oC, coming also at the cost of a lower reduction extent. Very recently, Gokon et al. also demonstrated redox reversibility of $Ba_ySr_{1-y}CoO_{3-\delta}$ utilizing air in both the reduction and oxidation half-cycles, finding that with an A-site distribution of y=3 the material

stores 208.1 kJ kg^{-1} and releases an average of -163.4, kJ kg,[228-] which are values in the range of Mn oxides, although those elements, especially Co, are less abundant. Nevertheless, these promising results show that there is room for designing new perovskite materials that can be reduced under air, which represents a more cost-effective option than using a sweep gas or vacuum.

In summary, the use of perovskites for thermochemical energy storage seems prominent, especially due to the possibility of tuning materials in a broad range of chemical compositions, although research efforts are still at lab scale. Furthermore, research on perovskite materials for this particular subject can benefit from the experience of more mature research lines in which perovskites have been widely used at high temperature, such as solid oxide fuel cells (SOFC), thermochemical solar-to-fuel production and especially chemical-looping-combustion. From the research in these areas vast knowledge on thermodynamics, ionic diffusion, O_2 exchange kinetics and materials durability can be extracted and applied to TCS systems.

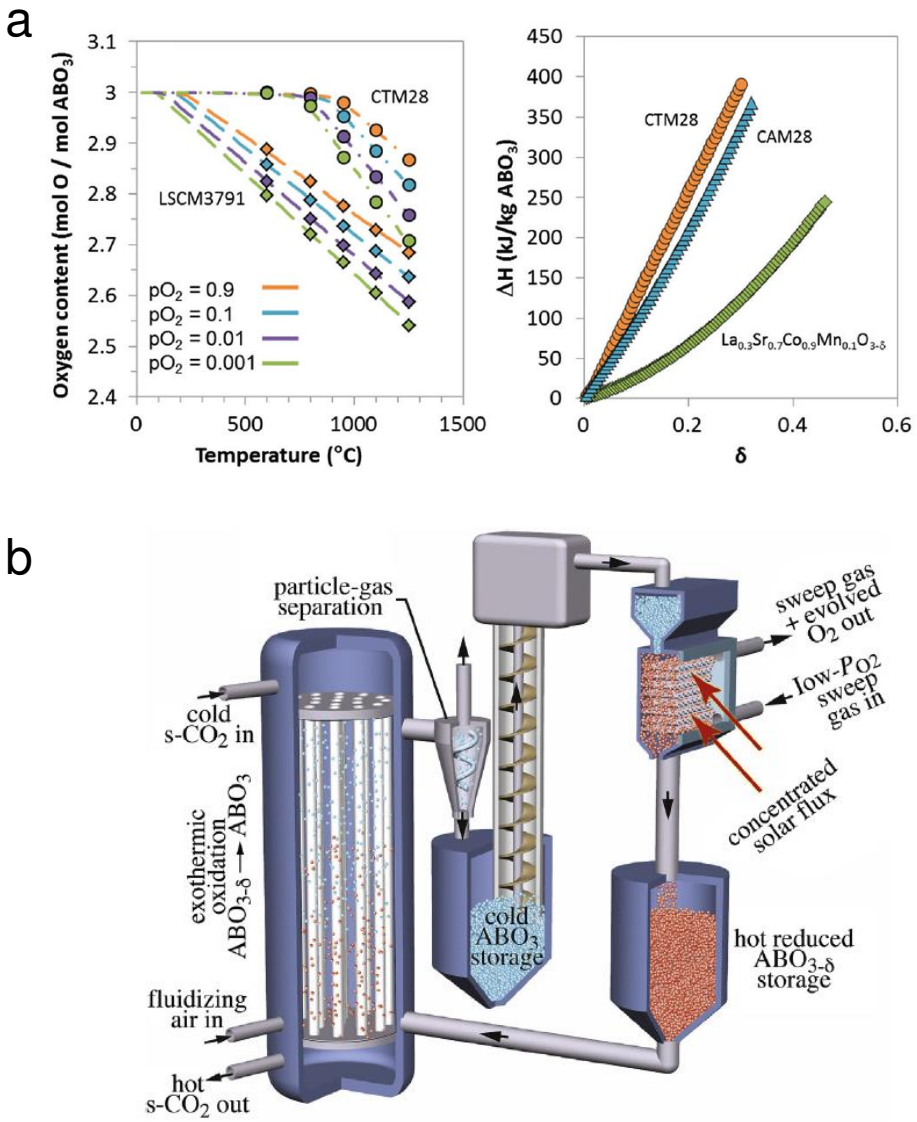

Figure 20. (a) Left, variation of the oxygen content with temperature for $La_{0.3}Sr_{0.7}Co_{0.9}Mn_{0.1}O_{3-\delta}$ compared with $CaTi_{0.2}Mn_{0.8}O_{3-\delta}$. Right, Dependence of the thermochemical energy storage density of three perovskites with the extent of reduction, δ. Reproduced from Ref [220] with permission of John Wiley & Sons, Inc. (b) Scheme of TCS system working with perovskites, which consists of two reactors, a directly irradiated falling particle receiver in which reduction at low pO_2 is performed, and a fluidized bed in which energy is released by re-oxidizing the perovskite with air. This unit operates also as a heat exchanger, since the exothermic reaction is used to heat supercritical CO_2, the heat transfer fluid that will drive the power block. Reprinted from Solar Energy, 151, Luca Imponenti,Kevin J. Albrecht,Jake W. Wands,Michael D. Sanders,Gregory S. Jackson, Thermochemical energy storage in strontium-doped calcium manganites for concentrating solar power applications, 1-13, Copyright (2017), with permission from Elsevier.

Table 4 summarizes the most promising redox candidates for high temperature thermochemical heat storage. In this section, materials aspects of state-of-the-art redox-based thermochemical storage systems have been analysed. On the following sections, reactor concepts and their integration in CSP plants will be discussed.

Table 4. Most promising redox TCS systems (*exp*=experimental; *the*=theoretical[151]). *These values do not take into account the sensible heat storage contributions of these oxide materials.

Reaction	Temperature, onset red./ox. (ºC)	Energy storage density* (kJ kg^{-1})	Max. No. cycles	Reference
$2\,BaO_2 \rightarrow 2\,BaO + O_2$	714/704 (885 *the.*)	474 (390 *exp*)	30 TGA	[156]
$2\,Co_3O_4 \rightarrow 6\,CoO + O_2$	943/927	844 (576 *exp*[161])	116; Fixed-bed reactor,Co_3O_4 honeycombs	[229]
$LiMn_2O_4 + Li_2MnO_3 \rightarrow 3LiMnO_2 + 0.5O_2$	970/886	~200 (*exp*)	45 TGA	[210]
$6\,(Mn_{0.75}Fe_{0.25})_2O_3 \rightarrow 4\,(Mn_{0.75}Fe_{0.25})_3O_4 + O_2$	990/895	271 (*exp*)	100 TGA	[206]
$Ca_{0.95}Sr_{0.05}MnO_3 \rightarrow Ca_{0.95}Sr_{0.05}MnO_{2.7} + 0.15O_2$	1000/500	555	1000, packed bed reactor, pO_2 swing,	[222]
$4\,CuO \rightarrow 2\,Cu_2O + O_2$	1042/1021 [161]	811 (806 *exp*)	20, TGA, isothermal 950 ºC, pO_2 swing,	[162]
$6\,(Cu_{0.33}Fe_{0.67})_2O_3 \rightarrow 4\,(Cu_{0.33}Fe_{0.67})_3O_4 + O_2$	1037/1038	333 (*exp*)	3 TGA	[161]
$(Mn_{0.33}Mg_{0.66})_3O_4 \rightarrow 3(Mn_{0.33}Mg_{0.66})O + 0.5O_2$	1500 (T_{max})	1070	10, fixed bed	[197]

3.2. Redox thermochemical heat storage reactor concepts and integration in concentrating solar power plants

3.2.1. Reactors types and experimental facilities

This section aims to provide the reader with a brief overview of current progress on reactors and experimental facilities utilized to evaluate the thermochemical heat storage systems described before. Contrarily to multicycle or kinetic evaluation of TCS materials using TGA or gram-scale lab reactors, literature encompassing development of pilot-scale TCS units is much scarcer. However, research in this ongoing activity is expected to grow faster on the next years due to the recent advances on materials development.

Table 5 shows a classification on traditional gas-solid reactors, their main advantages/disadvantages and other important parameters to take into consideration in the reactor selection. In principle, these type of reactors could be used for both the reduction and oxidation steps, although some particular configurations could be more advantageous for one of the reactions specifically. Here, it should be noted that some TCS integration concepts suggest the use of two independent reactors, especially when a directly-irradiated reactor is used for the reduction step. Thermochemical material features must also be accounted for. For instance, fluidized or moving bed reactors would be advisable for materials with low thermal conductivity and/or mass diffusivity (e.g. pure Mn_3O_4 pellets), since they promote gas-solid heat and mass transfer.

TCS reactors are also classified into directly-irradiated and indirectly-heated depending on whether storing medium absorbs solar radiation or not. In the first type, sun radiation is concentrated by the heliostats and, then directly focused on the reactor cavity. Such reactor consists of a ceramic cavity in which the redox material is placed and, normally, a quartz window that is

transparent in a wide range and it allows solar radiation to heat the reactant oxide. In this case. optical properties of the TCS material (e.g. absorptance and emissivity) can be also relevant to determine the operation temperature at a fixed irradiance and, then, the efficiency of the process. Conversely, in indirectly irradiated configurations charging proceeds by the heat transmission between a heat transfer fluid (air or, exceptionally sweep inert gas when a decrease on temperature is sought or low pO_2 is required to drive the reduction) and the oxide. In lab-scale experimental facilities this fact implies the incorporation of a pre-heating unit that brings the air flow to the require reduction temperature of the TCS system before it arrives to the reaction chamber[68,207,229]. In the following, redox reactors and lab-scale units commissioned to date will be described attending to such classification.

Table 5. Conventional gas-solid reactor concepts. Adapted from Ref. [68].

Reactor concept	Types	Particle size (mm)	Volume changes	Thermal conductivity	Disadvantages	Advantages	Application on redox thermochemical heat storage
Fixed bed	Direct/indirect contact reactor	> 2	Difficult to handle Big impact in reaction kinetic and process control	Direct contact: It can be low Indirect contact: It has to be improved by chemical modification of TCS material and by reactor design	Reaction kinetics is critical for load and unloading power with particle sizes in the upper range.	Low abrasion and attrition	Fixed bed reactor for $(Mn_{0.75}Fe_{0.25})_2O_3/(Mn_{0.75}Fe_{0.25})_3O_4$.; (~500 g)[207] Hybrid system Co_3O_4 honeycombs 90 kg[230]
Fluidized bed	Fluidized bed, pneumatic transport reactor, circulating fluidized bed, spouted, stage bed	< 1	Do not have much effect	Fluidizing improves the heat transfer coefficient	Impact of particle attrition, higher in circulating and pneumatic reactors Recovery of fines	Temperature uniformity Good heat transfer Improved gas/solid phase contact	Fluidized bed of 2.25 kg of Mn_2O_3[68]

Moving bed	Gravity assisted (vertical column, slit type, roof type), agitation assisted (rotary kiln, screw)	Wide range	Not beneficial	Improved by mixing effect	Agitation assisted reactor have temperature sensitive moving parts. Recovery of fines	Gravity assisted: soft impact of particle attrition Ability to continuously remove particles.	Directly irradiated rotary kiln with 250 g Co_3O_4[67] Directly irradiated rotary kiln with 10 g CuO[231,232]

Directly-irradiated reactors

First demonstration on redox Co_3O_4/CoO, thermochemical heat storage was reported by the experimental work described by Neises et al., utilizing a directly-irradiated solar rotary kiln (Fig. 21a) [67]. Redox reversibility was tested over 30 redox cycles and monitoring O_2 concentration. Results evidenced high material (95% Co_3O_4 mixed with 5% Al_2O_3) stability, proving the viability of such reactor configuration for Co-based TCS [67]. A numerical model that described the behavior of such reactor was further developed by Tescari et al. and validated with experimental results [233]. A falling particle receiver reactor was proposed in the frame of the PROMOTES project funded by the SunShot initiative [234]. Schrader modeled a $5kW_{th}$ reactor consisting in a gravity-assisted moving bed of Co_3O_4 particles, which are reduced by the sun radiation leaving the reactor as a CoO particle flow. Authors reported design parameters for optimum operation, resulting in 1112 ºC average outlet temperature [234].

The Cu-based redox couple was also tested experimentally with a directly-irradiated rotary kiln solar reactor (Fig. 21f-g) using the HoSIER solar furnace at IER-UNAM in Mexico [231,232]. With such configuration, the authors managed a proper thermal control on the reaction chamber avoid particle melting. Reported reduction conversion achieved 80% under Ar atmosphere. Additionally, redox cycles performed under air showed lower conversions, which were decreased cycle-to-cycle [231]. They further tested the reactor under non-rotational operation conditions, finding that such configuration performed worse than the rotary one. Namely, in such mode and with rather fast heating rates the front part of the copper oxide monolith suffered from melting and at low heating rates from severe thermal gradients. The use of rotary kilns for solar thermal applications was recently reviewed by Alonso et al. [235]. Moving beds have the benefit of better

contact of gas and solid phases, however, present challenges related to materials temperature acquisition, resulting less attractive for more fundamental studies [207]. For more detailed information about directly-irradiated reactors (receivers) we refer to the reviews by Ho[236,237].

Indirectly-heated reactors

The cobalt-based redox system has also been evaluated under a hybrid concept that couples sensible and thermochemical heat storage using cordierite honeycombs (Fig. 21b-c) [230]. This experimental work, carried out by the German Aerospace Center (DLR), was the first demonstration of thermochemical heat storage system in a pilot-plant. Such thermochemical heat storage system was commissioned at the Jülich Solar Tower in Germany [18]. The pilot-plant features a 90 kg-reactive phase (Co_3O_4) honeycomb-type reactor (Fig. 21b-c). This system additionally exploits the sensible heat storage capacity of the cordierite honeycomb, which is the main storage system operating in Jülich, and, in addition, the sensible heat of the Co_3O_4 reactant particles. Through this review paper we have generally only refer to the thermochemical heat storage capacity of the described materials, nevertheless, due to changes in temperature they also store sensible heat, which in some cases can represent a larger portion of the stored energy than the thermochemical one due to the high temperatures of operation [238]. Tescari et al. evaluated this system under a 22-cycle experimental campaign in which reaction conversion values were stable [238]. They further evidenced the exploitation of this hybrid system by comparison with an un-coated cordierite unit, which showed less storage capacity (25.3 kWh) than the Co_3O_4–coated one (47.0 kWh). Interestingly, numerical modelling assessments suggested a parabolic temperature distribution, which in turn caused the reaction to be delayed at the sides of the honeycomb respect to the center [239]. In summary, these highly promising preliminary results suppose a breakthrough in the field and will surely pave the route for TCS reactor up-scaling and incorporation in

demonstration, or future commercial CSP plants working with volumetric air receivers. Additionally, Agrafiotis et al. have suggested coupling of honeycombs coated with different oxide reactive materials, viz. Co_3O_4 and Mn_2O_3, in a novel *Cascaded Thermo-chemical Storage* [160,202]. This concept benefits from the different reduction temperatures that each of these redox couples present, by ordering them by increasing transition point from the low to the high temperature end. Hot air introduced into the first TCS unit of the cascade will trigger the reduction of such oxide, leaving that zone at temperatures still elevated to trigger the reduction of the second oxide with a lower transition temperature. Experimental tests at lab-scale have confirmed the proof-of-concept of this novel approach [160,202]. DLR researchers were also involved in experimental tests of a fixed bed reactor, in which 500 g of $(Mn_{0.75}Fe_{0.25})_2O_3$ granulates (~3 mm particle size) were assayed [207]. Stable reaction reversibility was observed for 17 cycles, although the granulates exhibited low mechanical strength upon cycling due to particle sintering [207]. Importantly, authors found that charging and discharging were limited by the rate at which heat was transfer into the solid and dissipated, respectively, most likely due to the poor thermal conductivity of the active material [207].

Indirectly-heated fluidized TCS reactors have been also subject of study for assessing pure Mn-oxide performance. Álvarez de Miguel et al. developed a 100-Wh multi-purpose TCS reactor in the frame of the EU-FP7 TCSPower project [68]. The design allowed working under both fixed-bed or fluidized-bed configurations (Fig. 21d-e). Authors further assessed the heat transfer characteristics in packed bed mode, developing a three-dimensional numerical model that was corroborated with experimental data [240].

This sub-section has explored current state of the art on reactors for redox-based TCS. The reader is encouraged to revisit the section 2 in which other designs using other chemical reactions

are described in order to have a broader picture of implications that other features such as higher pressures, gas-separation or agglomeration may have on reactor design and development.

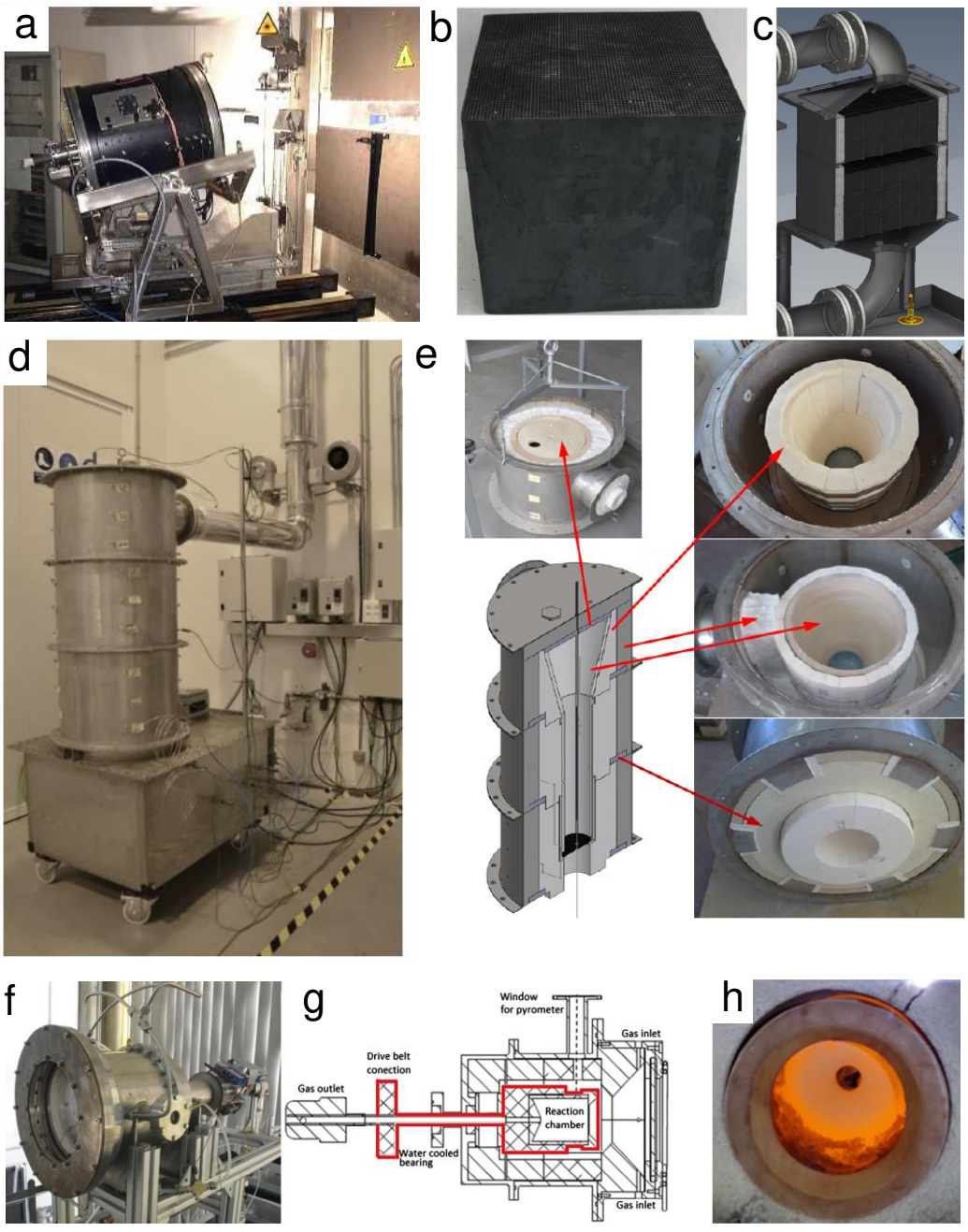

Figure 21. (a) Directly irradiated rotary kiln used for experimental characterization of Co oxides for TCS. Reprinted from Solar Energy, 86, M. Neises,S. Tescari,L. de Oliveira,M. Roeb,C. Sattler,B. Wong, Solar-heated rotary kiln for thermochemical energy storage, 3040-3048, Copyright (2012), with permission from Elsevier. (b) Co oxide-coated cordierite honeycomb and (c)

3D model of a TCS unit utilizing Co oxide coated honeycombs. Reprinted from Applied Energy, 189, Experimental evaluation of a pilot-scale thermochemical storage system for a concentrated solar power plant, S. Tescari, A. Singh, C. Agrafiotis, L. de Oliveira, S. Breuer, B. Schlögl-Knothe, M. Roeb, C. Sattler, 66-75, Copyright (2017), with permission of Elsevier. (d-e) Fluidized-bed reactor developed for testing Mn_2O_3 granulates for TCS applications Reprinted from Ref 174, with the permission of AIP Publishing. (f-g) Solar-driven rotary kiln used for testing copper oxides for TCS. (h) Reaction chamber after thermal treatment. Reprinted from Solar Energy, 115, Elisa Alonso, Carlos Pérez-Rábago, Javier Licurgo, Edward Fuentealba, Claudio A. Estrada, First experimental studies of solar redox reactions of copper oxides for thermochemical energy storage, 297-305, Copyright (2015), with permission from Elsevier.

3.2.2. Integration concepts and operation modes

This subsection addresses the different options for TCS system integration in CSP plants, and their viability analysis. Such studies explore how TCS units can be coupled with the other main components of a solar thermal power plant in the most efficient way, namely, how to integrate the storage unit with the solar field and the power block. Importantly the thermodynamic cycle of choice (Rankine, Brayton, etc.) has a direct impact in the operational temperatures of the TCS system. The way in which TCS media collects solar energy and its possible role as heat transfer fluid are also relevant aspects in the system integration. Additionally, CSP plants can incorporate one or several TCS reactors depending on storage medium and chemistry involved in the charging and discharging stages. For instance, TCS based on redox reactions could consider, if judged necessary, two different reactors, one for reduction and another for oxidation. As discussed in previous sections, some TCS reactors are meant to be *directly irradiated* with solar energy. This brings the concept of a reactor/receiver in which the solid oxide particles are reduced by the direct absorption of concentrated solar radiation coming from the solar field [222,234] (this concept is exemplified in Fig. 20b for the specific case of thermal storage with perovskite materials). Such a concept also implies conveying the solid particles from *directly irradiated* reduction reactor to the oxidation unit inside the plant. Therefore, this integration leads to the transport of the heat

storage medium or an active-type thermal storage system. In that case, the raise in temperature experienced by the TCS material during charging is driven by exchanging heat with the HTF (for example, air that was previously heated in the volumetric air receiver located on the top of the tower). In such type of reactors, the characteristics of the redox material and the reactor design chosen for storing solar energy have direct implications on the integration modes. The most comprehensive and deep study of this kind was elaborated by Ströhle et al.[238] Their relevant findings demonstrated that the actual reactor configuration (strongly correlated with the storing media particle size), influences both the optimum integration mode and the performance of the power plant, utilizing as TCS media the redox couple Mn_2O_3/Mn_3O_4.

Integration modes for passive reactors

According to Ströhle et al., a TCS unit can be incorporated to a CSP plant in either *parallel* or *serial* configurations. In the first arrangement, the HTF flow coming from the solar field is split into two streams, one directed to the TCS unit and the other to the power block (Fig. 22a). In the second configuration, the total HTF flows through both units. Ströhle and coworkers claimed that serial configuration is more suitable for fluidized bed reactors and parallel one will be ideal for packed bed reactors, illustrating the influence that the contacting pattern has on the TCS reactor integration. The main differences arise from the temperature distribution for each reactor configuration. In the case of packed-bed, the HTF outlet temperature matches well with the temperature at which the HTF exits the power block, guaranteeing low exergy losses in the mixing. On the other hand, due to faster gas-solid heat exchange and temperature spatial uniformity in a fluidized bed, the reactor outlet temperature is higher than the power block one, suggesting that

the HTF leaving the TCS unit should be directed to the power block. This indicates that serial configuration is the most appropriate for that type of reactors.

Analysis of packed bed reactors using Mn-oxide particles pointed out that thermochemical heat contributes in 14% of the total energy storage and the remaining stored heat was due to the sensible heat storage capacity of the Mn-oxide particles. Conversely, in the fluidized bed reactor, which exhibited 11% less energy storage density, all the Mn-oxide particles react due to enhanced mixing and gas-solid contact pattern, implying that the thermochemical portion of the total energy storage density was 64% [238]. In addition, parallel configuration shows higher flexibility on temperate and HTF flow adjustment, and with a packed bed enhanced, volumetric energy storage density due to lower presence of voids, i.e. less bed porosity, which makes this combination the ideal candidate for integration when considering indirectly-heated systems. However, the fact that just 14% of the heat storage of the redox couple Mn_2O_3/Mn_3O_4 accounts for chemical reaction suggests that Mn oxide particles that do not contribute to the reaction could be replace by cheaper inert solid particles used for sensible heat storage [238]. Motivated by this result, Ströhle et al. further proposed a sensible/thermochemical hybrid packed-bed concept as illustrated in Fig. 22b [241]. Here the thermochemical storage material composed of Mn_2O_3/Mn_3O_4 particles fill tubes located on top of the reactor and oxygen pressure adjustment in the tubes controls the redox reaction and then the TES working temperature. The remaining volume of the reactor is filled with inexpensive sensible storage media, such a pack bed of rocks. Use of oxygen partial pressure increases operation flexibility but at the expense of higher exergy losses driven by the need of pumping for controlling the TCS pressure [241].

Other TES concepts that involve hybridization of different thermal heat modes (sensible, latent or thermochemical) have been already mentioned through this review. In section 3.1.2,

Jafarian et al. reported sensible-latent-thermochemical heat storage system based on (molten) copper oxides [164]. In section 3.2.1, Agrafiotis et al. proposed cascade redox systems benefiting from the progressively decreasing transition temperatures of different metal oxide redox couples [242]. Bulfin et al. also suggested that some perovskite materials with low specific energy storage might be useful in a cascade configuration since those materials could work at ca. 400 ºC, compatible with other oxide pairs with increasing working temperatures.[243]

A novel hybridization concept has explored the combination of solar-driven steam-methane reforming and redox thermochemical storage based on redox cycles of cobalt oxides [244]. In their approach, Pantoleontos and co-workers integrate the TCS system for providing the energy requirements for the off-sun operation of the reforming reaction (highly endothermic, see section 2.2), which is the main commercial technology for production of H_2. This interesting work shows the potential of TCS systems to be coupled with other chemical process occurring at high temperature that could lead to their optimization and increase of overall energy efficiency.

Charging operation modes and directly-irradiated integration

One of the critical aspects when considering one redox pair or another is the maximum temperature needed for driving the endothermic reduction reaction, that is, the charge step. Relying on this fact, two main strategies could be applied if the reduction temperature of a specific redox couple needs to be lowered due to operational constraints. Namely, those are (1) working under vacuum pressure or (2) reducing the oxygen partial pressure ($pO_2 = 10^{-4}$ bar) [222] by using a sweep inert gas such as nitrogen or argon. The latter was chosen by Albrecht et al. for their thermodynamic modelling of perovskite-based storage system [245]. In that particular case, low pO_2 is required for reaching high levels of reduction extent (δ) that directly correlates with the heat stored. The novelty of that work

also resides on utilizing a defect chemistry model for extracting thermodynamic data. That was applied later for TCS system thermodynamic calculations and exergy assessment. Albrecht and co-workers found that the main source of exergy destruction was the oxidation reactor mainly driven by temperature gap between reduction and oxidation reactions [245]. A similar concept was proposed by Schrader et al., for the integration of directly-heated Co-based TCS system in a CSP plant coupled to an Air Brayton cycle [246]. They suggested a *directly-irradiated* falling-particle receiver type of reactor for carrying out the reduction step (Fig.22c-d). In this case, reduction is performed under low pressure by using vacuum pumping, favoring in this manner working under lower temperatures. They reported a maximum cycle efficiency of 44%, given that the temperature of the solar-thermochemical reactor during reduction is ca. 780 ºC and outlet pressure of the compressor is 30 bar [246].

Haseli et al. assessed the integration of Chemical Looping for Air Separation (CLAS) system based on CuO/Cu_2O redox reactions (with $MgAl_2O_4$ as inert support) into a CSP plant, also considering a two-reactor system [247]. This hybrid concept will couple the production of pure O_2 obtained by the reduction of a metal oxide, and the production of energy in the subsequent oxidation of the reduced metal oxide with air. One of the particularities of the CLAS concept is that steam is used as carrier gas for the reduction step, since it would allow an easy separation of the oxygen generated during the reduction and the steam simply by condensation. Obviously, the high-temperature stability of metal oxides under steam atmospheres is key for guaranteeing the feasibility of the process. Haseli et al. specifically chose the CuO/Cu_2O redox pair due to the both its high chemical energy storage and oxygen exchange capacity, reason why these materials have been widely studied for chemical looping combustion. They suggest the use of steam as sweep gas for the reduction because it can ease O_2 separation due to the facile condensation of water vapor.

Their simulations estimated a 41% of net efficiency of the overall process, 81% of energy storage refer to solar input, from which 26% was the chemical storage portion and a production of 0.023 m^3 O_2/MJ solar input [247]. This interesting concept widens the scope of thermochemical redox energy storage, making use of the oxygen generated during the reduction step. However, long-term experimental proof of metal oxide stability under high temperature steam atmospheres should be provided, since sintering can be promoted by steam.

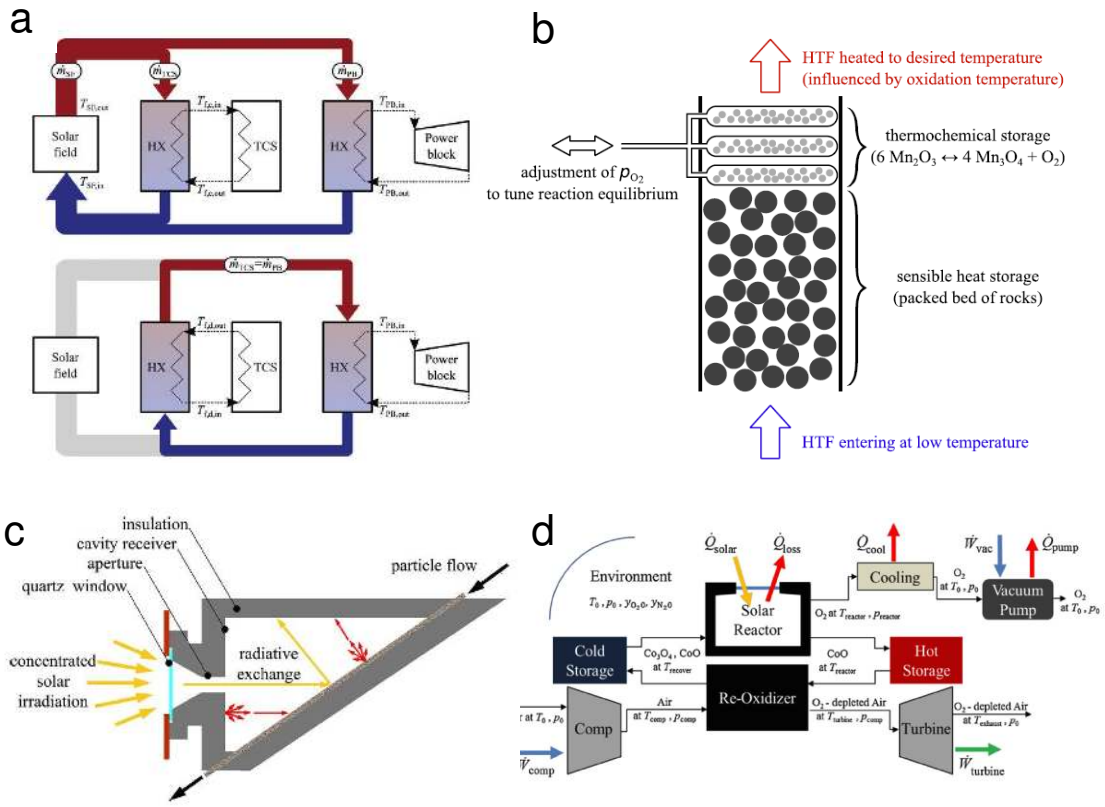

Figure 22. (a) Integration of a TCS system in parallel. The top schematic represent operation during on sun periods (charge) and the bottom during off sun (discharge). Reproduced from Ref [238] with permission of The Royal Society of Chemistry. (b) Sensible/thermochemical hybrid storage concept. Reprinted from Applied Energy, 196, S. Ströhle, A. Haselbacher, Z.R. Jovanovic, A. Steinfeld, 51-61, Copyright (2017) with permission from Elsevier (c) Schematic of a directly-irradiated solar reactor falling-particle receiver type to be integrated in flow diagram depicted in (d). Reprinted from Solar Energy,150, Andrew J. Schrader, Gianmarco De Dominicis, Garrett L. Schieber, Peter G. Loutzenhiser, 584-595 Copyright (2017) and Solar

This section has reviewed the stimulating, but still scarce, research related with integration analysis of TCS systems in CSP plants. We aim to provide the reader with a general perspective of the multi-scale nature on TCS comprising materials; reactor and integration research activities and illustrate their interplay of these different aspects. Despite the promise of these initial assessments of integration and new hybridization concepts that are laying the foundation of this activity, the field still feels the absence of detailed techno-economic evaluations that provide guidelines for process implementation, and eventually facilitate the integration of these systems in the CSP market.

3.3. Techno-economic assessments

Techno-economic assessments on TCS are very scarce. The work commented in section 2.2 by Peng et al. dealt with the techno-economic viability of thermochemical heat storage based on gas-gas reactions (ammonia synthesis and steam reforming of methane) [20]. Their study proved the high economic and energetic costs that reactions involving gas storage pose on CSP plants working with thermochemical heat storage. Recently, Bayón et al. reported a detailed assessment on gas-solid reactions encompassing the use of carbonates, hydroxides and oxides, benchmarked with molten salts [26]. Additionally, they included redox reactions involving chemical looping cycles, in which the reduction step entails the combustion of methane. These authors elaborated a comparison of those systems based on the total capital cost values and discharge temperatures, which is depicted in Fig. 23. This graph illustrates which thermal energy storage option would be optimal for a specific power cycle, depending on the discharge temperature. This fact emphasizes again the importance of determining experimentally the discharging temperature for many of the

reversible systems in which a hysteresis is observed between reduction and oxidation temperatures. Namely, in Fig. 23, Mn oxide discharging temperature, which will be the pair Mn_2O_3/Mn_3O_4, lies on the section in which CO_2 supercritical will be the most adequate power cycle. However, Fe-doped Mn-oxides, namely, $(Mn_{0.8}Fe_{0.2})_2O_3$/ $(Mn_{0.8}Fe_{0.2})_3O_4$, which exhibits an experimentally discharging temperature of ca. 880 ºC[204] matches better the Brayton cycle.[26] According to the data of Fig.23, the most promising reactions for Rankine steam cycles were those based the hydroxides $Ca(OH)_2$ (total capital cost, 4.78 \$ MJ^{-1}), $Sr(OH)_2$ (7.09 \$ MJ^{-1}) and $Ba(OH)_2$ (8.28 \$ MJ^{-1}). In the temperature range of potential use for supercritical CO_2 cycles, $CaCO_3/CaO$ (15.09 \$ MJ^{-1}) and BaO_2/BaO thermochemical cycles are the most economic options (23.93 \$ MJ^{-1}), whereas for Air Brayton or combined cycle, those are the carbonate system $SrCO_3/SrO$ (22.74 \$ MJ^{-1}). Chemical looping combustion (CLC) of methane reactions involving Fe_3O_4/FeO (18.87 \$ MJ^{-1}) and NiO/Ni (24.01 \$ MJ^{-1}) [26] are also included for sake of comparison, and they present a competitive cost, although they are not within the main scope of the present review because they require the use of a fossil fuel. Importantly, this work paves the path for further techno-economic assessments, which seems crucial in order to evaluate the industrial feasibility of mixed metal oxides that have shown remarkable TCS performance, such as perovskites, Li-Mn spinels or Fe-doped Mn oxides.

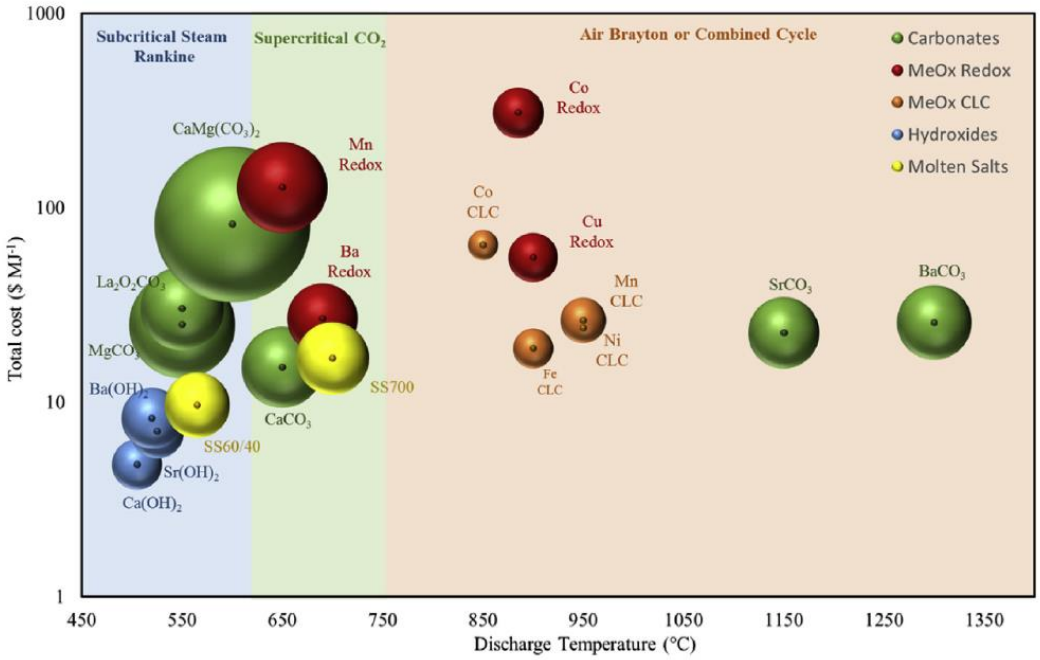

Figure 23. Total cost versus discharge temperature for the TCES systems evaluated in the techno-economic work. The size of the spheres represents the relative storage volume of the systems in L kWh_{th}^{-1}. Reprinted from Energy, 149, Bayon et al., Techno-economic assessment of solid–gas thermochemical energy storage systems for solar thermal power applications, 473-489, Copyright (2018), with permission from Elsevier.

3.4. Current challenges and future perspectives on redox systems

A great number of the research efforts summarized in this review have been successful in overcoming some of the main limitations of TCS, however this promising research field still encounters several challenges at all scales (materials, reactors and integration) that should be addressed by gaining further scientific insights on these systems in order to guarantee the feasibility of their commercial deployment. Some recommendations are provided below:

Predicting tools for identifying new redox pairs

Although the use of phase diagrams has been found to be an excellent predicting tool to understand phase transitions, such diagrams might be not sufficient to model or understand redox transformation in multicomponent systems in which more than two cations are involved. In this

respect, more efficient predicting tools should be elaborated, for instance, based on CALPHAD[197] or other thermodynamic libraries that could help in screening of promising redox candidates. Efforts should be focused on finding redox pairs with higher energy storage densities (chemical plus sensible) of ca. 1000 kJ kg^{-1} that could compete with carbonates or hydrides working at similar temperatures. Furthermore, low hysteresis temperature gaps should be ensured for guaranteeing high exergy efficiencies. On the other hand, selection of adequate materials based on thermodynamic criteria does not preclude further kinetic analysis to establish the feasibility of using those systems in TCS.

Establishing guidelines and protocols for accurate extraction of TCS relevant data

Thermogravimetric analysis has been broadly used in assessing redox reversibility and determination of kinetic parameters. TGA instruments available in the market present diverse configurations (i. e. vertical or horizontal gas flows) that require specific calibration and of which measurements needs cautiously analysis before reporting kinetic and thermodynamic data. Otherwise it could be the source of parametric divergence when comparing studies performed to similar materials. Namely, some TGA configurations might pose physical hurdles to oxidation reactions, adding mass transfer limitations that are eventually lumped in the kinetic parameters [248]. For instance, it was recently proved the impact that using a down-flow versus an up-flow of oxidizing air has on the rate of oxidation of $(Mn_{0.8}Fe_{0.2})_3O_4$ [205]. Differential Scanning Calorimetry (DSC) assessments are undoubtedly the main source of discrepancy in the community. It is obvious that one of the most valuable metrics for TCS systems is the heat absorbed/released and, accordingly, researchers in the field should reach a consensus in order to elaborate guidelines for accurately determine the energy storage density. In addition to the heat of reaction, the actual chemical energy storage density should also provide data on the sensible heat accumulated by the

thermochemical materials, which in some cases can represent a higher contribution than the chemical part. Other parameters such as porosity, apparent density and the volume of the reactor should be also considered for higher accuracy in the numerical values.

Limitations for an accurate determination of the reaction enthalpies arise from different sources. It is clear that due to the nature of gas-solid reactions, DSC sample encapsulation or use of lids is not recommended for measuring the heat released during the exothermic oxidation. In addition, alumina crucibles are commonly used, exhibiting lower heat conductivity than Pt ones. Furthermore, some oxidation reactions are generally slow, which results in broad DSC peaks that difficult an accurate integration. It is advisable that the DSC (normally found as DSC-TGA simultaneous equipment) is properly calibrated by using the melting points of standard metal references (e.g. Zn, Ag), covering the entire redox temperature window. Alternatively, calibration with other compounds, such as $CaCO_3$, has been suggested for improving the accuracy of reaction enthalpy measurements of ceramic materials in order to account for its lower thermal conductivity .[222] Recent efforts have been performed in the form of *Round Robin* tests in the frame of the Solar PACES Task III. [249,250] These analyses highlight the need of calibration adapted to the temperature range at which chemical reaction proceeds. Besides, more accurate measurements coupling various techniques (e.g. thermogravimetric measurements and mass spectrometry) are necessary. Application of alternative methods, based on combination of drop and acid-solution calorimetry, rather than DSC, as the recently reported by King et al., could be relevant for further advancing in the field.[198]

Advanced experimental and computational techniques for understanding redox kinetic mechanisms

Additional computational tools and high resolution spectroscopic techniques should be brought to the field to provide more mechanistic insights on how metal doping is influencing reactions kinetics or stabilizing the microstructure of the redox materials. Density Functional Theory (DFT) has been successfully used in sister fields such as thermochemical solar-to-fuel[251,252] production or chemical looping combustion[253], assessing redox behavior of similar type of oxides. Incorporation of advanced *in situ/operando* spectroscopy techniques such as Raman, X-ray photoelectron spectroscopy (XPS) or X-ray adsorption spectroscopy, to the already explored use of *in situ* XRD would be crucial for obtaining valuable information of temperature-resolved materials crystallographic ordering, phenomena occurring at the oxide surface and oxidation state transition taking place during the redox trade. This feedback will be crucial for gaining a deeper understanding of the reduction/oxidation at the atomic level, which in turn might facilitate strategies to improve materials kinetics and multicycle chemical stability.

Reactor engineering and process up-scaling

Redox TCS engineering has currently achieved a technology readiness level between 3 and 4. In spite of this prompt level of success, there is still room for improving reactor reliability and storage performance. Lessons learnt in other research fields involving concentrating solar energy and high-temperature chemistry could also be successfully applied to this aim. In this respect, redox TCS could take advantage of the exciting progress experienced on solar-driven thermochemistry in terms of reactor technology (for instance, on syngas production for which reactor development has contributed in greatly increasing process efficiencies[254]), gas management and operation (working with reduction and oxidations stages or handling low oxygen partial

pressure). In addition to reactor design, which will be assisted by computational fluid dynamics tools, mechanical properties of selected redox materials should be enhanced. For instance, resistance to attrition in the case of Mn oxides cycled in fluidized bed reactors, or a better control of the thermal/chemical expansion upon cycling of Co oxide-based porous structures, by, for instance, chemical modifications and/or addition of structural support materials.

Progress on redox TCS will require focusing on upscaling on the basis of the evaluation of integration in CSP plants. Furthermore, these systems should confirm its viability in light of techno-economic analysis and life cycle assessment. Assessing the optimum way for incorporating of the various redox pairs available, or its hybridization with sensible heat storage units, as those reported by Ströhle et al.[238,241] will offer useful guidelines for the industrial implementation. Currently relevant techno-economic analyses are scarce in the literature. Evaluations as those recently performed by Peng et al.[20] and Bayon et al.[26] , that could point towards which technical aspects contribute to improve the energy efficiency or to increase plant costs.

4. Conclusions

This work presents a comprehensive review on main TCS systems, paying special attention to those used at high temperatures (500-1000 ºC) and based on redox reactions. Many technological options are currently feasible and only additional detailed economic assessments allows discerning the most suitable one for a specific plant design. Thermochemical storage systems based on ammonia dissociation, hydrides ($TiH_{1.7}$ and CaH_2) and carbonates ($CaCO_3$ and $SrCO_3$) have superior energy storage densities and, in most cases, involves inexpensive materials. However, these chemical systems faced kinetic and/or reversibility limitations and require gas storage, which adds complexity to the process and implies the incorporation equipment that might have to operate at high pressures, which in turn increases the plant cost. In this respect, redox-based TCS appears as an interesting alternative since it can be more easily implemented in future CSP plants working with volumetric air receivers. Recent research progress focused in developing more efficient materials and reactors has been noteworthy, reaching certain level of maturity with the preliminary implementation of Co oxide-based TCS system in the Solar Tower Jülich facility. The easy tunability of some of these redox materials by chemical modification can lead to new compositions that outperform the pure oxides, as demonstrated for doped Mn oxides and perovskites. Overall, these facts demonstrate the potential of redox-based thermochemical heat storage as an efficient thermal energy storage option for future CSP plants working with volumetric air receivers, eventually increasing the on-demand production of electricity generated by this renewable energy technology. However, there is still room for improving the materials performance, design more efficient reactors and evaluate more optimum integration strategies, which points towards the necessity of continuing with the research on this promising energy storage class, which can

ultimately lead to a reduction in CSP plant cost and an increase in the share of solar electricity production.

5. Acknowledgments

This work has been partially supported by the projects TCS Power of the FP7 (ENERGY.2011.2.5-1), MULTISTOR (ENE2012-36937) of the Spanish Ministry of Economy and Competitiveness, the Iberdrola Foundation through the Energy and Environmental Research Grants 2014-2015, SOLARKITE project from "Ramón Areces" Foundation, by STAGE-STE grant agreement n° 609837 (Scientific and Technological Alliance for Guaranteeing the European Excellence in Concentrating Solar Thermal Electricity, ENERGY.2013.10.1.10), ALCCONES project from "Comunidad de Madrid" and European Structural Funds for their financial support to (S2013/MAE-2985). AJC thanks the financial support by Juan de la Cierva Formación Program (MICINN).

6. References

(1) Lewis, N. S.; Nocera, D. G. Powering the Planet: Chemical Challenges in Solar Energy Utilization. *Proc. Natl. Acad. Sci.* **2006**, *103*, 15729–15735.

(2) REN21. *Renewables 2017: Global Status Report*; 2017; Vol. 72.

(3) Renewable Energy Policy Network for the 21st Century (REN21). Renewables 2015 Gobal Status Report. **2015**, 4–5.

(4) Weinstein, L. A.; Loomis, J.; Bhatia, B.; Bierman, D. M.; Wang, E. N.; Chen, G. Concentrating Solar Power. *Chem. Rev.* **2015**, *115*, 12797–12838.

(5) Romero, M.; Steinfeld, A. Concentrating Solar Thermal Power and Thermochemical Fuels. *Energy Environ. Sci.* **2012**, *5*, 9234–9245.

(6) Romero, M.; González-Aguilar, J. Solar Thermal CSP Technology. *Wiley Interdiscip. Rev. Energy Environ.* **2014**, *3*, 42–59.

(7) Feldman, D.; Margolis, R.; Denholm, P. Stekli, J. Exploring the Potential Competitiveness of Utility-Scale Photovoltaics plus Batteries with Concentrating Solar Power , 2015 – 2030. Technical Report NREL/TP-6A20-66592**. 2016**.

(8) Sawin J., Seyboth K., W. F. *Renewables 2017 Global Status Report*; 2017.

(9) Lilliestam, J.; Labordena, M.; Patt, A.; Pfenninger, S. Empirically Observed Learning Rates for Concentrating Solar Power and Their Responses to Regime Change. *Nat. Energy* **2017**, *2*, 17094.

(10) Santos, J. J. C. S.; Palacio, J. C. E.; Reyes, A. M. M.; Carvalho, M.; Freire, A. J. R.; Barone, M. A. Concentrating Solar Power. *Adv. Renew. Energies Power Technol.* **2018**, *1*, 373–402.

(11) IRENA. *Irena Power to Change 2016.*; 2016.

(12) Benoit, H.; Spreafico, L.; Gauthier, D.; Flamant, G. Review of Heat Transfer Fluids in Tube-Receivers Used in Concentrating Solar Thermal Systems: Properties and Heat Transfer Coefficients. *Renew. Sustain. Energy Rev.* **2016**, *55*, 298–315.

(13) Zhang, H.; Benoit, H.; Gauthier, D.; Degrève, J.; Baeyens, J.; López, I. P.; Hemati, M.; Flamant, G. Particle Circulation Loops in Solar Energy Capture and Storage: Gas–solid Flow and Heat Transfer Considerations. *Appl. Energy* **2016**, *161*, 206–224.

(14) Reyes-Belmonte, M. A.; Sebastián, A.; Romero, M.; González-Aguilar, J. Optimization of a Recompression Supercritical Carbon Dioxide Cycle for an Innovative Central Receiver Solar Power Plant. *Energy* **2016**, *112*, 17–27.

(15) SUN to LIQUID: Fuels from concentrated solar power http://www.sun-to-liquid.eu/

(16) Fend, T. High Porosity Materials as Volumetric Receivers for Solar Energetics. *Opt. Appl.* **2010**, *40*, 271–284.

(17) Ávila-Marín, A. L. Volumetric Receivers in Solar Thermal Power Plants with Central Receiver System Technology: A Review. *Sol. Energy* **2011**, *85*, 891–910.

(18) Zunft, S.; Hänel, M.; Krüger, M.; Dreißigacker, V.; Göhring, F.; Wahl, E. Jülich Solar Power Tower—Experimental Evaluation of the Storage Subsystem and Performance Calculation. *J. Sol. Energy Eng.* **2011**, *133*, 031019.

(19) Kuravi, S.; Trahan, J.; Goswami, D. Y.; Rahman, M. M.; Stefanakos, E. K. Thermal Energy Storage Technologies and Systems for Concentrating Solar Power Plants. *Prog. Energy Combust. Sci.* **2013**, *39*, 285–319.

(20) Peng, X.; Root, T. W.; Maravelias, C. T. Storing Solar Energy with Chemistry: The Role of

Thermochemical Storage in Concentrating Solar Power. *Green Chem.* **2017**, *19*, 2427–2438.

(21) Zu, C. X.; Li, H. Thermodynamic Analysis on Energy Densities of Batteries. *Energy Environ. Sci.* **2011**, *4*, 2614–2624.

(22) Zhang, H.; Baeyens, J.; Cáceres, G.; Degrève, J.; Lv, Y. Thermal Energy Storage: Recent Developments and Practical Aspects. *Prog. Energy Combust. Sci.* **2016**, *53*, 1–40.

(23) Gil, A.; Medrano, M.; Martorell, I.; Lázaro, A.; Dolado, P.; Zalba, B.; Cabeza, L. F. State of the Art on High Temperature Thermal Energy Storage for Power Generation. Part 1—Concepts, Materials and Modellization. *Renew. Sustain. Energy Rev.* **2010**, *14*, 31–55.

(24) Medrano, M.; Gil, A.; Martorell, I.; Potau, X.; Cabeza, L. F. State of the Art on High-Temperature Thermal Energy Storage for Power Generation. Part 2—Case Studies. *Renew. Sustain. Energy Rev.* **2010**, *14*, 56–72.

(25) Mehos, M.; Turchi, C.; Vidal, J.; Wagner, M.; Ma, Z.; Ho, C.; Kolb, W.; Andraka, C.; Alan Kruizenga. *Concentrating Solar Power Gen3 Demonstration Roadmap*; 2017.

(26) Bayon, A.; Bader, R.; Jafarian, M.; Fedunik-Hofman, L.; Sun, Y.; Hinkley, J.; Miller, S.; Lipiński, W. Techno-Economic Assessment of Solid–gas Thermochemical Energy Storage Systems for Solar Thermal Power Applications. *Energy* **2018**, *149*, 473–484.

(27) Concentrating Solar Power: Efficiently Leveraging Equilibrium Mechanisms for Engineering New Thermochemical Storage | Department of Energy http://energy.gov/eere/sunshot/concentrating-solar-power-efficiently-leveraging-equilibrium-mechanisms-engineering-new (accessed Dec 16, 2015).

(28) Fernandez, A. I.; Martínez, M.; Segarra, M.; Martorell, I.; Cabeza, L. F. Selection of

Materials with Potential in Sensible Thermal Energy Storage. *Sol. Energy Mater. Sol. Cells* **2010**, *94*, 1723–1729.

(29) Liu, M.; Steven Tay, N. H.; Bell, S.; Belusko, M.; Jacob, R.; Will, G.; Saman, W.; Bruno, F. Review on Concentrating Solar Power Plants and New Developments in High Temperature Thermal Energy Storage Technologies. *Renew. Sustain. Energy Rev.* **2016**, *53*, 1411–1432.

(30) Turchi, C. S.; Vidal, J.; Bauer, M. Molten Salt Power Towers Operating at 600–650 °C: Salt Selection and Cost Benefits. *Sol. Energy* **2018**, *164*, 38–46.

(31) Olivares, R. I.; Chen, C.; Wright, S. The Thermal Stability of Molten Lithium–Sodium–Potassium Carbonate and the Influence of Additives on the Melting Point. *J. Sol. Energy Eng.* **2012**, *134*, 041002.

(32) Ding, W.; Shi, H.; Jianu, A.; Xiu, Y.; Bonk, A.; Weisenburger, A.; Bauer, T. Molten Chloride Salts for next Generation Concentrated Solar Power Plants: Mitigation Strategies against Corrosion of Structural Materials. *Sol. Energy Mater. Sol. Cells* **2019**, *193*, 298–313.

(33) Mohan, G.; Venkataraman, M.; Gomez-Vidal, J.; Coventry, J. Thermo-Economic Analysis of High-Temperature Sensible Thermal Storage with Different Ternary Eutectic Alkali and Alkaline Earth Metal Chlorides. *Sol. Energy* **2018**, *176*, 350–357.

(34) Becattini, V.; Motmans, T.; Zappone, A.; Madonna, C.; Haselbacher, A.; Steinfeld, A. Experimental Investigation of the Thermal and Mechanical Stability of Rocks for High-Temperature Thermal-Energy Storage. *Appl. Energy* **2017**, *203*, 373–389.

(35) Calvet, N.; Gomez, J. C.; Faik, A.; Roddatis, V. V.; Meffre, A.; Glatzmaier, G. C.; Doppiu,

S.; Py, X. Compatibility of a Post-Industrial Ceramic with Nitrate Molten Salts for Use as Filler Material in a Thermocline Storage System. *Appl. Energy* **2013**, *109* , 387–393.

(36) Gutierrez, A.; Miró, L.; Gil, A.; Rodríguez-Aseguinolaza, J.; Barreneche, C.; Calvet, N.; Py, X.; Inés Fernández, A.; Grágeda, M.; Ushak, S.; et al. Advances in the Valorization of Waste and By-Product Materials as Thermal Energy Storage (TES) Materials. *Renew. Sustain. Energy Rev.* **2016**, *59*, 763–783.

(37) Felderhoff, M.; Urbanczyk, R.; Peil, S. Thermochemical Heat Storage for High Temperature Applications – A Review. *Green* **2013**, *3*, 113–123.

(38) Wu, J.; Long, X. feng. Research Progress of Solar Thermochemical Energy Storage. *Int. J. Energy Res.* **2015**, *39*, 869–888.

(39) Nomura, T.; Okinaka, N.; Akiyama, T. Technology of Latent Heat Storage for High Temperature Application: A Review. *ISIJ Int.* **2010**, *50*, 1229–1239.

(40) Khare, S.; Dell'Amico, M.; Knight, C.; McGarry, S. Selection of Materials for High Temperature Latent Heat Energy Storage. *Sol. Energy Mater. Sol. Cells* **2012**, *107*, 20–27.

(41) Qureshi, Z. A.; Ali, H. M.; Khushnood, S. Recent Advances on Thermal Conductivity Enhancement of Phase Change Materials for Energy Storage System: A Review. *Int. J. Heat Mass Transf.* **2018**, *127*, 838–856.

(42) Bellan, S.; Alam, T. E.; González-Aguilar, J.; Romero, M.; Rahman, M. M.; Goswami, D. Y.; Stefanakos, E. K. Numerical and Experimental Studies on Heat Transfer Characteristics of Thermal Energy Storage System Packed with Molten Salt PCM Capsules. *Appl. Therm. Eng.* **2015**, *90*, 970–979.

(43) Graham, M.; Shchukina, E.; Castro, P. F. De; Shchukin, D. Nanocapsules Containing Salt

Hydrate Phase Change Materials for Thermal Energy Storage. *J. Mater. Chem. A* **2016**, *4*, 16906–16912.

(44) Linder, M. *Advances in Thermal Energy Storage Systems*; Elsevier, 2015.

(45) Prengle, H. W.; Sun, C.-H. Operational Chemical Storage Cycles for Utilization of Solar Energy to Produce Heat or Electric Power. *Sol. Energy* **1976**, *18*, 561–567.

(46) Wentworth, W. E.; Chen, E. Simple Thermal Decomposition Reactions for Storage of Solar Thermal Energy. *Sol. Energy* **1976**, *18*, 205–214.

(47) Ervin, G. Solar Heat Storage Using Chemical Reactions. *J. Solid State Chem.* **1977**, *61*, 51–61.

(48) Fujii, I.; Tsuchiya, K. Experimental Study of Thermal Energy Storage by Use of Reversible Chemical Reactions. *Altern. Energy Sources, Vol. 9* **1978**, *9*, 4021–4035.

(49) Bowrey, R. G.; Jutsen, J. Energy Storage Using the Reversible Oxidation of Barium Oxide. *Sol. Energy* **1978**, *21*, 523–525.

(50) Prengle, H.; Hunt, J.; Mauk, C.; Sun, E. Solar Energy with Chemical Storage for Cogeneration of Electric Power and Heat. *Sol. Energy* **1980**, *24*, 373–384.

(51) Chubb, T. A. Analysis of Gas Dissociation Solar Thermal Power System. *Sol. Energy* **1975**, *17*, 129–136.

(52) Chubb, T. A.; Nemecek, J. J.; Simmons, D. E. Design of a Small Thermochemical Receiver for Solar Thermal Power. *Sol. Energy* **1979**, *23*, 217–221.

(53) Fahim, M. A.; Ford, J. D. Energy Storage Using the BaO_2/BaO Reaction Cycle. *Chem. Eng. J.* **1983**, *27*, 21–28.

(54) Chadda, D.; Ford, J. D.; Fahim, M. A. Chemical Energy Storage by the Reaction Cycle CuO/Cu_2O. *Int. J. Energy Res.* **1989**, *13*, 63–73.

(55) Ramade, S. M.; Lee, M.-C.; Prengle, H. W. Chemical Storage of Solar Energy Kinetics of Heterogeneous SO_3 and H_2O Reaction-Reaction Analysis and Reactor Design. *Sol. Energy* **1990**, *44*, 321–332.

(56) Mayorova, A. F.; Mudretsova, S. N.; Mamontov, M. N.; Levashov, P. A.; Rusin, A. D. Thermoanalysis of the System BaO_2-BaO-O_2. *Thermochim. Acta* **1993**, *217*, 241–249.

(57) K. Lovegrove. Thermodynamic Limits on the Performance of a Solar Thermochemical Energy Storage System. *Int. J. Energy Res.* **1993**, *17*, 817–829.

(58) McCrary, J. H.; McCrary, G. E.; Chubb, T. A.; Won, Y. S. An Experimental Study of SO_3 Dissociation as a Mechanism for Converting and Transporting Solar Energy. *Sol. Energy* **1981**, *27*, 433–440.

(59) De Maria, G.; D'Alessio, L.; Coffari, E.; Paolucci, M.; Tiberio, C. A. Thermochemical Storage of Solar Energy with High-Temperature Chemical Reactions. *Sol. Energy* **1985**, *35* , 409–416.

(60) Levitan, R.; Rosin, H.; Levy, M. Chemical Reactions in a Solar Furnace—Direct Heating of the Reactor in a Tubular Receiver. *Sol. Energy* **1989**, *42*, 267–272.

(61) Dunn, R.; Lovegrove, K.; Burgess, G. A Review of Ammonia-Based Thermochemical Energy Storage for Concentrating Solar Power. *Proc. IEEE* **2012**, *100*, 391–400.

(62) Pardo, P.; Deydier, A.; Anxionnaz-Minvielle, Z.; Rougé, S.; Cabassud, M.; Cognet, P. A Review on High Temperature Thermochemical Heat Energy Storage. *Renew. Sustain. Energy Rev.* **2014**, *32*, 591–610.

(63) SunShot Initiative http://energy.gov/eere/sunshot/sunshot-initiative.

(64) Deutsch, M.; Mueller, D.; Aumeyr, C.; Jordan, C.; Gierl-Mayer, C.; Weinberger, P.; Winter, F.; Werner, A. Systematic Search Algorithm for Potential Thermochemical Energy Storage Systems. *Appl. Energy* **2016**, *183*, 113–120.

(65) Manuel Romero; Jose Gonzalez-Aguilar; Eduardo Zarza. Concentrating Solar Thermal Power. In *Energy Efficiency and Renewable Energy Handbook*; Yogi Goswami, Kreith, F., Eds.; CRC Press, 2015; pp 1237–1346.

(66) Lovegrove, K.; Luzzi, A; Soldiani, I.; Kreetz, H. Developing Ammonia Based Thermochemical Energy Storage for Dish Power Plants. *Sol. Energy* **2004**, *76*, 331–337.

(67) Neises, M.; Tescari, S.; de Oliveira, L.; Roeb, M.; Sattler, C.; Wong, B. Solar-Heated Rotary Kiln for Thermochemical Energy Storage. *Sol. Energy* **2012**, *86*, 3040–3048.

(68) Miguel, S. Á. De; Gonzalez-Aguilar, J.; Romero, M. 100-Wh Multi-Purpose Particle Reactor for Thermochemical Heat Storage in Concentrating Solar Power Plants. *Energy Procedia* **2014**, *49*, 676–683.

(69) Pardo, P.; Anxionnaz-Minvielle, Z.; Rougé, S.; Cognet, P.; Cabassud, M. $Ca(OH)_2$/CaO Reversible Reaction in a Fluidized Bed Reactor for Thermochemical Heat Storage. *Sol. Energy* **2014**, *107*, 605–616.

(70) Laing, D.; Lehmann, D.; Bahl, C. Concrete Storage for Solar Thermal Power Plants and Industrial Process Heat. In *IRES III 2008, 3rd International Renewable Energy Storage Conference*; 2008; pp 1–6.

(71) *Mathur, Anoop. Using Encapsulated Phase Change Material in Thermal Energy Storage for Baseload Concentrating Solar Power (EPCM-TES). No DE-EE0003589. 2013.*

doi:10.2172/1184415

(72) Chen, C.; Aryafar, H.; Warrier, G.; Lovegrove, K. M.; Lavine, A. S. Ammonia Synthesis for Producing Supercritical Steam in the Context of Solar Thermochemical Energy Storage. *Conf. Proc. SolarPACES 2015* **2016**.

(73) Lavine, A. S.; Lovegrove, K. M.; Jordan, J.; Bran, G.; Chen, C.; Aryafar, H.; Sepulveda, A. Thermochemical Energy Storage with Ammonia : Aiming for the SunShot Cost Target. In *Conference proceedings SolarPACES 2015*; 2016; pp 2–9.

(74) Chen, C.; Aryafar, H.; Lovegrove, K. M.; Lavine, A. S. Modeling of Ammonia Synthesis to Produce Supercritical Steam for Solar Thermochemical Energy Storage. *Sol. Energy* **2017**, *155*, 363–371.

(75) Chen, C.; Lovegrove, K. M.; Sepulveda, A.; Lavine, A. S. Design and Optimization of an Ammonia Synthesis System for Ammonia-Based Solar Thermochemical Energy Storage. *Sol. Energy* **2018**, *159* , 992–1002.

(76) Levy, M.; Levitan, R.; Rosin, H.; Rubin, R. Solar Energy Storage via a Closed-Loop Chemical Heat Pipe. *Sol. Energy* **1993**, *50*, 179–189.

(77) DeLancey, G. B.; Kovenklioglu, S.; Ritter, A. B.; Schneider, J. C. Cyclohexane Dehydrogenation for Thermochemical Energy Conversion. *Ind. Eng. Chem. Process Des. Dev.* **1983**, *22*, 639–645.

(78) Wong, B.; Brown, L.; Buckingham, R.; Sweet, W.; Russ, B.; Gorensek, M. Sulfur Dioxide Disproportionation for Sulfur Based Thermochemical Energy Storage. *Sol. Energy* **2015**, *118*, 134–144.

(79) Pegasus Project:Renewable PowEr Generation by Solar PArticle Receiver Driven SUlphur

Storage Cycle https://www.pegasus-project.eu/.

(80) Harries, D. N.; Paskevicius, M.; Sheppard, D. A.; Price, T. E. C.; Buckley, C. E. Concentrating Solar Thermal Heat Storage Using Metal Hydrides. *Proc. IEEE* **2012**, *100*, 539–549.

(81) Fellet, M.; Buckley, C. E.; Paskevicius, M.; Sheppard, D. A. Research on Metal Hydrides Revived for Next-Generation Solutions to Renewable Energy Storage. *MRS Bull.* **2013**, *38* , 1012–1013.

(82) Paskevicius, M.; Sheppard, D. A.; Williamson, K.; Buckley, C. E. Metal Hydride Thermal Heat Storage Prototype for Concentrating Solar Thermal Power. *Energy* **2015**, *88*, 469–477.

(83) Chaise, A.; de Rango, P.; Marty, P.; Fruchart, D.; Miraglia, S.; Olivès, R.; Garrier, S. Enhancement of Hydrogen Sorption in Magnesium Hydride Using Expanded Natural Graphite. *Int. J. Hydrogen Energy* **2009**, *34*, 8589–8596.

(84) Rönnebro, E.; Whyatt, G.; Powell, M.; Westman, M.; Zheng, F.; Fang, Z. Metal Hydrides for High-Temperature Power Generation. *Energies* **2015**, *8*, 8406–8430.

(85) Urbanczyk, R.; Peinecke, K.; Peil, S.; Felderhoff, M. Development of a Heat Storage Demonstration Unit on the Basis of Mg_2FeH_6 as Heat Storage Material and Molten Salt as Heat Transfer Media. *Int. J. Hydrogen Energy* **2017**, *42*, 13818–13826.

(86) Sheppard, D. A.; Corgnale, C.; Hardy, B.; Motyka, T.; Zidan, R.; Paskevicius, M.; Buckley, C. E. Hydriding Characteristics of $NaMgH_2F$ with Preliminary Technical and Cost Evaluation of Magnesium-Based Metal Hydride Materials for Concentrating Solar Power Thermal Storage. *RSC Adv.* **2014**, *4*, 26552–26562.

(87) Sheppard, D. A.; Humphries, T. D.; Buckley, C. E. What Is Old Is New Again. *Mater.*

Today **2015**, *18*, 414–415.

(88) Dieterich, M.; Bürger, I.; Linder, M. Open and Closed Metal Hydride System for High Thermal Power Applications: Preheating Vehicle Components. *Int. J. Hydrogen Energy* **2017**, *42*, 11469–11481.

(89) Nasri, M.; Burger, I.; Michael, S.; Friedrich, H. E. Waste Heat Recovery for Fuel Cell Electric Vehicle with Thermochemical Energy Storage. *2016 Elev. Int. Conf. Ecol. Veh. Renew. Energies* **2016**, 1–6.

(90) Shkatulov, A.; Ryu, J.; Kato, Y.; Aristov, Y. Composite Material "$Mg(OH)_2$/Vermiculite": A Promising New Candidate for Storage of Middle Temperature Heat. *Energy* **2012**, *44*, 1028–1034.

(91) Cot-Gores, J.; Castell, A.; Cabeza, L. F. Thermochemical Energy Storage and Conversion: A-State-of-the-Art Review of the Experimental Research under Practical Conditions. *Renew. Sustain. Energy Rev.* **2012**, *16*, 5207–5224.

(92) Mastronardo, E.; Kato, Y.; Bonaccorsi, L.; Piperopoulos, E.; Milone, C. Thermochemical Storage of Middle Temperature Wasted Heat by Functionalized C/$Mg(OH)_2$ Hybrid Materials. *Energies* **2017**, *10*, 70.

(93) Mastronardo, E.; Bonaccorsi, L.; Kato, Y.; Piperopoulos, E.; Lanza, M.; Milone, C. Strategies for the Enhancement of Heat Storage Materials Performances for MgO/H_2 O/$Mg(OH)_2$ Thermochemical Storage System. *Appl. Therm. Eng.* **2017**, *120*, 626–634.

(94) Piperopoulos, E.; Mastronardo, E.; Fazio, M.; Lanza, M.; Galvagno, S.; Milone, C. Enhancing the Volumetric Heat Storage Capacity of $Mg(OH)_2$ by the Addition of a Cationic Surfactant during Its Synthesis. *Appl. Energy* **2018**, *215*, 512–522.

(95) Shkatulov, A.; Krieger, T.; Zaikovskii, V.; Chesalov, Y.; Aristov, Y. Doping Magnesium Hydroxide with Sodium Nitrate: A New Approach to Tune the Dehydration Reactivity of Heat-Storage Materials. *ACS Appl. Mater. Interfaces* **2014**, *6*, 19966–19977.

(96) Rosemary, J. K.; Bauerle, G. L.; Springer, T. H. Solar Energy Storage Using Reversible Hydration-Dehydration of CaO-$Ca(OH)_2$. *J. Energy* **1979**, *3*, 321–322.

(97) Darkwa, K. Thermochemical Energy Storage in Inorganic Oxides: An Experimental Evaluation. *Appl. Therm. Eng.* **1998**, *18*, 387–400.

(98) Criado, Y. A.; Alonso, M.; Abanades, J. C. Kinetics of the $CaO/Ca(OH)_2$ Hydration/Dehydration Reaction for Thermochemical Energy Storage Applications. *Ind. Eng. Chem. Res.* **2014**, *53*, 12594–12601.

(99) Sakellariou, K. G.; Tsongidis, N. I.; Karagiannakis, G.; Konstandopoulos, A. G. Shortlisting of Composite CaO-Based Structured Bodies Suitable for Thermochemical Heat Storage with the $CaO/Ca(OH)_2$ Reaction Scheme. *Energy & Fuels* **2017**, *31*, 6548–6559.

(100) Xu, M.; Huai, X.; Cai, J. Agglomeration Behavior of Calcium Hydroxide/Calcium Oxide as Thermochemical Heat Storage Material: A Reactive Molecular Dynamics Study. *J. Phys. Chem. C* **2017**, *121*, 3025–3033.

(101) Álvarez Criado, Y.; Alonso, M.; Abanades, J. C. Composite Material for Thermochemical Energy Storage Using $CaO/Ca(OH)_2$. *Ind. Eng. Chem. Res.* **2015**, *54*, 9314–9327.

(102) Criado, Y. A.; Alonso, M.; Abanades, J. C. Enhancement of a $CaO/Ca(OH)_2$ Based Material for Thermochemical Energy Storage. *Sol. Energy* **2016**, *135*, 800–809.

(103) Sakellariou, K. G.; Karagiannakis, G.; Criado, Y. A.; Konstandopoulos, A. G. Calcium Oxide Based Materials for Thermochemical Heat Storage in Concentrated Solar Power

Plants. *Sol. Energy* **2015**, *122*, 215–230.

(104) Sakellariou, K. G.; Criado, Y. A.; Tsongidis, N. I.; Karagiannakis, G.; Konstandopoulos, A. G. Multi-Cyclic Evaluation of Composite CaO-Based Structured Bodies for Thermochemical Heat Storage via the $CaO/Ca(OH)_2$ Reaction Scheme. *Sol. Energy* **2017**, *146*, 65–78.

(105) Afflerbach, S.; Kappes, M.; Gipperich, A.; Trettin, R.; Krumm, W. Semipermeable Encapsulation of Calcium Hydroxide for Thermochemical Heat Storage Solutions. *Sol. Energy* **2017**, *148*, 1–11.

(106) Roßkopf, C.; Haas, M.; Faik, A.; Linder, M.; Wörner, A. Improving Powder Bed Properties for Thermochemical Storage by Adding Nanoparticles. *Energy Convers. Manag.* **2014**, *86*, 93–98.

(107) Roßkopf, C.; Afflerbach, S.; Schmidt, M.; Görtz, B.; Kowald, T.; Linder, M.; Trettin, R. Investigations of Nano Coated Calcium Hydroxide Cycled in a Thermochemical Heat Storage. *Energy Convers. Manag.* **2015**, *97*, 94–102.

(108) Schaube, F.; Koch, L.; Wörner, A.; Müller-Steinhagen, H. A Thermodynamic and Kinetic Study of the De- and Rehydration of $Ca(OH)_2$ at High H_2O Partial Pressures for Thermo-Chemical Heat Storage. *Thermochim. Acta* **2012**, *538*, 9–20.

(109) Yan, J.; Zhao, C. Y. First-Principle Study of $CaO/Ca(OH)_2$ Thermochemical Energy Storage System by Li or Mg Cation Doping. *Chem. Eng. Sci.* **2014**, *117*, 293–300.

(110) Yan, J.; Zhao, C. Y. Thermodynamic and Kinetic Study of the Dehydration Process of $CaO/Ca(OH)_2$ Thermochemical Heat Storage System with Li Doping. *Chem. Eng. Sci.* **2015**, *138*, 86–92.

(111) Shkatulov, A.; Aristov, Y. Modification of Magnesium and Calcium Hydroxides with Salts: An Efficient Way to Advanced Materials for Storage of Middle-Temperature Heat. *Energy* **2015**, *85*, 667–676.

(112) Schaube, F.; Wörner, A.; Tamme, R. High Temperature Thermochemical Heat Storage for Concentrated Solar Power Using Gas–Solid Reactions. *J. Sol. Energy Eng.* **2011**, *133*, 031006.

(113) Schaube, F.; Kohzer, A.; Schütz, J.; Wörner, A.; Müller-Steinhagen, H. De- and Rehydration of $Ca(OH)_2$ in a Reactor with Direct Heat Transfer for Thermo-Chemical Heat Storage. Part A: Experimental Results. *Chem. Eng. Res. Des.* **2012**, *91*, 864–856.

(114) Schaube, F.; Utz, I.; Wörner, A.; Müller-Steinhagen, H. De- and Rehydration of $Ca(OH)_2$ in a Reactor with Direct Heat Transfer for Thermo-Chemical Heat Storage. Part B: Validation of Model. *Chem. Eng. Res. Des.* **2013**, *91*, 865–873.

(115) Ströhle, S.; Haselbacher, A.; Jovanovic, Z. R.; Steinfeld, A. Transient Discrete-Granule Packed-Bed Reactor Model for Thermochemical Energy Storage. *Chem. Eng. Sci.* **2014**, *117*, 465–478.

(116) Shao, H.; Nagel, T.; Roßkopf, C.; Linder, M.; Wörner, A.; Kolditz, O. Non-Equilibrium Thermo-Chemical Heat Storage in Porous Media: Part 2 – A 1D Computational Model for a Calcium Hydroxide Reaction System. *Energy* **2013**, *60*, 271–282.

(117) Criado, Y. A.; Alonso, M.; Abanades, J. C.; Anxionnaz-Minvielle, Z. Conceptual Process Design of a $CaO/Ca(OH)_2$ Thermochemical Energy Storage System Using Fluidized Bed Reactors. *Appl. Therm. Eng.* **2014**, *73*, 1087–1094.

(118) Criado, Y. A.; Huille, A.; Rouge, S.; Abanades, J. C. Experimental Investigation and Model

Validation of a $CaO/Ca(OH)_2$ Fluidized Bed Reactor for Thermochemical Energy Storage Applications. *Chem. Eng. J.* **2017**, *313*, 1194–1205.

(119) Rougé, S.; A. Criado, Y.; Soriano, O.; Abanades, J. C. Continuous $CaO/Ca(OH)_2$ Fluidized Bed Reactor for Energy Storage: First Experimental Results and Reactor Model Validation. *Ind. Eng. Chem. Res.* **2017**, *56*, 844–852.

(120) Schmidt, M.; Szczukowski, C.; Roßkopf, C.; Linder, M.; Wörner, A. Experimental Results of a 10 KW High Temperature Thermochemical Storage Reactor Based on Calcium Hydroxide. *Appl. Therm. Eng.* **2014**, *62*, 553–559.

(121) Schmidt, M.; Gutierrez, A.; Linder, M. Thermochemical Energy Storage with $CaO/Ca(OH)_2$ - Experimental Investigation of the Thermal Capability at Low Vapor Pressures in a Lab Scale Reactor. *Appl. Energy* **2017**, *188*, 672–681.

(122) Schmidt, M.; Gollsch, M.; Giger, F.; Grün, M.; Linder, M. Development of a Moving Bed Pilot Plant for Thermochemical Energy Storage with $CaO/Ca(OH)_2$. In *Solar PACES 2015*; Cape Town.

(123) Kyaw, K.; Matsuda, H.; Hasatani, M. Applicability Of Carbonation / Decarbonation Reactions For Storing Thermal Energy From Nuclear Reactors. *J. Chem. Eng. Japan* **1996**, *29*, 119–125.

(124) Blamey, J.; Anthony, E. J.; Wang, J.; Fennell, P. S. The Calcium Looping Cycle for Large-Scale CO_2 Capture. *Prog. Energy Combust. Sci.* **2010**, *36*, 260–279.

(125) Perejón, A.; Romeo, L. M.; Lara, Y.; Lisbona, P.; Martínez, A.; Valverde, J. M. The Calcium-Looping Technology for CO_2 Capture: On the Important Roles of Energy Integration and Sorbent Behavior. *Appl. Energy* **2016**, *162*, 787–807.

(126) Chacartegui, R.; Alovisio, A.; Ortiz, C.; Valverde, J. M.; Verda, V.; Becerra, J. A. Thermochemical Energy Storage of Concentrated Solar Power by Integration of the Calcium Looping Process and a CO_2 Power Cycle. *Appl. Energy* **2016**, *173*, 589–605.

(127) Ortiz, C.; Chacartegui, R.; Valverde, J. M.; Alovisio, A.; Becerra, J. A. Power Cycles Integration in Concentrated Solar Power Plants with Energy Storage Based on Calcium Looping. *Energy Convers. Manag.* **2017**, *149*, 815–829.

(128) Alovisio, A.; Chacartegui, R.; Ortiz, C.; Valverde, J. M.; Verda, V. Optimizing the CSP-Calcium Looping Integration for Thermochemical Energy Storage. *Energy Convers. Manag.* **2017**, *136*, 85–98.

(129) Flamant, G.; Hernandez, D.; Bonet, C.; Traverse, J.-P. Experimental Aspects of the Thermochemical Conversion of Solar Energy; Decarbonation of $CaCO_3$. *Sol. Energy* **1980**, *24*, 385–395.

(130) Obermeier, J.; Müller, B.; Müller, K.; Arlt, W. Energy Storage and Transportation Based on Solar Irradiation-Aided CaO-Looping. *Energy Technol.* **2016**, *4*, 123–135.

(131) Sarrion, B.; Valverde, J. M.; Perejon, A.; Perez-Maqueda, L.; Sanchez-Jimenez, P. E. On the Multicycle Activity of Natural Limestone/Dolomite for Thermochemical Energy Storage of Concentrated Solar Power. *Energy Technol.* **2016**, *4*, 1013–1019.

(132) Benitez-Guerrero, M.; Sarrion, B.; Perejon, A.; Sanchez-Jimenez, P. E.; Perez-Maqueda, L. A.; Manuel Valverde, J. Large-Scale High-Temperature Solar Energy Storage Using Natural Minerals. *Sol. Energy Mater. Sol. Cells* **2017**, *168*, 14–21.

(133) Benitez-Guerrero, M.; Valverde, J. M.; Sanchez-Jimenez, P. E.; Perejon, A.; Perez-Maqueda, L. A. Multicycle Activity of Natural $CaCO_3$ Minerals for Thermochemical

Energy Storage in Concentrated Solar Power Plants. *Sol. Energy* **2017**, *153*, 188–199.

(134) Humphries, T. D.; Møller, K. T.; Rickard, W. D. A.; Sofianos, M. V.; Liu, S.; Buckley, C. E.; Paskevicius, M. Dolomite: A Low Cost Thermochemical Energy Storage Material. *J. Mater. Chem. A* **2019**, *7*, 1206–1215.

(135) Aihara, M.; Nagai, T.; Matsushita, J.; Negishi, Y.; Ohya, H. Development of Porous Solid Reactant for Thermal-Energy Storage and Temperature Upgrade Using Carbonation/Decarbonation Reaction. *Appl. Energy* **2001**, *69*, 225–238.

(136) Sanchez-Jimenez, P. E.; Valverde, J. M.; Perez-Maqueda, L. A. Multicyclic Conversion of Limestone at Ca-Looping Conditions: The Role of Solid-Sate Diffusion Controlled Carbonation. *Fuel* **2014**, *127*, 131–140.

(137) Zhao, M.; Shi, J.; Zhong, X.; Tian, S.; Blamey, J.; Jiang, J.; Fennell, P. S. A Novel Calcium Looping Absorbent Incorporated with Polymorphic Spacers for Hydrogen Production and CO_2 Capture. *Energy Environ. Sci.* **2014**, *7*, 3291–3295.

(138) Obermeier, J.; Sakellariou, K. G.; Tsongidis, N. I.; Baciu, D.; Charalambopoulou, G.; Steriotis, T.; Müller, K.; Karagiannakis, G.; Konstandopoulos, A. G.; Stubos, A.; et al. Material Development and Assessment of an Energy Storage Concept Based on the CaO-Looping Process. *Sol. Energy* **2017**, *150*, 298–309.

(139) Sánchez Jiménez, P. E.; Perejón, A.; Benítez Guerrero, M.; Valverde, J. M.; Ortiz, C.; Pérez Maqueda, L. A. High-Performance and Low-Cost Macroporous Calcium Oxide Based Materials for Thermochemical Energy Storage in Concentrated Solar Power Plants. *Appl. Energy* **2019**, *235*, 543–552.

(140) Benitez-Guerrero, M.; Valverde, J. M.; Perejon, A.; Sanchez-Jimenez, P. E.; Perez-

Maqueda, L. A. Low-Cost Ca-Based Composites Synthesized by Biotemplate Method for Thermochemical Energy Storage of Concentrated Solar Power. *Appl. Energy* **2018**, *210*, 108–116.

(141) Sakellariou, K. G.; Tsongidis, N. I.; Karagiannakis, G.; Konstandopoulos, A. G.; Baciu, D.; Charalambopoulou, G.; Steriotis, T.; Stubos, A.; Arlt, W. Development and Evaluation of Materials for Thermochemical Heat Storage Based on the $CaO/CaCO_3$ Reaction Couple. *AIP Conf. Proc.* **2016**, *1734*, 050040.

(142) André, L.; Abanades, S. Evaluation and Performances Comparison of Calcium, Strontium and Barium Carbonates during Calcination/Carbonation Reactions for Solar Thermochemical Energy Storage. *J. Energy Storage* **2017**, *13*, 193–205.

(143) Rhodes, N. R.; Barde, A.; Randhir, K.; Li, L.; Hahn, D. W.; Mei, R.; Klausner, J. F.; AuYeung, N. Solar Thermochemical Energy Storage Through Carbonation Cycles of $SrCO_3$ /SrO Supported on $SrZrO_3$. *ChemSusChem* **2015**, *8*, 3793–3798.

(144) Bagherisereshki, E.; Tran, J.; Lei, F.; AuYeung, N. Investigation into $SrO/SrCO_3$ for High Temperature Thermochemical Energy Storage. *Sol. Energy* **2018**, *160*, 85–93.

(145) Price 3mol% Yttria Stabilized Zirconia (YSZ) Powder ready-to-press grade http://www.inframat.com/products/4039OR-9502.htm.

(146) Takasu, H.; Ryu, J.; Kato, Y. Application of Lithium Orthosilicate for High-Temperature Thermochemical Energy Storage. *Appl. Energy* **2017**, *193*, 74–83.

(147) Ortiz, C.; Romano, M. C.; Valverde, J. M.; Binotti, M.; Chacartegui, R. Process Integration of Calcium-Looping Thermochemical Energy Storage System in Concentrating Solar Power Plants. *Energy* **2018**, *155*, 535–551.

(148) Kurtulus, K.; Coskun, A.; Ameen, S.; Yilmaz, C.; Bolatturk, A. Thermoeconomic Analysis of a CO_2 compression System Using Waste Heat into the Regenerative Organic Rankine Cycle. *Energy Convers. Manag.* **2018**, *168*, 588–598.

(149) Meroueh, L.; Yenduru, K.; Dasgupta, A.; Jiang, D.; AuYeung, N. Energy Storage Based on $SrCO_3$ and Sorbents—A Probabilistic Analysis towards Realizing Solar Thermochemical Power Plants. *Renew. Energy* **2018**, *133*, 770–786.

(150) Jakobsen, J.; Roussanaly, S.; Anantharaman, R. A Techno-Economic Case Study of CO_2 capture, Transport and Storage Chain from a Cement Plant in Norway. *J. Clean. Prod.* **2017**, *144*, 523–539.

(151) General Atomics. *Thermochemical heat storage for concentrated solar power thermochemical system reactor design for thermal energy storagePhase II Final Report for the Period; 2011*

(152) Müller, D.; Knoll, C.; Artner, W.; Harasek, M.; Gierl-Mayer, C.; Welch, J. M.; Werner, A.; Weinberger, P. Combining In-Situ X-Ray Diffraction with Thermogravimetry and Differential Scanning Calorimetry – An Investigation of Co_3O_4 , MnO_2 and PbO_2 for Thermochemical Energy Storage. *Sol. Energy* **2017**, *153*, 11–24.

(153) Momma, K.; Izumi, F. VESTA 3 for Three-Dimensional Visualization of Crystal, Volumetric and Morphology Data. *J. Appl. Crystallogr.* **2011**, *44*, 1272–1276.

(154) Jondo, J. L.; Phok, S.; Galez, P.; Jorda, J.-L. Studies in the BaO_2–BaO–CuO System. *Cryst. Eng.* **2002**, *5*, 419–425.

(155) Jorda, J. L.; Jondo, T. K. Barium Oxides: Equilibrium and Decomposition of BaO_2. *J. Alloys Compd.* **2001**, *327* , 167–177.

(156) Carrillo, A. J.; Sastre, D.; Serrano, D. P.; Pizarro, P.; Coronado, J. M. Revisiting the BaO_2 /BaO Redox Cycle for Solar Thermochemical Energy Storage. *Phys. Chem. Chem. Phys.* **2016**, *18* , 8039–8048.

(157) Chen, X.; Jung, T.; Park, J.; Kim, W.-S. Preparation of Tunable (BaSrMg)O for Oxygen Chemisorption: Formation Mechanism and Characterization. *Inorg. Chem.* **2015**, *54*, 5419–5425.

(158) Jung, T.; Na, J.-G.; Cho, D. W.; Park, J.-H.; Yang, R. T. $Ba_xSr_{1-x}O$/MgO Nano-Composite Sorbents for Tuning the Transition Pressure of Oxygen: Application to Air Separation. *Chem. Eng. Sci.* **2015**, *137*, 532–540.

(159) Chen, X.; Jung, T.; Park, J.; Kim, W.-S. Preparation of Single-Phase Three-Component Alkaline Earth Oxide of (BaSrMg)O: A High Capacity and Thermally Stable Chemisorbent for Oxygen Separation. *J. Mater. Chem. A* **2015**, *3*, 258–265.

(160) Agrafiotis, C.; Roeb, M.; Sattler, C. Exploitation of Thermochemical Cycles Based on Solid Oxide Redox Systems for Thermochemical Storage of Solar Heat. Part 4: Screening of Oxides for Use in Cascaded Thermochemical Storage Concepts. *Sol. Energy* **2016**, *139*, 695–710.

(161) Block, T.; Schmücker, M. Metal Oxides for Thermochemical Energy Storage: A Comparison of Several Metal Oxide Systems. *Sol. Energy* **2016**, *126*, 195–207.

(162) Deutsch, M.; Horvath, F.; Knoll, C.; Lager, D.; Gierl-Mayer, C.; Weinberger, P.; Winter, F. High-Temperature Energy Storage: Kinetic Investigations of the CuO/Cu_2O Reaction Cycle. *Energy & Fuels* **2017**, *31*, 2324–2334.

(163) Setoodeh Jahromy, S.; Birkelbach, F.; Jordan, C.; Huber, C.; Harasek, M.; Werner, A.;

Winter, F. Impact of Partial Pressure, Conversion, and Temperature on the Oxidation Reaction Kinetics of Cu_2O to CuO in Thermochemical Energy Storage. *Energies* **2019**, *12* , 508.

(164) Jafarian, M.; Arjomandi, M.; Nathan, G. J. Thermodynamic Potential of Molten Copper Oxide for High Temperature Solar Energy Storage and Oxygen Production. *Appl. Energy* **2017**, *201*, 69–83.

(165) Price cobalt http://www.infomine.com/investment/metal-prices/cobalt/ (accessed Jul 27, 2017).

(166) Block, T.; Knoblauch, N.; Schmücker, M. The Cobalt-Oxide/Iron-Oxide Binary System for Use as High Temperature Thermochemical Energy Storage Material. *Thermochim. Acta* **2013**, *577*, 25–32.

(167) Agrafiotis, C.; Roeb, M.; Schmücker, M.; Sattler, C. Exploitation of Thermochemical Cycles Based on Solid Oxide Redox Systems for Thermochemical Storage of Solar Heat. Part 1: Testing of Cobalt Oxide-Based Powders. *Sol. Energy* **2014**, *102*, 189–211.

(168) Agrafiotis, C.; Tescari, S.; Roeb, M.; Schmücker, M.; Sattler, C. Exploitation of Thermochemical Cycles Based on Solid Oxide Redox Systems for Thermochemical Storage of Solar Heat. Part 3: Cobalt Oxide Monolithic Porous Structures as Integrated Thermochemical Reactors/Heat Exchangers. *Sol. Energy* **2015**, *114*, 459–475.

(169) Carrillo, A. J.; Moya, J.; Bayón, A.; Jana, P.; de la Peña O'Shea, V. A.; Romero, M.; Gonzalez-Aguilar, J.; Serrano, D. P.; Pizarro, P.; Coronado, J. M. Thermochemical Energy Storage at High Temperature via Redox Cycles of Mn and Co Oxides: Pure Oxides versus Mixed Ones. *Sol. Energy Mater. Sol. Cells* **2014**, *123*, 47–57.

(170) Andre, L.; Abanades, S.; Cassayre, L. High-Temperature Thermochemical Energy Storage Based on Redox Reactions Using Co-Fe and Mn-Fe Mixed Metal Oxides. *J. Solid State Chem.* **2017**, *253*, 6–14.

(171) André, L.; Abanades, S.; Cassayre, L. Experimental Investigation of Co–Cu, Mn–Co, and Mn–Cu Redox Materials Applied to Solar Thermochemical Energy Storage. *ACS Appl. Energy Mater.* **2018**, *1*, 3385–3395.

(172) Tamayo, A.; Rodríguez, M.; Arroyo, C.; Beltran-Heredia, J.; Rubio, F. Dependence of the Synthetic Strategy on the Thermochemical Energy Storage Capability of $Cu_xCo_{3-x}O_4$ Spinels. *J. Eur. Ceram. Soc.* **2018**, *38*, 1583–1591.

(173) Agrafiotis, C.; Roeb, M.; Schmücker, M.; Sattler, C. Exploitation of Thermochemical Cycles Based on Solid Oxide Redox Systems for Thermochemical Storage of Solar Heat. Part 2: Redox Oxide-Coated Porous Ceramic Structures as Integrated Thermochemical Reactors/Heat Exchangers. *Sol. Energy* **2015**, *114*, 440–458.

(174) Pagkoura, C.; Karagiannakis, G.; Zygogianni, A.; Lorentzou, S.; Kostoglou, M.; Konstandopoulos, A. G.; Rattenburry, M.; Woodhead, J. W. Cobalt Oxide Based Structured Bodies as Redox Thermochemical Heat Storage Medium for Future CSP Plants. *Sol. Energy* **2014**, *108*, 146–163.

(175) Muroyama, A. P.; Schrader, A. J.; Loutzenhiser, P. G. Solar Electricity via an Air Brayton Cycle with an Integrated Two-Step Thermochemical Cycle for Heat Storage Based on Co_3O_4/CoO Redox Reactions II: Kinetic Analyses. *Sol. Energy* **2015**, *122*, 409–418.

(176) Agrafiotis, C.; Block, T.; Senholdt, M.; Tescari, S.; Roeb, M.; Sattler, C. Exploitation of Thermochemical Cycles Based on Solid Oxide Redox Systems for Thermochemical Storage

of Solar Heat . Part 6 : Testing of Mn-Based Combined Oxides and Porous Structures. *Sol. Energy* **2017**, *149*, 227–244.

(177) Bush, H. E.; Loutzenhiser, P. G. Solar Electricity via an Air Brayton Cycle with an Integrated Two-Step Thermochemical Cycle for Heat Storage Based on Fe_2O_3/Fe_3O_4 Redox Reactions: Thermodynamic and Kinetic Analyses. *Sol. Energy* **2018**, *174*, 617–627.

(178) Scheffe, J. R.; Li, J.; Weimer, A. W. A Spinel Ferrite/Hercynite Water-Splitting Redox Cycle. *Int. J. Hydrogen Energy* **2010**, *35*, 3333–3340.

(179) Muhich, C. L.; Aston, V. J.; Trottier, R. M.; Weimer, A. W.; Musgrave, C. B. First-Principles Analysis of Cation Diffusion in Mixed Metal Ferrite Spinels. *Chem. Mater.* **2016**, *28*, 214–226.

(180) Scheffe, J. R.; McDaniel, A. H.; Allendorf, M. D.; Weimer, A. W. Kinetics and Mechanism of Solar-Thermochemical H_2 Production by Oxidation of a Cobalt Ferrite–zirconia Composite. *Energy Environ. Sci.* **2013**, *6*, 963.

(181) Scheffe, J. R.; Allendorf, M. D.; Coker, E. N.; Jacobs, B. W.; McDaniel, A. H.; Weimer, A. W. Hydrogen Production via Chemical Looping Redox Cycles Using Atomic Layer Deposition-Synthesized Iron Oxide and Cobalt Ferrites. *Chem. Mater.* **2011**, *23*, 2030–2038.

(182) Kodama, T.; Gokon, N.; Yamamoto, R. Thermochemical Two-Step Water Splitting by ZrO_2-Supported $Ni_xFe_{3-x}O_4$ for Solar Hydrogen Production. *Sol. Energy* **2008**, *82*, 73–79.

(183) Fresno, F.; Yoshida, T.; Gokon, N.; Fernández-Saavedra, R.; Kodama, T. Comparative Study of the Activity of Nickel Ferrites for Solar Hydrogen Production by Two-Step Thermochemical Cycles. *Int. J. Hydrogen Energy* **2010**, *35*, 8503–8510.

(184) Ehrhart, B.; Coker, E.; Siegel, N.; Weimer, A. Thermochemical Cycle of a Mixed Metal Oxide for Augmentation of Thermal Energy Storage in Solid Particles. *Energy Procedia* **2014**, *49*, 762–771.

(185) Pike, J.; Hanson, J.; Zhang, L.; Chan, S. Synthesis and Redox Behavior of Nanocrystalline Hausmannite (Mn_3O_4). *Chem. Mater.* **2007**, *42*, 5609–5616.

(186) Fritsch, S.; Navrotsky, A. Thermodynamic Properties of Manganese Oxides. *J. Am. Ceram. Soc.* **1996**, *79*, 1761–1768.

(187) Otto, E. M. Equilibrium Pressures of Oxygen over Mn_2O_3-Mn_3O_4 at Various Temperatures. *J. Electrochem. Soc.* **1964**, *111*, 88.

(188) Barin, I. *Thermochemical Data of Pure Substances*; Barin, I., Ed.; Wiley-VCH Verlag GmbH: Weinheim, Germany, 1995.

(189) Zaki, M.; Hasan, M.; Pasupulety, L.; Kumari, K. Thermochemistry of Manganese Oxides in Reactive Gas Atmospheres: Probing Catalytic MnO_x Compositions in the Atmosphere of CO+ O_2. *Thermochim. Acta* **1998**, *311*, 97–103.

(190) Marugán, J.; Botas, J. A.; Martín, M.; Molina, R.; Herradón, C. Study of the First Step of the Mn_2O_3/MnO Thermochemical Cycle for Solar Hydrogen Production. *Int. J. Hydrogen Energy* **2012**, *37*, 7017–7025.

(191) Marugán, J.; Botas, J. A.; Molina, R.; Herradón, C. Study of the Hydrogen Production Step of the Mn_2O_3/MnO Thermochemical Cycle. *Int. J. Hydrogen Energy* **2014**, *39* , 5274–5282.

(192) Botas, J. A.; Marugán, J.; Molina, R.; Herradón, C. Kinetic Modelling of the First Step of Mn_2O_3/MnO Thermochemical Cycle for Solar Hydrogen Production. *Int. J. Hydrogen Energy* **2012**, *37*, 18661–18671.

(193) Alonso, E.; Hutter, C.; Romero, M.; Steinfeld, A.; Gonzalez-Aguilar, J. Kinetics of Mn_2O_3 –Mn_3O_4 and Mn_3O_4 –MnO Redox Reactions Performed under Concentrated Thermal Radiative Flux. *Energy & Fuels* **2013**, *27*, 4884–4890.

(194) Rao, C. N. R.; Dey, S. Solar Thermochemical Splitting of Water to Generate Hydrogen. *Proc. Natl. Acad. Sci.* **2017**, *2017*, 201700104.

(195) Lei, Q.; Bader, R.; Kreider, P.; Lovegrove, K.; Lipiński, W. Thermodynamic Analysis of a Combined-Cycle Solar Thermal Power Plant with Manganese Oxide-Based Thermochemical Energy Storage. *E3S Web Conf.* **2017**, *22*, 00102.

(196) Wang, M.; Sundman, B. Thermodynamic Assessment of the Mn-O System. *Metall. Mater. Trans. B* **1992**, *23*, 821–831.

(197) Randhir, K.; King, K.; Rhodes, N.; Li, L.; Hahn, D.; Mei, R.; Auyeung, N.; Klausner, J.; Lansing, E. Magnesium-Manganese Oxides for High Temperature Thermochemical Energy Storage. *J. Energy Storage* **2019**, *21*, 599–610.

(198) King, K.; Randhir, K.; Klausner, J. Calorimetric Method for Determining the Thermochemical Energy Storage Capacities of Redox Metal Oxides. *Thermochim. Acta* **2019**, *673*, 105–118.

(199) Karagiannakis, G.; Pagkoura, C.; Zygogianni, A.; Lorentzou, S.; Konstandopoulos, A. G. Monolithic Ceramic Redox Materials for Thermochemical Heat Storage Applications in CSP Plants. *Energy Procedia* **2014**, *49*, 820–829.

(200) Carrillo, A. J.; Serrano, D. P.; Pizarro, P.; Coronado, J. M. Thermochemical Heat Storage Based on the Mn_2O_3/Mn_3O_4 Redox Couple: Influence of the Initial Particle Size on the Morphological Evolution and Cyclability. *J. Mater. Chem. A* **2014**, *2*, 19435–19443.

(201) Carrillo, A. J.; Serrano, D. P.; Pizarro, P.; Coronado, J. M. Design of Efficient Mn-Based Redox Materials for Thermochemical Heat Storage at High Temperatures. *AIP Conf. Proc.* **2016**, *2*, 050009.

(202) Agrafiotis, C.; Becker, A.; Roeb, M.; Sattler, C. Exploitation of Thermochemical Cycles Based on Solid Oxide Redox Systems for Thermochemical Storage of Solar Heat. Part 5: Testing of Porous Ceramic Honeycomb and Foam Cascades Based on Cobalt and Manganese Oxides for Hybrid Sensible/Thermochemical Heat S. *Sol. Energy* **2016**, *114*, 440–458.

(203) Wong, B.; Brown, L.; Schaube, F.; Tamme, R.; Sattler, C. Oxide Based Thermochemical Heat Storage. In *16th Solar PACES International Symposium, Perpignan, France.*; 2010; pp 1–8.

(204) Carrillo, A. J.; Serrano, D. P.; Pizarro, P.; Coronado, J. M. Improving the Thermochemical Energy Storage Performance of the Mn_2O_3/Mn_3O_4 Redox Couple by the Incorporation of Iron. *ChemSusChem* **2015**, *8*, 1947–1954.

(205) Carrillo, A. J.; Serrano, D. P.; Pizarro, P.; Coronado, J. M. Understanding Redox Kinetics of Iron-Doped Manganese Oxides for High Temperature Thermochemical Energy Storage. *J. Phys. Chem. C* **2016**, *120*, 27800–27812.

(206) Wokon, M.; Block, T.; Nicolai, S.; Linder, M.; Schmuecker, M. Thermodynamic and Kinetic Investigation of a Technical Grade Manganese-Iron Binary Oxide for Thermochemical Energy Storage. *Sol. Energy* **2017**, *153*, 471–485.

(207) Wokon, M.; Kohzer, A.; Linder, M. Investigations on Thermochemical Energy Storage Based on Technical Grade Manganese-Iron Oxide in a Lab-Scale Packed Bed Reactor. *Sol.*

Energy **2017**, *153*, 200–214.

(208) Carrillo, A. J.; Serrano, D. P.; Pizarro, P.; Coronado, J. M. Manganese Oxide-Based Thermochemical Energy Storage: Modulating Temperatures of Redox Cycles by Fe–Cu Co-Doping. *J. Energy Storage* **2016**, *5*, 169–176.

(209) Preisner, N. C.; Block, T.; Linder, M.; Leion, H. Stabilizing Particles of Manganese-Iron Oxide with Additives for Thermochemical Energy Storage. *Energy Technol.* **2018**, *6*, 2154-2165.

(210) Varsano, F.; Alvani, C.; La Barbera, A.; Masi, A.; Padella, F. Lithium Manganese Oxides as High-Temperature Thermal Energy Storage System. *Thermochim. Acta* **2016**, *640*, 26–35.

(211) Hlongwa, N. W.; Sastre, D.; Iwuoha, E.; Carrillo, A. J.; Ikpo, C.; Serrano, D. P.; Pizarro, P.; Coronado, J. M. Exploring the Thermochemical Heat Storage Capacity of AMn_2O_4 (A = Li or Cu) Spinels. *Solid State Ionics* **2018**, *320*, 316-324

(212) Kubicek, M.; Bork, A. H.; Rupp, J. L. M. Perovskite Oxides – a Review on a Versatile Material Class for Solar-to-Fuel Conversion Processes. *J. Mater. Chem. A* **2017**, *5*, 11983–12000.

(213) Evdou, A.; Zaspalis, V.; Nalbandian, L. $La_{1-x}Sr_xFeO_{3-\delta}$ Perovskites as Redox Materials for Application in a Membrane Reactor for Simultaneous Production of Pure Hydrogen and Synthesis Gas. *Fuel* **2010**, *89*, 1265–1273.

(214) Michalsky, R.; Neuhaus, D.; Steinfeld, A. Carbon Dioxide Reforming of Methane Using an Isothermal Redox Membrane Reactor. *Energy Technol.* **2015**, *3*, 784–789.

(215) Ezbiri, M.; Allen, K. M.; Gàlvez, M. E.; Michalsky, R.; Steinfeld, A. Design Principles of

Perovskites for Thermochemical Oxygen Separation. *ChemSusChem* **2015**, *8*, 1966–1971.

(216) He, F.; Li, X.; Zhao, K.; Huang, Z.; Wei, G.; Li, H. The Use of $La_{1-x}Sr_xFeO_3$ Perovskite-Type Oxides as Oxygen Carriers in Chemical-Looping Reforming of Methane. *Fuel* **2013**, *108*, 465–473.

(217) Rydén, M.; Leion, H.; Mattisson, T.; Lyngfelt, A. Combined Oxides as Oxygen-Carrier Material for Chemical-Looping with Oxygen Uncoupling. *Appl. Energy* **2014**, *113*, 1924–1932.

(218) Babiniec, S. M.; Coker, E. N.; Miller, J. E.; Ambrosini, A. Investigation of $La_xSr_{1-x}Co_yM_{1-y}O_{3-\delta}$ (M=Mn, Fe) Perovskite Materials as Thermochemical Energy Storage Media. *Sol. Energy* **2015**, *118* , 451–459.

(219) Zhang, Z.; Andre, L.; Abanades, S. Experimental Assessment of Oxygen Exchange Capacity and Thermochemical Redox Cycle Behavior of Ba and Sr Series Perovskites for Solar Energy Storage. *Sol. Energy* **2016**, *134*, 494–502.

(220) Babiniec, S. M.; Coker, E. N.; Miller, J. E.; Ambrosini, A. Doped Calcium Manganites for Advanced High-Temperature Thermochemical Energy Storage. *Int. J. Energy Res.* **2016**, *40*, 280–284.

(221) Imponenti, L.; Albrecht, K. J.; Braun, R. J.; Jackson, G. S. Measuring Thermochemical Energy Storage Capacity with Redox Cycles of Doped-$CaMnO_3$. *ECS Trans.* **2016**, *72*, 11–22.

(222) Imponenti, L.; Albrecht, K. J.; Wands, J. W.; Sanders, M. D.; Jackson, G. S. Thermochemical Energy Storage in Strontium-Doped Calcium Manganites for Concentrating Solar Power Applications. *Sol. Energy* **2017**, *151*, 1–13.

(223) Jackson, G. S.; Imponenti, L.; Albrecht, K. J.; Miller, D. C.; Braun, R. J. Inert and Reactive Oxide Particles for High-Temperature Thermal Energy Capture and Storage for Concentrating Solar Power. *J. Sol. Energy Eng.* **2019**, *141*, 021016.

(224) Bork, A. H.; Povoden-Karadeniz, E.; Rupp, J. L. M. Modeling Thermochemical Solar-to-Fuel Conversion: CALPHAD for Thermodynamic Assessment Studies of Perovskites, Exemplified for (La,Sr)MnO_3. *Adv. Energy Mater.* **2017**, *7*, 1601086.

(225) Emery, A. A.; Saal, J. E.; Kirklin, S.; Hegde, V. I.; Wolverton, C. High-Throughput Computational Screening of Perovskites for Thermochemical Water Splitting Applications. *Chem. Mater.* **2016**, *28*, 5621–5634.

(226) Lau, C. Y.; Dunstan, M. T.; Hu, W.; Grey, C. P.; Scott, S. A. Large Scale in Silico Screening of Materials for Carbon Capture through Chemical Looping. *Energy Environ. Sci.* **2017**, *10* , 818–831.

(227) Imponenti, L.; Albrecht, K. J.; Kharait, R.; Sanders, M. D.; Jackson, G. S. Redox Cycles with Doped Calcium Manganites for Thermochemical Energy Storage to 1000 °C. *Appl. Energy* **2018**, *230*, 1–18.

(228) Gokon, N.; Yawata, T.; Bellan, S.; Kodama, T.; Hyun-seok, C. Thermochemical Behavior of Perovskite Oxides Based on La_xSr_{1-x}(Mn, Fe, Co)$O_{3-\delta}$ and $Ba_ySr_{1-y}CoO_{3-\delta}$ Redox System for Thermochemical Energy Storage at High Temperatures. *Energy* **2019**, *171*.

(229) Karagiannakis, G.; Pagkoura, C.; Halevas, E.; Baltzopoulou, P.; Konstandopoulos, A. G. Cobalt/Cobaltous Oxide Based Honeycombs for Thermochemical Heat Storage in Future Concentrated Solar Power Installations: Multi-Cyclic Assessment and Semi-Quantitative Heat Effects Estimations. *Sol. Energy* **2016**, *133*, 394–407.

(230) Tescari, S.; Singh, A.; Agrafiotis, C.; de Oliveira, L.; Breuer, S.; Schlögl-Knothe, B.; Roeb, M.; Sattler, C. Experimental Evaluation of a Pilot-Scale Thermochemical Storage System for a Concentrated Solar Power Plant. *Appl. Energy* **2017**, *189*, 66–75.

(231) Alonso, E.; Pérez-Rábago, C.; Licurgo, J.; Fuentealba, E.; Estrada, C. A. First Experimental Studies of Solar Redox Reactions of Copper Oxides for Thermochemical Energy Storage. *Sol. Energy* **2015**, *115*, 297–305.

(232) Alonso, E.; Pérez-Rábago, C.; Licurgo, J.; Gallo, A.; Fuentealba, E.; Estrada, C. A. Experimental Aspects of CuO Reduction in Solar-Driven Reactors: Comparative Performance of a Rotary Kiln and a Packed-Bed. *Renew. Energy* **2017**, *105*, 665–673.

(233) Tescari, S.; Neises, M.; de Oliveira, L.; Roeb, M.; Sattler, C.; Neveu, P. Thermal Model for the Optimization of a Solar Rotary Kiln to Be Used as High Temperature Thermochemical Reactor. *Sol. Energy* **2013**, *95*, 279–289.

(234) Schrader, A. J.; De Dominicis, G.; Schieber, G. L.; Loutzenhiser, P. G. Solar Electricity via an Air Brayton Cycle with an Integrated Two-Step Thermochemical Cycle for Heat Storage Based on Co_3O_4 /CoO Redox Reactions III: Solar Thermochemical Reactor Design and Modeling. *Sol. Energy* **2017**, *150*, 584–595.

(235) Alonso, E.; Gallo, A.; Roldán, M. I.; Pérez-Rábago, C. A.; Fuentealba, E. Use of Rotary Kilns for Solar Thermal Applications : Review of Developed Studies and Analysis of Their Potential. *Sol. Energy* **2017**, *144*, 90–104.

(236) Ho, C. K. A Review of High-Temperature Particle Receivers for Concentrating Solar Power. *Appl. Therm. Eng.* **2016**, *109*, 958–969.

(237) Ho, C. K. Advances in Central Receivers for Concentrating Solar Applications. *Sol. Energy*

2017, *152*, 38–56.

(238) Ströhle, S.; Haselbacher, A.; Jovanovic, Z. R.; Steinfeld, A. The Effect of the Gas–solid Contacting Pattern in a High-Temperature Thermochemical Energy Storage on the Performance of a Concentrated Solar Power Plant. *Energy Environ. Sci.* **2016**, *9*, 1375–1389.

(239) Singh, A.; Tescari, S.; Lantin, G.; Agrafiotis, C.; Roeb, M.; Sattler, C. Solar Thermochemical Heat Storage via the Co_3O_4/CoO Looping Cycle: Storage Reactor Modelling and Experimental Validation. *Sol. Energy* **2017**, *144*, 453–465.

(240) de Miguel, S. Á.; Bellan, S.; de María, J. M. G.; González-Aguilar, J.; Romero, M. Numerical Modelling of a 100-Wh Lab-Scale Thermochemical Heat Storage System for Concentrating Solar Power Plants. *AIP Conf. Proc.* **2016**, *1743*, 050005.

(241) Ströhle, S.; Haselbacher, A.; Jovanovic, Z. R.; Steinfeld, A. Upgrading Sensible-Heat Storage with a Thermochemical Storage Section Operated at Variable Pressure: An Effective Way toward Active Control of the Heat-Transfer Fluid Outflow Temperature. *Appl. Energy* **2017**, *196*, 51–61.

(242) Agrafiotis, C.; Becker, A.; Roeb, M.; Sattler, C. Hybrid Sensible/Thermochemical Storage of Solar Energy in Cascades of Redox-Oxide-Pair-Based Porous Ceramics. In *Volume 2: Photovoltaics; Renewable-Non-Renewable Hybrid Power System; Smart Grid, Micro-Grid Concepts; Energy Storage; Solar Chemistry; Solar Heating and Cooling; Sustainable Cities and Communities, Transportation; Symposium on Integrated/Sustainable Buil*; ASME, 2015; p V002T14A002.

(243) Bulfin, B.; Vieten, J.; Agrafiotis, C.; Roeb, M.; Sattler, C. Applications and Limitations of

Two Step Metal Oxide Thermochemical Redox Cycles; a Review. *J. Mater. Chem. A* **2017**, *5*, 18951–18966.

(244) Pantoleontos, G.; Koutsonikolas, D.; Lorentzou, S.; Karagiannakis, G.; Lekkos, C. P.; Konstandopoulos, A. G. Dynamic Simulation and Optimal Heat Management Policy of a Coupled Solar Reforming – Heat Storage Process. *Chem. Eng. Res. Des.* **2017**, 1–17.

(245) Albrecht, K. J.; Jackson, G. S.; Braun, R. J. Thermodynamically Consistent Modeling of Redox-Stable Perovskite Oxides for Thermochemical Energy Conversion and Storage. *Appl. Energy* **2016**, *165*, 285–296.

(246) Schrader, A. J.; Muroyama, A. P.; Loutzenhiser, P. G. Solar Electricity via an Air Brayton Cycle with an Integrated Two-Step Thermochemical Cycle for Heat Storage Based on Co_3O_4/CoO Redox Reactions: Thermodynamic Analysis. *Sol. Energy* **2015**, *118*, 485–495.

(247) Haseli, P.; Jafarian, M.; Nathan, G. J. High Temperature Solar Thermochemical Process for Production of Stored Energy and Oxygen Based on CuO/Cu_2O Redox Reactions. *Sol. Energy* **2017**, *153*, 1–10.

(248) Stamatiou, A.; Steinfeld, A.; Jovanovic, Z. R. On the Effect of the Presence of Solid Diluents during Zn Oxidation by CO_2. *Ind. Eng. Chem. Res.* **2013**, *52*, 1859–1869.

(249) Coronado, J. M.; Cabeza, L. F.; Ding, Y.; Lanchi, M.; Navarro, H.; Nieto-Maestre, J.; Prieto, C.; Sau, S.; Senneca, O.; Tregambi, C.; et al. Round Robin Test on Enthalpies of Redox Materials for Thermochemical Heat Storage. In *Solar PACES 2016*; 2016.

(250) Lucio, B.; Bayon, A.; Olivares, R.; Navarro, M. E.; Ding, Y.; Senneca, O.; Tregambi, C.; Lanchi, M.; Sau, S.; Vidal, J.; et al. Round Robin Test on Enthalpies of Redox Materials for Thermochemical Heat Storage: Perovskites. In *Proceeedings of the SolarPACES 2019,*

October 2-5, 2018. Casablanca, Morocco; 2018.

(251) Michalsky, R.; Botu, V.; Hargus, C. M.; Peterson, A. A.; Steinfeld, A. Design Principles for Metal Oxide Redox Materials for Solar-Driven Isothermal Fuel Production. *Adv. Energy Mater.* **2015**, *5*, 1401082.

(252) Muhich, C. L.; Ehrhart, B. D.; Witte, V. A; Miller, S. L.; Coker, E. N.; Musgrave, C. B.; Weimer, A. W. Predicting the Solar Thermochemical Water Splitting Ability and Reaction Mechanism of Metal Oxides: A Case Study of the Hercynite Family of Water Splitting Cycles. *Energy Environ. Sci.* **2015**, *8*, 3687–3699.

(253) Bazhenova, E.; Honkala, K. Screening the Bulk Properties and Reducibility of Fe-Doped Mn_2O_3 from First Principles Calculations. *Catal. Today* **2017**, *285*, 104–113.

(254) Marxer, D.; Furler, P.; Takacs, M.; Steinfeld, A. Solar Thermochemical Splitting of CO_2 into Separate Streams of CO and O_2 with High Selectivity, Stability, Conversion, and Efficiency. *Energy Environ. Sci.* **2017**, *10*, 1142–1149.

Biographies

Alfonso J. Carrillo holds M.Sc. in Chemical Engineering by Universidad de Salamanca (Spain), M.Sc. in Renewable Energies by Universidad de León (Spain) and a Ph.D. in Chemical Engineering by Universidad Rey Juan Carlos (Spain). His Ph.D. research was conducted at IMDEA Energy (Spain) focusing on oxides for solar thermochemical energy storage. Then, he moved to the Electrochemical Materials Laboratory to perform his postdoctoral research on redox materials for solar-to-fuel thermochemical conversion, first at ETH Zurich (Switzerland), and after at the Massachusetts Institute of Technology, MIT (USA), where he was 2018 MIT-Eni Energy Fellow. Currently, he is Juan de la Cierva Research Fellow at the Instituto de Tecnología Química, UPV-CSIC, in Valencia, Spain.

Jose González-Aguilar holds MSc in Physics (University of Cantabria, Spain, 1994), Ph.D. in Physics (University of Cantabria, Spain, 1999) and Habilitation à Diriger des Recherches (University Paul Sabatier, Toulouse, France, 2007). Ramón y Cajal research Fellow 2009. Senior researcher at IMDEA Energy Institute (2009 – present). His research interests concern concentrating solar energy systems and technologies, with special emphasis on high flux optical engineering, modelling and characterization; innovative heat transfer fluids for solar thermal power plants; high-temperature thermal storage; production of commodities and chemicals by solar thermochemistry and high-temperature heat exchangers.

Manuel Romero received his PhD in Chemical Engineering from the University of Valladolid Spain in 1990. He is the Deputy Director of the IMDEA Energy Institute and Principal Researcher of the High Temperature Processes Unit. He was Director of the Renewable Energy Division of CIEMAT and Director of the “Plataforma Solar de Almería”. He is author of more than 90 articles, he has participated in more than 45 R&D projects in energy research, 15 of them financed by the

European Commission. In 2009 he received the “Farrington Daniels Award” for his contributions to the development of high temperature solar concentrating systems.

Juan M. Coronado conducted his doctoral studies at the Catalysis and Petrochemistry Institute (ICP-CSIC) and he received his Ph.D in Chemistry from the Complutense University of Madrid. He was a Marie Skłodowska Curie Fellow and “Ramón y Cajal” researcher. He was appointed as researcher at CIEMAT and a senior researcher in IMDEA Energy (Spain). Recently, he re-joined ICP-CSIC as research scientist. He is co-author of more than 120 articles in peer–reviewed journals. Currently, his research is focused on the development of catalysts and redox oxides for cleaner fuel production and energy storage.

Graphical abstract